The Dissertation Committee for Mahdi Heidari Moghadam Certifies that this is the approved version of the following dissertation:

Time-dependent Analysis of Jet-grouted Tunnels in Difficult Ground Conditions

Committee:

Fulvio Tonon, Supervisor

John Tassoulas, Co-Supervisor

Jorge Zornberg

Chadi El Mohtar

Ran Chen

Time-dependent Analysis of Jet-grouted Tunnels in Difficult Ground Conditions

by

Mahdi Heidari Moghadam, B.S.;M.S.;M.S.

Dissertation

Presented to the Faculty of the Graduate School of

The University of Texas at Austin

in Partial Fulfillment

of the Requirements

for the Degree of

Doctor of Philosophy

The University of Texas at Austin

December 2013

Dedication

To my wife, Fereshteh,

my Parents,

and my sons, Puyan and Mahan

Acknowledgements

I would like to thank my supervisor, Professor Fulvio Tonon, for his valuable courses and guidance, and constant support throughout my PhD studies and research. I am also grateful to my co-supervisor, Professor John Tassoulas, for his instrumental guidance and constant support. I express my appreciation to the committee chair, Dr. Jorge Zornberg, and to the graduate studies committee chair, Dr. Howard Liljestrand, for their special support. I should also express my gratitude to the other committee members, particularly Dr. Ran Chen, for his time and comments. Through my PhD studies in the last three years, I had the chance to enjoy unique instructors and classmates. I would like to thank them and to wish the best for them. I want to specifically thank my best friends, Mahdi Habibi and Hossein Roodi, for their friendship and advice.

I am indebted to J.F. Shea, Maccaferri, Grace, and CSI Inc. for their financial support through the International Tunneling Consortium established by Dr. Fulvio Tonon at the University of Texas at Austin.

Time-dependent Analysis of Jet-grouted Tunnels in Difficult Ground Conditions

Mahdi Heidari Moghadam, Ph.D.

The University of Texas at Austin, 2013

Supervisors: Fulvio Tonon

John Tassoulas

In this study, excavation of jet-grouted tunnels in ground with strong time-dependent behavior is analyzed. The constant growth of population has led to a constant increase in the price of lands and thus infrastructures. Underground alternatives are becoming more economical. Furthermore, advances in the construction technology have made it feasible to construct tunnels in difficult ground conditions. By providing a grouted arch ahead of the tunnel face, jet-grouting has proved effective for the stability and performance of tunnels in difficult conditions. Given the limited depth of jet-grouting into the face, the jet-grouted arch is loaded soon after installation, when the rigidity of the grouted material is growing significantly. The simultaneous loading and hardening of the jet-grouting makes the tunnel response depend on the excavation rate. Furthermore, in difficult tunneling conditions, the ground material is associated with highly viscous behavior. This behavior is synonymous with delayed deformation depending on the level and duration of the ground loading by the tunnel excavation. In order to show the importance of the time-dependent behaviors, the full-face and the sequential excavation method are compared using three-dimensional and two-dimensional finite element analyses. First, a three-dimensional model is constructed and its results are validated

against available analytical solutions for time-independent behaviors. The hardening of the jet-grouting is then introduced into the model by embedding jet-grouting elements through the analysis. In order to account for the ground viscous behavior, an advanced viscoplastic constitutive model is adopted, numerically implemented in FORTRAN, and used in conjunction with finite element software ABAQUS. The excavation methods are compared for the well documented study case of Tartaiguille tunnel. The results indicate that the full-face method outperforms the sequential method in the studied case by installing the tunnel invert closer to the face. The two-dimensional analysis of the tunnel is conducted by using the convergence-confinement method. To this end, a new approach is introduced to use the method for tunnels in time-dependent conditions. The effect of the jet-grouting hardening and the ground viscous behavior is characterized within the new approach by deriving the ground convergence curves. The reverse dependency of these mechanisms on the tunnel advance rate leads to an optimum advance rate, at which minimum tunnel convergence develops.

Table of Contents

INTRODUCTION

Chapter 1: Introduction

Technological advances and space limitations have increased the favorability of underground alternatives. Underground transit is more frequently used to solve the problem of rapid transit in highly populated areas, where free surface space and ecological issues are of great importance. Advances in the excavation and support of ground have also made it feasible to construct larger underground structures in more problematic ground conditions. However, the analysis, design, and construction of tunnels are still mainly based on empirical rules. More complexity of the circumstances encountered in the construction of tunnels calls for more accurate analysis methods and systematic procedures for the excavation of tunnels.

The modern design of a tunnel requires an accurate analysis of the ground-support interaction in the tunnel (Lunardi, 2008). The virgin ground is under an in situ stress in equilibrium with the ground weight. Replacement of part of the ground with the structure entails disturbance of the in situ stress state, and the interacting stresses would no longer be the in situ stresses except for an ideal rigid structure. The primary unknown quantity for the structure design, the interaction loads depend on the intensity and extent of this disturbance. The latter also depends primarily on the mechanical response of both the ground and the structure. The response of the supports could be well characterized because the support structures are designed within elastic behavior. The response of the ground, on the other hand, is quite complicated even within small deformation. The ground behavior is in fact associated with residual (plastic) deformations even for small magnitudes of deformation (Holtz et al., 2011).

This dissertation investigates tunneling in difficult ground conditions. Difficult ground conditions generally include ground with little or no cohesion (relative to the in situ stress), medium to high deformability (Chern et al., 1998), and viscous characteristics. In these conditions, the ground is mainly composed of incompetent soil or soft rock such as shale rocks. These geomaterials are composed mainly of clay particles, which cause peculiar phenomena in geotechnical engineering. Slake deterioration, swelling, incompetent strength and stiffness, and time-dependent response are issues related to these types of ground.

In difficult ground conditions, tunnels are associated with significant delayed deformation. This type of deformation is related, particularly to the ground viscous behavior. The time-dependent behavior is represented by increase in ground settlement over time in shallow tunnels or increase in support forces over time in deep tunnels (Hoek, 2001). In order to take account of ground viscous behavior, an accurate time-dependent constitutive model is of marked importance. The constitutive model is necessary to account for the geomaterials fundamental characteristics such as critical state, strength softening, and rate-dependent response. The model is also necessary to provide a straightforward procedure for the identification of the model parameters.

Time-dependency of the ground response gives rise to the dependency of the tunnel response to the excavation method and rate in difficult conditions. The full-face and the sequential tunneling methods are well established in the tunneling industry (Tonon, 2010). The full-face method has proved superior, particularly in difficult ground conditions (Tonon, 2011). Contrary to the sequential method, in the full-face method, the completion of the support structure is accelerated by installation of the tunnel invert adjacent to the face. The achieved acceleration in the ground support prevents excessive loading of the ground, which is crucial in the rate of the ground delayed deformation. Therefore, the

consideration of the longitudinal distance between the tunnel face and the invert installation is also necessary in the time-dependent analysis of the tunnel in difficult ground conditions. The consideration of this distance requires a three-dimensional model in the finite element method.

In difficult ground conditions, tunnels require intensive support measures. Tunnels for urban facilities are usually built near the ground surface, where the ground is typically recent alluvium with little consolidation and thus poor mechanical properties. These tunnels often display considerable deformation and stability concerns. The control of the tunnel deformation in these difficult conditions is of primary importance.

To control the ground deformation induced by tunnel driving, sub-horizontal jet-grouting is becoming increasingly common as an effective method (Pelizza and Peila, 1993). This method is a pre-confinement measure, whereby the deformation is controlled from the very initiation, i.e. a few tunnel diameters ahead of the excavation face. Jet-grouting umbrellas are made up of successively implemented sub-horizontal columns. Jet-grouting is used to limit ground surface settlement, tunnel convergence (pre-convergence in particular), face extrusion, and hence to help stability of the face and cavity in the tunnels excavated in difficult ground conditions (Lunardi, 2008).

Despite successful use of jet-grouting method, the analysis and construction of jet-grouted umbrellas have little been investigated. Cast within the transitional zone (a few tunnel diameters behind and ahead of face), the large part of loading on jet-grouted umbrellas takes place when the jet-grout rigidity develops rapidly. This simultaneous loading and hardening of the jet-grouting requires accounting for the hardening of the jet-grouting umbrella in the analyses of the jet-grouted tunnels.

The three-dimensional problem of the tunnel excavation is still treated within a simplified two-dimensional plane strain model in practice (Karakus, 2007). The

convergence-confinement method is a two-dimensional method which can account for the three-dimensional effects by considering a two-dimensional plane strain model of the tunnel cross-section and a one-dimensional longitudinal profile of the tunnel deformation (AFTES, 2001). The latter represents the longitudinal supportive effect of the face on the tunnel (ground self-support). However, this method has been basically formulated for tunnels with time-independent behavior, and needs be developed for such time-dependent behaviors as the ground viscosity and the support hardening.

In this study, the excavation of jet-grouted tunnels in difficult ground conditions is analyzed by using three-dimensional and two-dimensional finite element models. The analyses take into account the time-dependent mechanisms of the jet-grouting hardening and the ground viscous behavior. The hardening of the jet-grouting over time is accounted for by using two approaches: embedding a series of jet-grouting elements at the jet-grouted zone during the analysis and using a chemoplastic model. In order to account for the ground viscous behavior, the viscoplastic CJS model is adopted (Purwodihardjo, 2004). The model is numerically implemented in FORTRAN, and used in conjunction with finite element software ABAQUS. The superiority of the full-face method in difficult conditions is probed by comparing the method to the sequential method in three-dimensional models with different distances between the face and the invert installation. The comparison is made in reference to the ground properties encountered in Tartaiguille tunnel, where both methods were applied. Finally, to make the time-dependent analyses achievable in practice, the convergence-confinement method is developed for tunnels in time-dependent conditions by introducing a new approach to account for the jet-grouting hardening and the ground viscous behavior.

This dissertation has three main parts. In the first part, the viscoplastic ground model and the chemoplastic jet-grouting model are explained in detail. In the second part,

the tunnel in time-dependent ground conditions is investigated by using three-dimensional models. The investigation begins with the validation of the model in time-independent conditions. The third part addresses the two-dimensional analysis of the tunnel using the convergence-confinement method and the new procedure for calculating the ground response curve in time-dependent conditions.

TIME-DEPENDENT CONSTITUTIVE MODELS

Chapter 2: Ground Viscous Behavior

2.1. INTRODUCTION

The importance of the ground properties is varied in the analysis of different earth structures. In the case of structures such as buildings, bridges, and pavements, the ground furnishes the support required for the stability of the structure against the externally applied loads. The ground-structure interaction in these cases could therefore be considered as statically determinate. The load on the ground may be determined by invoking the equilibrium of the structure. Hence, the mechanical behavior of the ground has negligible influence in the analysis of these structures. In the case of structures such as retaining walls, the interaction is still quite determinate. In this case, the structure provides the stability of the ground, and thus the interacting forces may be still determined from the equilibrium of the supported ground. Accordingly, the ultimate strength of the ground is the only geomaterial property required in the analysis of these structure

The ground mechanical characteristics are of particular importance in the analysis of tunnels. The ground-structure interaction in tunnels is generally statically indeterminate as opposed to the above-mentioned structures. In particular, in deep tunnels, the ultimate equilibrium approach predicts failure loads which are associated with impractical excessive tunnel deformation. This fact confirms that the design ground-structure loads cannot be estimated with accounting only for the ultimate properties of the structures and the ground. In order to have an accurate estimate of the interacting forces and deformations, the geomaterial and the structure mechanical response and its possible evolution over time need be characterized throughout the tunnel deformation and age.

Tunnels in difficult ground conditions are typically associated with significant delayed deformation. The delayed response of a tunnel may be related to various phenomena:

a) support delayed behavior: hardening of concrete final lining, shotcrete primary lining, jet-grouted pre-lining, cemented rock bolts, lining creep, shrinkage, etc.

b) ground delayed behavior: consolidation, creep, swelling, weathering

c) accumulative damage to supports: as a result of service; frost and thaw; corrosion

This dissertation addresses the time-dependent response of jet-grouted tunnels in ground with viscous behavior. Herein, only hardening of the jet-grouting and concrete lining, and ground viscous response are studied.

Fig. 1 shows the convergence of the Mont Terri reconnaissance gallery during face advancement and stoppage (Boidy et al., 2002). The gallery crosses sedimentary clay formations, including Dogger shale and Triassic anhydrite marls. The tunnel is about 370 m deep with a finished average diameter of 2.35 m.

The gallery was excavated without any support system until the gallery face reached TM 874.6, where excavation was stopped for one month. The followings are observed:

a) Significant displacement increment during the excavation of the section, related to the instantaneous response of the tunnel to the quick change in the tunnel geometry

b) Moderate displacement during excavation pauses, due to the ground viscous nature

Delayed deformation of the ground or the support can lead to several issues, e.g. an increase in the support demand over time, or a time-increasing convergence of the tunnel. In some cases, the tunnel delayed deformation can reach 70% of the total tunnel deformation (Rousset, 1988).

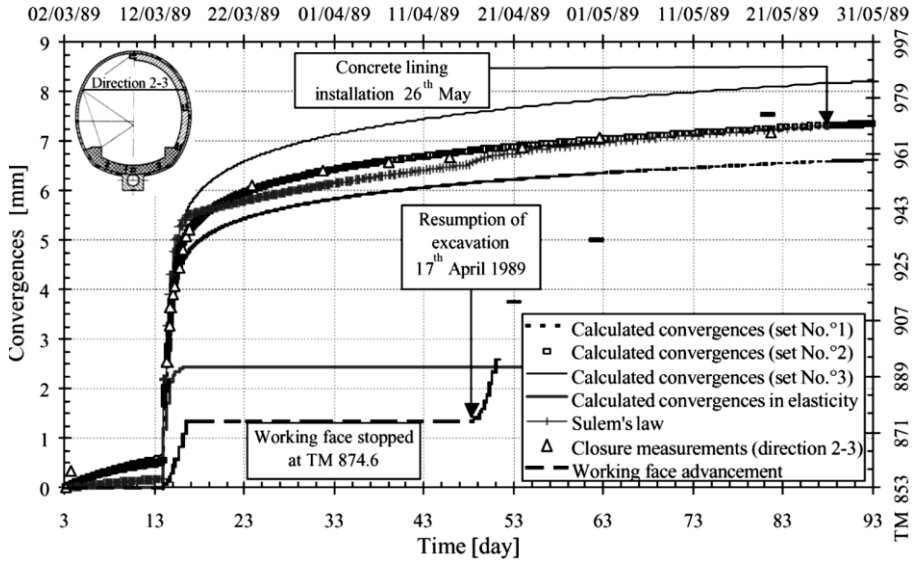

Figure 1: Tunnel convergence as measured during face advance and stoppage (after Boidy et al., 2002)

2.2. EXPERIMENTAL RESULTS

The delayed response of viscous geomaterials is attributed to the viscous sliding of minerals against each other. This delayed response gives rise to time-dependent increasing deformation and stress in the ground and supports. The viscous behavior of geomaterials is typically identified in three types of tests.

2.2.1. Tests with controlled deformation rate

Many experimenters have shown that the deformation rate influences the response of the geomaterial, particularly clays and soft rocks (Adachi and Oka, 1982; Hicher, 1985; Fodil et al., 1998; Murakami et al., 1996; Zhu and Yin, 2000). Fig. 2 shows the dependency of the stress response on the applied strain rate. We see that the material strength depends on the applied strain rate. By increasing the shear strain rate, the geomaterial strength increases.

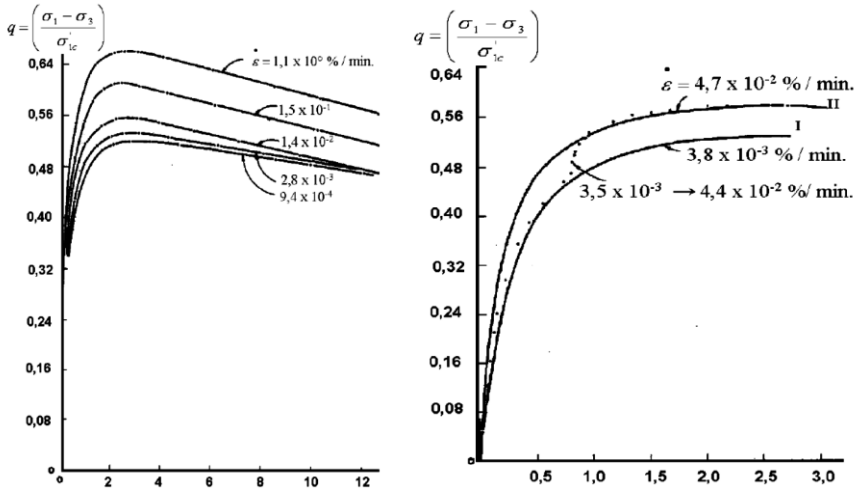

Figure 2: Loading rate effect (after Murakami et al., 1996)

Fig. 3 shows the effect of the strain rate on the effective stress path (Hicher, 1985). It is notable that the critical state line remains unaffected by the strain rate. Similar results can be found on tests conducted by Adachi and Oka (1982), and Zhu and Yin (2000). They showed that the peak strength is affected by the applied strain rate while the residual strength is almost constant.

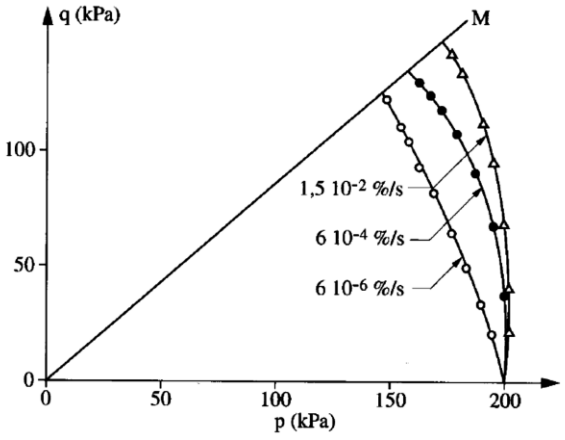

Figure 3: Effect of loading rate on stress path (after Hicher, 1985)

2.2.2. Tests with controlled load (creep)

The creep test is another type of test that is frequently used to assess the time-dependent behavior of geomaterials. In this test, the stresses on the material are constant during the test, and the deformation response is measured over time.

The existence of creep response under an isotropic stress state is a matter of debate, and conflicting results have been presented. Maekawa et al. (1991) showed that for high levels of isotropic stresses, the volumetric flow is very significant. In general, the viscosity of the geomaterial response to the isotropic stress state is significantly lower than to the deviatoric stress state. Accordingly, in many models, the material creep due to the isotropic stress is neglected.

A number of studies on the viscous behavior of soils have been carried out on the secondary deformation in the odometer consolidation test. In an odometer test, the stress field in the sample is not isotropic. Because the lateral strain vanishes, the volume change can be directly measured with the change in the sample height. Fig. 4 shows the evolution of the axial strain with time in the odometer tests performed by Fodil et al. (1998) on a natural clay. A relatively high permeability for clay due to the presence of fine sand allowed for the separation of the primary consolidation phase from the secondary drained creep phase. The slope of the axial strain versus the logarithm of time defines the coefficient of the secondary consolidation (creep) phase.

Standard triaxial tests have been widely used to study the creep behavior under deviatoric stress state (Bishop, 1966; Tavenas et al., 1978; Akai et al., 1977). The volumetric and deviatoric deformation increments are typically monitored with time. Fig. 4 shows the variation of volumetric and shear strain in the tests performed by Akai et al. (1977). Dilation and shear strain occur with primarily decreasing and ultimately increasing

rate. As shown, at higher load levels, the initial rate of deformation is higher, but its variation with time is of less intensity.

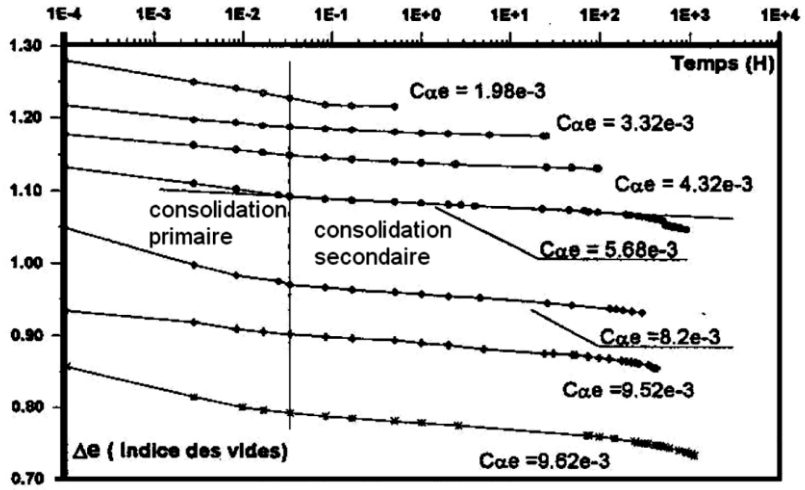

Figure 4: Oedometric creep as secondary consolidation (after Fodil et al., 1998)

Fig. 5 shows that the strain rate in a creep test increases with increasing the applied load. In general, the rock deforms in a creep test in three distinct phases (Fig. 6):

1) primary or transitional creep: the creep strain rate decreases with time
2) secondary or stationary creep: the creep strain rate is constant
3) tertiary creep: the creep rate increases due to the development of damage to the rock structure

The primary creep phase always takes place in the beginning of the creep test. The tertiary creep phase also occurs ensuing large deformation or large loads (close to rock strength). The secondary creep phase is however so short-lived that a direct transition from the primary to the tertiary phase may be assumed.

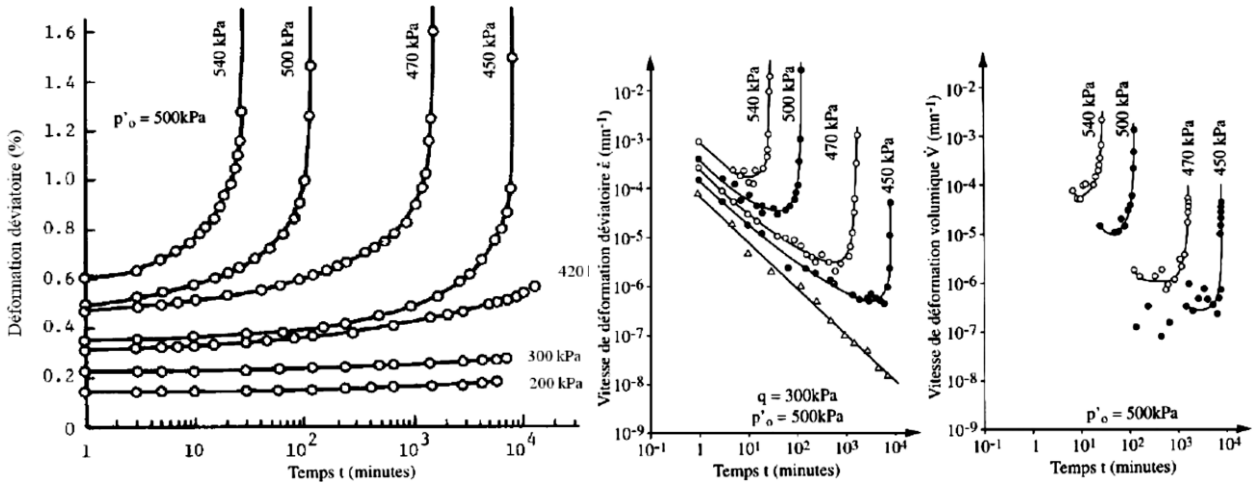

Figure 5: Triaxial drained test on Ohya soft rock (after Akai et al., 1977)

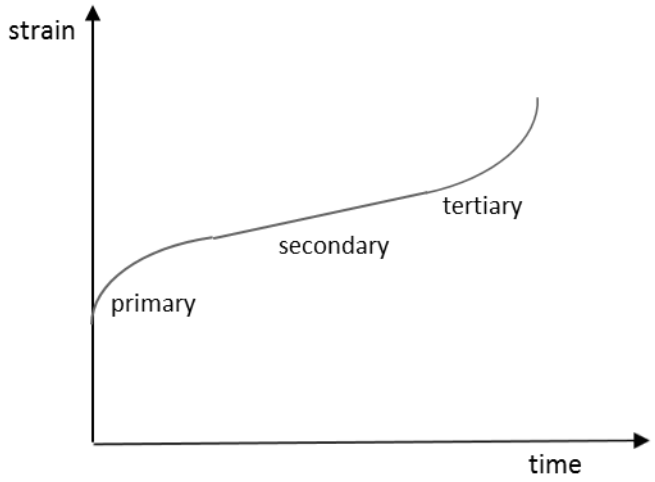

Figure 6: Different deformation phases in creep test

Undrained creep tests have been the subject of a large number of studies on geomaterials viscous behavior (Tavenas et al., 1978; Kavazanjian and Mitchell, 1980; Sekiguchi, 1984; Murakami et al., 1996; Lin et al., 1998; Zhu et al., 1999). The undrained creep test can be performed in a relatively short time because the sample consolidation need not be fulfilled. On the other hand, the pore pressure changes during the test, which

causes a change with time of the effective stresses. Hence, the term creep may be considered improper for this type of test. Primary and tertiary creep phases have been detected in the undrained tests as well (Sekiguchi, 1984).

2.2.3. Tests with constant deformation (relaxation)

In a relaxation test, the deformation is applied instantly and then kept constant during the test while the reduction of the stress response is measured. As shown in Fig. 7, the load decreases linearly with the logarithm of time. The rate of relaxation increases with an increase in the imposed deformation level.

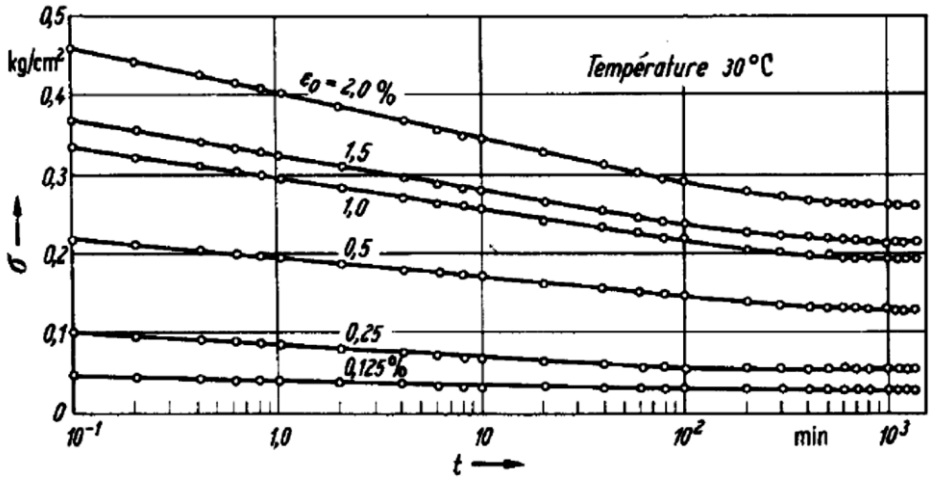

Figure 7: Evolution of axial stress with time in undrained relaxation test (after Murakami et al., 1996)

The following points may be drawn from the presented experimental data:

- The strength and the stress-strain curve are influenced by the applied strain rate
- Each strain rate is associated with a response curve. A change in the strain rate leads to a change in the material response curve

- The critical state defined by the critical line in the meridional stress plane is independent of the applied strain rate
- The amount and rate of delayed deformation is controlled by the level of the shear stress
- A direct transition from the primary to the tertiary phase may be assumed (no secondary phase)
- The deformation rate increases dramatically when the applied load is close to the material peak strength (tertiary creep)
- The rate of stress relaxation increases with the level of the imposed deformation

2.3. THEORETICAL MODELING

A constitutive model for the material viscous behavior basically describes the rate dependent response of the material on the basis of experimental data from laboratory or field tests. Several models have been proposed to describe the viscous behavior of geomaterials. In general, these models can be divided into two types: models that explicitly account for the time effect and models that implicitly account for the time effect through time evolving state variables. In general, three approaches are followed in the constitutive modeling of viscous geomaterials.

2.3.1. Empirical modeling

Empirical models are derived by simple interpretation of experimental observations. On the basis of the secondary consolidation data (Aristorenas, 1992; Kharchafi, 1995), a linear relation between the volumetric strain and the logarithm of time is well established. Singh and Mitchell (1968) proposed a power law relation for the axial deformation rate in a triaxial creep test. Tavenas et al. (1978) suggested different load dependency but identical power for the volumetric and shear deformation as

$$\dot{\epsilon}_v(t) = f(\sigma)(\frac{t_i}{t})^m \qquad \dot{\epsilon}_d(t) = g(\sigma)(\frac{t_i}{t})^m$$

Bjerrum (1973) delineated the effect of delayed deformation by the curves shown in Fig. 8. According to these curves, the compression index C_c is independent of the time, but the overconsolidation stress σ'p increases with time or strain rate. The curves show that the decrease in the void ratio during the delayed deformation gives the material an overconsolidation as if it has been subject to a higher load. In fact, material hardening occurs through increased density and elastic limit during the creep phase. The curves assume that the relationship between the axial force and deformation can be represented by parallel curves associated with different times. Accordingly, the instantaneous and delayed deformations can be calculated as:

$$\delta_i = \frac{C_c}{1+e_0}\log\left(\frac{p_0+\Delta p}{p_c}\right) \qquad \delta_d = \frac{C_c}{1+e_0}\log(\frac{p_c}{p_0})$$

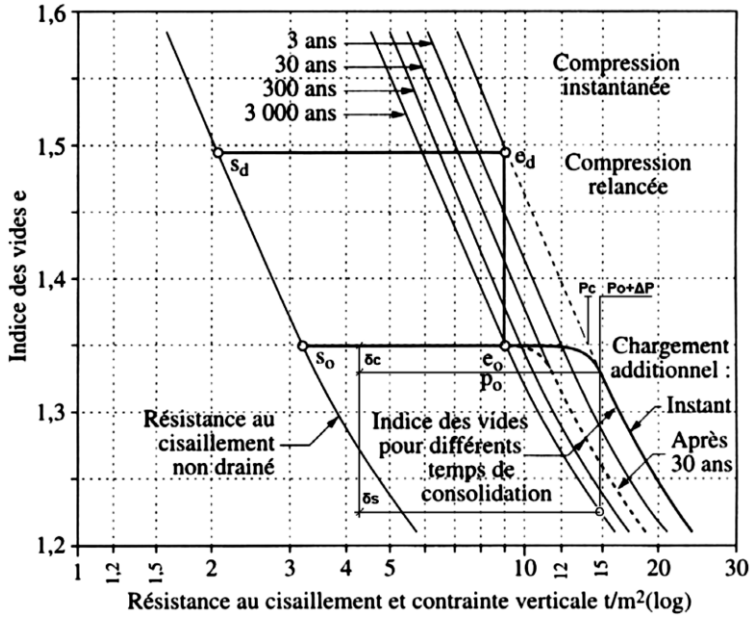

Figure 8: Bjerrum (1973) curves for delayed deformation in oedometric test

Borja and Kavazanjian (1985), and Pestana and Whittle (1998) extended Bjerrum's curves for three-dimensional modeling of clays delayed behavior. Garlanger (1972) describes the different consolidation curves using the following equation:

$$e = e_0 - C_r\, log(\frac{p_c}{p_0}) - C_c\, log(\frac{p}{p_c}) - C_a\, log(\frac{t_i + t}{t_i})$$

where e is the void ratio, Cr is the recompression index, Cc is the compression index, and Cα is the coefficient of secondary consolidation. σ'_o, σ'_c and σ' are initial, preconsolidation, and applied stress respectively, and t is the reference time (end of primary consolidation).

In general, empirical models are not intrinsic, but depend on the stress path and the boundary conditions. Therefore, they may be applied only within the same loading and boundary conditions as they are derived. These relationships can nonetheless be used to describe the primary creep phase.

2.3.2. Rheological models

Rheological models use a different approach to model the geomaterial viscous behavior. They are composed of three primary one-dimensional conceptual elements: Hooke spring element representing elastic behavior, Newton damper element representing viscous behavior, and St. Venant slipping element representing plastic behavior (Table 1).

Hook spring	
Newton damper	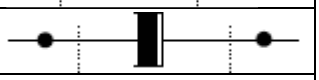
St. Venant slider	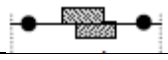

Table 1: Basic elements of rheological models

A number of rheological models have been suggested in the literature by taking different number, different configuration (in series, parallel, or a combination of both), or

different constitutive rules (linear or nonlinear) for the principal elements. In general, the models may be classified as viscoelastic or viscoplastic.

The viscoelastic approach is the simplest approach to take into account the viscous behavior. This approach has been applied to several types of materials such as soil, rock and concrete. The simplest model may be conceived as to consist a linear damper element whereby shear stress τ relates to the shear strain rate $\dot{\gamma}$ by a constant viscosity η as:

$$\tau = \eta\,\dot{\gamma}$$

This model represents a damper with Newtonian fluid. No relaxation process is possible with this model. The viscosity has thus a dimension of stress-time.

Maxwell's model shown in Table 2 consists of a linear spring and a linear damper in series. The governing constitutive differential equation for this model is obtained as follows:

$$\dot{\gamma} = \frac{\dot{\tau}}{G} + \frac{\tau}{\eta}$$

Model	Representation
Maxwell	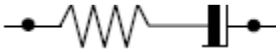
Kelvin	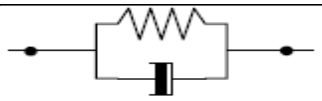
Burger	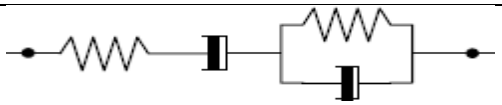

Table 2: Viscoelastic rheological models

This model can describe the secondary creep as well as the relaxation test through elastic deformation recovery over time. The response of this model in the creep test is:

$\tau = cte \qquad \gamma(t) = \frac{\tau}{G} + \frac{\tau}{\eta} t$

The response of the model in the relaxation test is:

$\varepsilon = cte \qquad \tau(t) = G\varepsilon \exp\left(-\frac{G}{\eta} t\right)$

Kelvin-Voight model is another basic viscoelastic model which corresponds to a parallel assembly of a linear spring and a linear damper element. The differential equation obtained for the model is:

$\tau = G\gamma + \eta\dot{\gamma}$

Unlike Maxwell model, Kelvin-Voight model can describe an asymptotic exponential response in the creep test as follows:

$\gamma(t) = \frac{\tau}{G}(1 - \exp\left(-\frac{G}{\eta} t\right))$

This model fails to model the relaxation test because the damper element in parallel to the spring element prevents any immediate deformation to be imposed.

Burgers model consists of a serial assembly of Kelvin and Maxwell models as shown in Table 2. In the creep test, the deformation response of this model is the sum of Kelvin and Maxwell models deformation responses:

$\gamma(t) = \frac{\tau}{G^M} + \frac{\tau}{\eta^M} t + \frac{\tau}{G^K}(1 - \exp\left(-\frac{G^K}{\eta^K} t\right))$

Therefore, this model can reproduce the primary and the secondary creep phases (Nomikos et al., 2011). Different rheological models have been proposed based on the basic Maxwell and Kelvin assemblies. More complex viscoelastic models may also be constructed by using a variety of assemblage of Kelvin and Maxwell models.

A major part of geomaterials viscous deformation is not recoverable. Hence, viscoelastic models may be used only for problems with monotonic loading paths. In addition, the viscous deformation occurs for loads beyond certain limits. In order to account for this fact and also the nonlinearity of the material response due to inelastic deformation,

the viscoelastic models require elements with complex constitutive equations. On the other hand, by using plastic elements, viscoplastic models can treat inelasticity directly and with markedly less complexity.

Bingham model is a rigid-viscoplastic model. According to this model, the viscoplastic shear deformation occurs only for loads exceeding a certain stress limit. The shear strain rate in this model is obtained as

$$\dot{\gamma} = 0 \qquad \tau < \tau_0 \ ; \qquad \dot{\gamma} = \frac{\tau - \tau_0}{\eta} \qquad \tau \geq \tau_0$$

This model describes rigid-viscoplastic deformations. By adding a spring element in series to Bingham model, Madejski (1960) proposed an elasto-viscoplastic model, which was used in other elasto-viscoplastic models such as Fritz (1984) and Rousset (1990).

Komamura and Huang (1974) combined Kelvin-Voight viscoelastic model and Bingham viscoplastic model in series. The strain response in the creep test using this model can be expressed as:

$$\gamma(t) = \frac{\tau - \tau_0}{\eta^B} t + \frac{\tau}{G^K}(1 - \exp\left(-\frac{G^K}{\eta^K} t\right))$$

CVICS model is a viscoelastic-plastic model. It results from serial assemblage of Burgers and Mohr-Coulomb models. The plastic part can describe the instantaneous irreversible deformation. This model is implemented in the finite difference code FLAC. Other viscoplastic models are derived based on Maxwell, Kelvin-Voight, and Bingham elementary models.

2.3.3. Viscoplastic models

Different approaches have been adopted in the literature to model three-dimensional viscoplastic deformation. A number of models uses the overstress concept to model viscoplastic deformation. The idea was first introduced by Perzyna (1966) within metal plasticity. In this theory, the stress state is no longer limited to the yield surface, and

the viscous strain rate relates to the distance of the stress state and the evolving yield surface. As such, the strain rate is decomposed into an elastic and a viscoplastic part as:

$$\dot{\varepsilon}_{ij} = \dot{\varepsilon}_{ij}^{e} + \dot{\varepsilon}_{ij}^{vp}$$

Perzyna (1966) suggested the following equation for the hardening yield surface defined by F=0. The size of the surface depends on the viscous deformation history as

$$F\left(\sigma_{ij}, \varepsilon_{kl}^{vp}\right) = \frac{f\left(\sigma_{ij}\right)}{\kappa\left(\varepsilon_{kl}^{vp}\right)} - 1$$

The flow rule in this model is written as

$$\dot{\varepsilon}_{ij}^{vp} = \gamma < \phi(F) > \frac{\partial g}{\partial \sigma_{ij}}$$

where γ represents the material viscosity, and g is the viscoplastic potential function, which is identical to the yield function F in case of associated plasticity. ϕ is the flow function. Nguyen-Minh (1986), Rousset (1988) and Panet (1995) showed that the use of a power law flow function allows for satisfactory calibration of viscoplastic deformation in laboratory or in situ measurements. However, for most geomaterials, experiments indicate a linear relationship between the maximum strength and the logarithm of the imposed strain rate. A power law flow function fails to reproduce this observation, and generally overestimates the strength of soft rocks. Consequently, Katona (1984), Laigle and Kolmayer (1998) and Fodil et al. (1998) proposed an exponential relationship of the form

$$\phi(F) = \exp(F^{n}) - 1$$

Several viscoplastic models have been developed using this approach (Dafalias et al., 1982; Rousset, 1988; Fodil et al., 1998; Laigle and Kolmayer, 1998; Purwodihardjo and Cambou, 2005). This approach has several advantages:

- The plasticity criterion is directly involved
- The viscous behavior can be described along a wide range of loading paths

- The formulation is amenable to numerical implementation such as finite element method
- Identification of the model parameters is generally simple

However, Mimura and Sekiguchi (1985), and Adachi et al. (1996) showed that the structure of this theory fails to describe the deformation acceleration during the tertiary creep phase.

Olszak and Perzyna (1966) modified the overstress theory by introducing an unsteady yield surface which was explicitly dependent on a time scalar variable. In these types of models, the viscoplastic yield surface is given by

$$F\left(\sigma_{ij}, \varepsilon_{kl}^{vp}, \beta\right) = 0$$

where β is a scalar time-dependent parameter. The yield surface is often used as the potential surface to determine the direction of the viscoplastic deformation as

$$\dot{\varepsilon}_{ij}^{vp} = \gamma \frac{\partial F}{\partial \sigma_{ij}}$$

where γ is a positive multiplier which is obtained from the consistency condition as

$$\gamma = -\frac{\frac{\partial F}{\partial \sigma_{mn}} \dot{\sigma}_{mn} + \frac{\partial F}{\partial \beta} \dot{\beta}}{\frac{\partial F}{\partial \sigma_{mn}} \frac{\partial F}{\partial \varepsilon_{mn}^{vp}}}$$

As such, unlike the basic overstress theory, the viscoplastic strain rate in this concept is determined in terms of the stress *rate*. Further, the stress state will be bound to the yield surface, and the loading-unloading criterion again holds. However, the explicit dependence of constitutive equations on time impairs the generality of the model. For instance, these types of models may predict viscous deformation continue even after a complete removal of loads. In general, the explicit use of time in constitutive equations allows for the direct use of experimental data and thus a good agreement between the simulation and the

experiment. However, the specified model may not show such a good performance in other loading paths.

In order to simulate the tertiary creep phase in the drained as well as the undrained conditions, Aubry et al. (1985) introduced a damage mechanism into their model. The accelerated rock failure in the tertiary creep phase was accounted for by damaging the viscosity parameter and the Young's modulus of the material. The constitutive equations depend explicitly on time.

Kaliakin and Dafalias (1990) are credited for the bounding surface approach in viscoplasticity. They constructed an elasto-viscoplastic model based on the bounding surface, the critical state, and Perzyna overstress concepts. The bounding surface is a boundary surface in the stress space which limits the stress state. The stress state can exist in the inner area between the yield surface and the bounding surface (see Fig. 9). The state of the material is defined in terms of the stress and the internal variables q_n. For each stress state σ_{ij}, there is a single image stress $\bar{\sigma}_{ij}$ on the bounding surface.

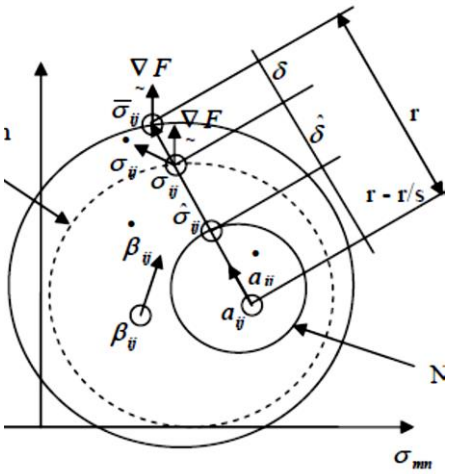

Figure 9: Bounding surface concept

The bounding surface is defined by

$$F(\bar{\sigma}_{ij}, q_n) = 0$$

The bounding surface changes always outwards. The flow rule is defined in terms of the yield function gradient and the potential gradient as:

$$\dot{\varepsilon}_{ij}^{p} = < \gamma > \frac{\partial G}{\partial \sigma_{ij}} \qquad \gamma = \frac{1}{K^p} \frac{\partial F}{\partial \sigma_{ij}} \dot{\sigma}_{ij}$$

The plastic modulus changes monotonically with the distance between the stress state and the corresponding image point as

$$K^p = \bar{K}^p + H \frac{\delta}{< r - s\,\delta >}$$

where $\bar{K}^p$ is the plastic modulus obtained from the consistency condition on the bounding surface. H is a scalar hardening function, and δ, r and s are shown in Fig. 9. Kaliakin and Dafalias (1989) proposed a simple version of this model, where the plastic deformation is decomposed into immediate and delayed parts. The latter can eliminate the difficulties associated with fast loading and failure modeling in the classical theory of viscoplasticity.

At failure, where the plastic modulus tends to vanish, the evolution of the bounding surface also vanishes. This leads to a constant rate of viscoplastic strain, which represents the secondary creep phase. As such, in this model the failure and the secondary creep are synonymous, which is not fully evidenced by experimental data. However, this model has several advantages:

- Simple formulation (isotropic (scalar) hardening)
- Applicability to both drained as well as undrained conditions
- Applicability to both normally consolidated and over-consolidated clays

In conclusion, the significance of the delayed response in geomaterials and concrete-type materials is well established. The amplitude of the viscous deformation in some cases may exceed by several times the immediate deformation. To take this behavior

in the analysis of structures, several models have been developed, ranging from rather simple empirical models to more advanced rheological models and complicated viscoplastic constitutive models.

The empirical models can be used for qualitative studies. However, for structures requiring more precision, the rheological models and the viscoplastic models need be employed. The rheological models have a decent capability in representing the uniaxial viscous behavior. Several authors have extended these models for three-dimensional problems, but this extension is concomitant with a loss of simplicity in these models.

The majority of viscoplastic models proposed in the literature have been developed based on the Perzyna overstress model. This model is developed within the framework of classic plasticity theory, and is also quite amenable to numerical implementation. This model lacks the capability to account for the accelerating tertiary creep phase. Efforts have been made to overcome this deficiency by introducing unsteady yield surface or damage theory. The time factor however is explicitly involved in these approaches, limiting their applicability to certain loading paths.

Bounding surface viscoplastic models follow another approach in describing the viscous behavior of geomaterials. They can satisfactorily reproduce the response of both normally consolidated and overconsolidated clays in the drained as well as the undrained conditions. Moreover, their formulation is fairly simple (isotropic hardening). However, they fail to account for the accelerating tertiary creep.

2.4. VISCOPLASTIC CJS MODEL

Ground viscous behavior is an important characteristic of tunneling in difficult ground conditions. Strictly related to the properties of the natural ground, the delayed deformation is typically observed in ground with considerable amount of highly plastic

clays. The tunnel time-dependent response in difficult conditions typically derives from three time-dependent mechanisms of ground viscous behavior, ground consolidation, and ground swelling. Here, we treat only the ground viscous behavior by analyzing the tunnel in undrained conditions and using a viscoplastic model for the ground.

CJS model is a viscoplastic model developed over years by incorporating important concepts such as critical state, strain softening, non-associativity, and bounding surface theory into a basic Mohr-Coulomb model (Hicher and Shao, 2008). Furthermore, the model parameters can be identified using standard triaxial tests (Purwodihardjo, 2004).

This study employs a version of the model which includes only isotropic hardening. This version is suitable for monotonic loading as in tunneling. In unloading, the model response is completely elastic and identical, which is inconsistent with experimental reality. The advantage of this model is therefore mainly in its relative simplicity and its ability to provide an acceptable precision in monotonic loading with a minimum number of parameters and of experimental tests.

This model is based on non-linear elasticity and two mechanisms of plasticity. It also takes into account the dependency on the density of the material through the critical state. The plastic deformations are generated from an isotropic and a deviatoric mechanism. Fig. 10 shows the yield surfaces associated with these mechanisms in CJS model. The total strain in the model is then decomposed in four parts

$$\dot{\varepsilon_{ij}} = \dot{\varepsilon_{ij}}^{e} + \dot{\varepsilon_{ij}}^{ip} + \dot{\varepsilon_{ij}}^{dp} + \dot{\varepsilon_{ij}}^{vd}$$

which are elastic strain, plastic strain due to isotropic mechanism, plastic strain due to deviatoric mechanism, and viscous plastic strain, respectively.

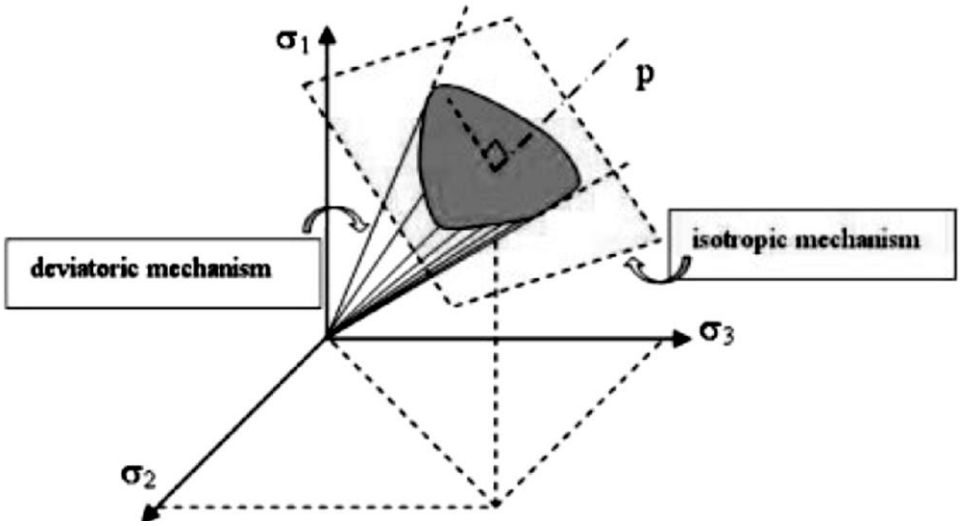

Figure 10: Yield surfaces associated with deviatoric and isotropic mechanisms in stress space in CJS model

2.4.1. Elastic behavior

CJS model uses a non-linear elastic response. The elastic part of the deformation depends on the level of the confinement pressure as well. The elastic law is given by the following incremental non-linear equation:

$$\dot{\varepsilon_{ij}}^{e} = \frac{\dot{S_{ij}}}{2G} + \frac{\dot{I}_1}{9K}\delta_{ij}$$

where I_1 and S_{ij} are the first invariant and the deviatoric part of the stress tensor, respectively. K and G are the tangent bulk and shear modulus, respectively, which depend on the stress state through a power law:

$$K = K_0{}^{e}\left(\frac{I_1}{3P_a}\right)^n \quad ; \quad G = G_0\left(\frac{I_1}{3P_a}\right)^n$$

K_0^e, G_0, and n are model parameters while Pa is the atmospheric pressure which equals 100 kPa.

2.4.2. Isotropic plastic mechanism

The yield surface associated with this mechanism is a plane perpendicular to the hydrostatic axis. The yield surface is given by

$$f^i(I_1, Q) = \frac{I_1}{3} - (Q + T_r) = 0$$

The yield surface's evolution is defined by an isotropic hardening mechanism depending on a scalar variable Q and T_r is a parameter of the model to take into account the cohesion. The hardening rule has the form

$$\dot{Q} = {K_0}^p (\frac{Q}{P_a})^n {\dot{\varepsilon}_v}^{ip}$$

${K_0}^p$ is the tangent plastic bulk modulus and n is a parameter of the model which can be determined by experiment.

2.4.3. Deviatoric plastic mechanism

For the sake of simplicity no kinematic hardening but only isotropic hardening was taken into account in the model used in this paper. The yield surface can be defined by the following equation:

$$f^d(\sigma_{ij}, R) = s_{II}\, h(\theta) - R(I_1 + 3\, T_r) = 0$$

$$h(\theta) = (1 - \sqrt{54}\, \gamma\, \frac{s_{III}}{{s_{II}}^3})^{\frac{1}{6}} \quad ; \quad s_{II} = \sqrt{s_{ij} s_{ij}} \quad ; \quad s_{III} = \det(s_{ij})$$

where γ is a parameter of the model. s_{II} and s_{III} are the second and third invariants of the deviatoric stress, respectively. θ is the Lode angle.

The evolution of the yield surface is characterized by the evolution of R with the internal variable p. The relationship between R and p is written as

$$R = \frac{A R_m p}{A p + R_m}$$

where R_m is a parameter that corresponds to the mean slope of the peak surface and A is a parameter of the model. The evolution of (the hardening parameter) p is defined by

$$\dot{p} = \dot{\lambda}^d I_1 (\frac{I_1}{3P_a})^{-1.5}$$

Substituting p in terms of R, we can express the deviatoric mechanism hardening as

$$\dot{R} = A(1 - \frac{R}{R_m})^2 \dot{p}$$

The deviatoric flow rule is given by

$$\dot{\varepsilon_{ij}}^{dp} = \dot{\lambda}^d [\frac{\partial f^d}{\partial \sigma_{ij}} - \left(\frac{\partial f^d}{\partial \sigma_{kl}} n_{kl}\right) n_{ij}]$$

where $\dot{\lambda}^d$ is a magnitude parameter of the incremental plastic strain for the deviatoric plastic mechanism. This flow rule corresponds to a non-associated plastic mechanism. Tensor n_{ij} is a symmetrical tensor so that tr(n^2)=1, and it is a tangential tensor to the surface corresponding to the potential function. It is defined by

$$n_{ij} = \frac{\beta' \left(\frac{S_{ij}}{S_{II}}\right) - \delta_{ij}}{\sqrt{\beta'^2 + 3}} \qquad \beta' = sgn(S_{ij}\, \dot{e_{ij}}^{dp}) \beta (\frac{S_{II}}{{S^c}_{II}} - 1)$$

where ${s^c}_{II}$ represents the second invariant of the deviatoric stress on the critical surface and β is a parameter of the model. The critical surface is defined by

$$f^c(\sigma_{ij}, R) = {s^c}_{II}\, h(\theta) - R_c(I_1 + 3\, T_r) = 0$$

where R_c represents the mean slope of the critical surface. The critical surface defines stress states with no volume change. The normal to the yield surface may be calculated as

$$\frac{\partial f^d}{\partial \sigma_{ij}} = Q_{ij} - R\delta_{ij} \quad ; \quad Q_{ij} = \frac{1}{h^5(\theta)} [\left(1 + \frac{\gamma}{2}\cos(3\theta)\right) \frac{q_{ij}}{q_{II}} + \frac{\gamma\sqrt{54}}{6q_{II}^2} dev\left(\frac{\partial \det(\boldsymbol{q})}{\partial q_{ij}}\right)]$$

The peak surface is the locus of stress states corresponding to the peak of the stress-strain curve in the standard triaxial tests.

2.4.4. Critical state behavior

Two important phenomena can be drawn from the drained triaxial tests:

- The peak resistance increases with the initial density of the material,
- The material tends to a state called the critical state, which is characterized by a null volume variation and a constant ratio of q/p independent of the initial density

To take into account these phenomena in this model, the slope of the peak surface varies as a function of the mean effective stress and the density of the material. Numerous experiments have also demonstrated an increase in the peak angle with a decrease of the mean pressure. In this model, this evolution is expressed through the peak slope Rm defined by

$$R_m = R_c + \mu \ln\left(\frac{3p_c}{I_1}\right) \quad ; \quad p_c = p_{c_0} \exp(c\varepsilon_v) \quad ; \quad \varepsilon_v = \frac{\Delta e}{1 + e_0}$$

where μ is a parameter of the model, and p_c is a critical pressure. c is a model parameter, p_{c_0} is a critical pressure corresponding to the initial density, ε_v is the accumulated volume strain, and e represents the void ratio. This formulation, however, leads to an unrealistic increase in the peak friction angle for mean pressures less than a threshold pressure p_{seuil}. For these mean pressures, the peak slope R_m is defined by

$$R_m = R_c + \mu \ln\left(\frac{3p_c}{I_1}\right) \frac{\ln(\frac{m_0 . p_c}{p_{seuil}})}{\ln(\frac{3\, m_0 . p_c}{I_1})} \quad ; \quad p_{seuil} = p_a \ln(\frac{p_a + p_c}{p_a})$$

Parameter m_o allows to choose the limit of the peak angle for a given density when the mean pressure approaches zero.

2.4.5. Strain softening mechanism

In the original CJS model, the definition of the critical state allows the strain softening of soils which is linked to the dilatancy of soils to be taken into account. But in the other case, such as for the overconsolidated clay, the strain softening of the material is generally linked to the cracking which does not develop a significant evolution of the density. In this case, it is necessary to define another strain softening mechanism which is not directly linked to the volume strain. So in this paper, the proposed model takes into account the strain softening of soils which depends on the accumulated deviatoric strain. This model is made up of three portions, an elastoplastic portion up to the peak strength, a

softening portion in which the strength (R_c and T_r) reduces from the peak to residual, and finally, a constant residual strength portion. In this model, post peak values of the strength parameters, i.e. R_c and T_r will be defined as functions of the second invariant of the deviatoric strain, $e_{II} = \sqrt{e_{ij}e_{ij}}$. The following equations are used to define the softening of the strength parameters:

If $e_{II} \leq {e_{II}}^0$:

$R_c = R_{c_{peak}}$; $T_r = T_{r_{peak}}$

If ${e_{II}}^0 \leq e_{II} \leq {e_{II}}^f$:

$$R_c = R_{c_{peak}} - \left(R_{c_{peak}} - R_{c_{res}}\right)\sqrt{1 - \frac{\left({e_{II}}^f - e_{II}\right)^2}{\left({e_{II}}^f - {e_{II}}^0\right)^2}}$$

$$T_r = T_{r_{peak}} - \left(T_{r_{peak}} - T_{r_{res}}\right)\sqrt{1 - \frac{\left({e_{II}}^f - e_{II}\right)^2}{\left({e_{II}}^f - {e_{II}}^0\right)^2}}$$

If $e_{II} \geq {e_{II}}^f$:

$R_c = R_{c_{res}}$; $T_r = T_{r_{res}}$

where the subscripts *res* and *peak* refer to the residual and peak value, respectively. Fig. 11 shows the second kind of strain softening behavior in CJS model.

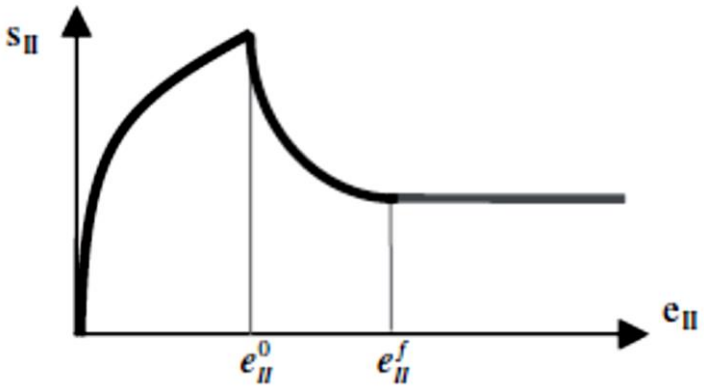

Figure 11: Second kind of strain softening in the CJS model

2.4.6. Viscous behavior

The viscous effect of the soil is taken into account through a creep surface which is bounded by the current (artificial) state of stress surface. It means that the creep surface can evolve but the evolution is limited by the state of stress surface. The current state of stress surface is a surface homothetic to the yield surface. Meanwhile, the evolution of state of stress surface is limited by the yield surface (elastoplastic concept). The evolution of the yield surface is limited by the peak surface.

The basic formulation for this viscous mechanism is inspired by the overstress model of Perzyna (1966). To keep within the framework of elastoplasticity is the reason for using this formulation. The idea is, therefore, starting from the general framework of elastoplasticity and introducing a modeling of viscous effects. It has been shown that this model is incapable for introducing the accelerated deformation phenomenon in the case of tertiary creep (Adachi et al., 1990). Therefore, in this paper a formulation has been proposed to allow the tertiary creep to be taken into account in the model.

Thus, three important terms have to be defined in the framework of this model. The first one is the viscosity of the material, the second one is the function of retardation and the last one is the direction of the viscoplastic strain. The evolution of the viscous strain is as follows:

$$\dot{\varepsilon_{ij}}^{vd} = \frac{1}{\eta}(F_v)^m {G_{ij}}^{vd}$$

where η is the viscosity of the material, F_v is the function of retardation, and ${G_{ij}}^{vd}$ is the direction of the viscoplastic strain. The viscosity of the material is a function of the distance of the state of stress R_e from the peak surface R_m. This function is defined by

$$\eta = \eta_0[1 - \left(\frac{R_e}{R_m}\right)^2]^k$$

where η_0 is a parameter of the model, R_e is the mean slope of the current state of stress surface, R_m is the mean slope of the peak surface, and k is a parameter of the model.

The delay function F_v is inspired by the bounding surface theory (Kaliakin and Dafalias, 1990). This function is defined by

$$F_v = \frac{R_e - R_v}{R_m - R_v}$$

where R_v corresponds to the mean slope of the creep surface. The power m in the given viscous flow rule is defined by

$$m = m_1 + m_2 \frac{R_e}{R_m}$$

where m_1 and m_2 are parameters of the model. The retardation function, F_v, takes an important role because it will drive the evolution of the primary creep, the secondary creep and the tertiary creep where the secondary creep will be reduced to a passing point between the primary creep and the tertiary creep. The primary creep, in the creep test, can be modeled when the creep surface increases and approaches the current state of stress surface. In this case, the viscous strain rate decreases with the creep surface approaching the stress surface.

This viscous flow rule can represent the tertiary creep behavior, which occurs at stress states near the peak surface. For these stress states, F_v equals one while the viscosity η vanishes. Thus, the rate of the viscoplastic strain becomes infinite (rupture). It is noteworthy that the tertiary creep behavior due to the proximity of the stress state and the peak surface may also occur as a result of the strength softening at elevated shear strains.

Like the yield surface, a viscous surface is used in a number of models to take into account the evolution of the delayed plastic deformation. Lade and Liu (1998) studied the yield and the creep potential surfaces, representing the direction of the instantaneous and delayed deformation rate, respectively (Fig. 12). They used two stress paths of constant

confining pressure and constant stress ratio in the triaxial test. The orientation of the delayed (plastic) strain rate is seen to be almost identical to the orientation of the instantaneous (plastic) strain rate. In other words, identical delayed and instantaneous potential surfaces can be used.

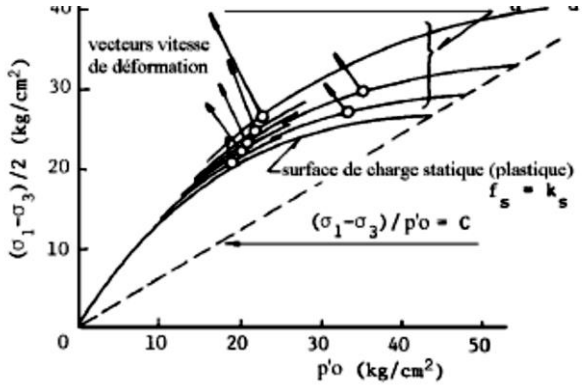

Figure 12: Yield vs viscous surface (after Lade and Liu (1998))

Thus, the same potential surface may be used for the direction of the viscoplastic strain rate as

$$G_{ij}{}^{vd} = \frac{\partial f^e}{\partial \sigma_{ij}} - \left(\frac{\partial f^e}{\partial \sigma_{kl}} n_{kl}\right) n_{ij}$$

where f^e is the state of stress surface which is homothetic to the yield surface for the deviatoric mechanism. It is defined by

$$f^e(\sigma_{ij}, R_e) = s_{II}\, h(\theta) - R_e(I_1 + 3\, T_r) = 0$$

The peak surface is defined by

$$f^r(\sigma_{ij}, R_m) = s_{II}\, h(\theta) - R_m(I_1 + 3\, T_r) = 0$$

The creep surface is defined by

$$f^v(\sigma_{ij}, R_v) = s_{II}\, h(\theta) - R_v(I_1 + 3\, T_r) = 0$$

The evolution of the creep surface is given by

$$R_v = R_e(1 - \frac{1}{\exp\left(A^v \frac{R_m}{R_e} {e_{II}}^{vd}\right)})$$

A^v is a parameter and ${e_{II}}^{vd}$ is the accumulated deviatoric viscoplastic strain defined by $\dot{e}_{II}^{vd} = \sqrt{\dot{e}_{ij}^{vd} \dot{e}_{ij}^{vd}}$

where $\dot{e}_{ij}^{vd}$ is the deviatoric viscoplastic strain rate. Fig. 13 schematically displays the different surfaces used in the model in the deviatoric and meridional plane, respectively.

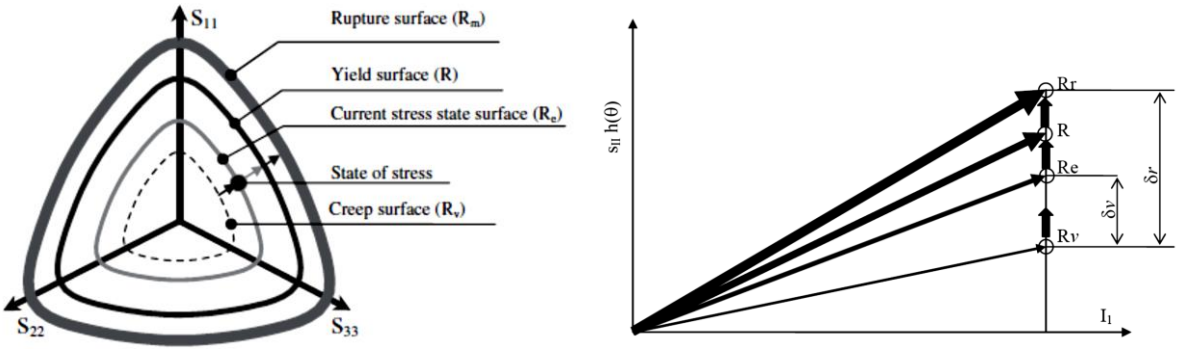

Figure 13: Viscous, stress, yield, and peak surface in deviatoric and meridional plane

2.4.7. Model parameters and performance

The parameters of the model elastoplastic mechanism can be identified by using classical laboratory tests. The procedure for calibrating these parameters is described in Maleki (1998). Identification of the model elastoplastic parameters requires:

- Two triaxial tests at different confining pressures
- One isotropic test to determine the parameters of the isotropic mechanism
- Isotropic unloading and triaxial reloading to specify the value of elastic parameters

Identification of the model viscoplastic parameters requires three creep tests at different deviatoric stress with measurement of the sample volume change (Purwodihardjo,

2004). In the identification procedure, some parameters are exactly determined from the experimental data, but the rest of the parameters can be evaluated only through fitting the calculated results to the experimental curves. Table 3 gives the list of the internal variables used in the model. Table 4 summarizes the parameters of the model along with their values used in the subsequent analyses.

Fig. 14 displays the performance of this model to reproduce the test results on the tunnel ground samples. Fig. 14 indicates a satisfactory agreement between the results of the model and the measured data. The numerical implementation of the model by the author (in color) is also validated by the complete coincidence with the results obtained in Purwodihardjo (2005) (barely visible in black) by using the finite difference method.

Fig. 15 shows the effect of the loading rate on the response of the ground material in the undrained conditions. The material peak and residual strength are seen to markedly decrease with reducing the deformation rate because of the increased development of the delayed plastic deformation.

STATE VARIABLES	SYMBOLE
Size of isotropic yield surface	Q
Size of deviatoric yield surface	R
Cohesion	T_r
Critical slope	R_c
Critical pressure	p_c
Equivalent shear strain	e_{II}
Size of viscous surface	R_v

Table 3: Model internal variables

MECHANISM	PARAMETER	SYMBOLE	VALUE
Elastic	Elastic bulk modulus	$K_0{}^e$ (MPa)	*139*
	Elastic shear modulus	G_0 (MPa)	*27*
	Non-linearity exponent	n	*0.7*
Isotropic plastic	Plastic modulus	$K_0{}^p$ (MPa)	*139*
Deviatoric plastic	Yield surface shape factor	γ	*0.3616*
	Peak critical slope	$R_{c_{peak}}$	*0.0784*
	Residual critical slope	$R_{c_{res}}$	*0.0784*
	Dilatancy parameter	β	*-0.005*
	Hardening parameter	A (kPa^{-1})	*2*
	Initial critical pressure	p_{c_0} (MPa)	*17*
	Critical line slope in e-ln(p') plane	c	*60*
	Dilatancy parameter	μ	*0.033*
	Low confinement parameter	m_0	*2.5*
	Peak cohesion parameter	$T_{r_{peak}}$ (MPa)	*11.825*
	Residual cohesion parameter	$T_{r_{res}}$ (MPa)	*7.112*
	Deviatoric strain at peak strength	$e_{II}{}^0$	*0.02*
	Deviatoric strain at residual strength	$e_{II}{}^f$	*0.065*
Viscous plastic	Hardening parameter	A^v	*125*
	Base viscosity	η_0 (sec)	10^8
	Tertiary viscosity parameter	k	*6*
	Delay function parameter	m_1	*0.3*
	Delay function parameter	m_2	*0*

Table 4: Model parameters and their values

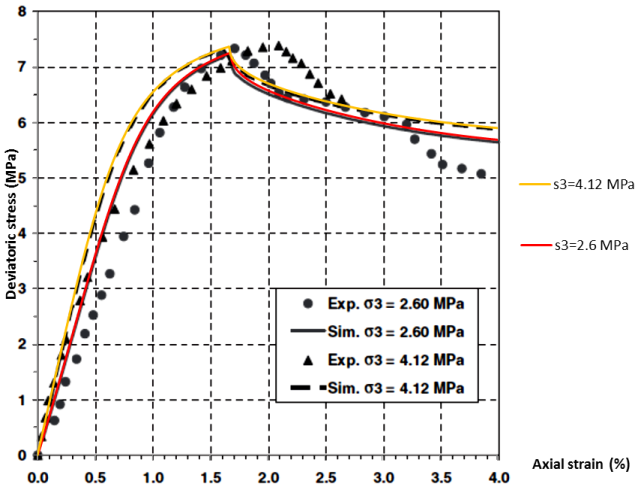

Figure 14: Numerical simulation of drained triaxial tests (ID test)

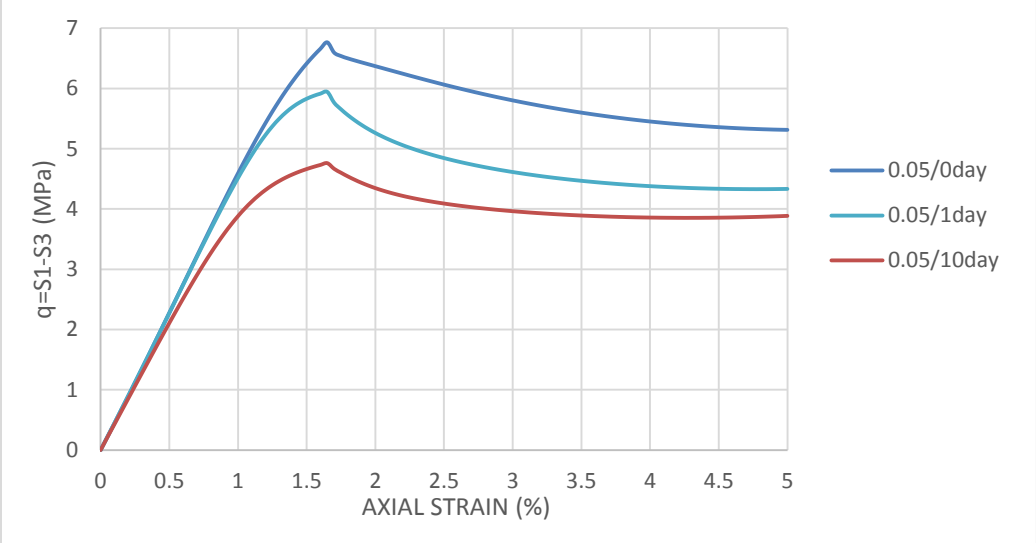

Figure 15: Undrained traiaxial test at different rates (s3=1.2 MPa)

Chapter 3: Jet-grouting Hardening Behavior

3.1. INTRODUCTION

Tunnel linings are critical in providing short term and long term stability and serviceability of tunnels. In short term, they prevent ground failure due to excavation, and in long term, they prevent ground delayed failure. They confine the ground deformation for the functionality of the tunnel as well as the adjacent surface or underground structures. In addition, they furnish the safety of the tunnel during its construction. In general, linings help stability of the tunnel in three following ways:

- Bearing: providing tunnel stability through direct bearing pressure against the excavated ground, the precarious rock blocks, etc.
- Confinement: providing tunnel stability through increasing confining pressure and thus ground shear capacity
- Reinforcement: providing tunnel stability through directly strengthening the ground

Cement-based linings are frequently used in tunnels. In addition to financial advantages, cast-in-place (CIP) linings can fit irregular tunnel profiles, and thus provide immediate support for the tunnel. They are also more resistant to fire. Hence, the use of these linings is well-established in the tunneling industry.

Jet-grouting is a rather modern method to enhance the properties of the ground by injecting mortar under high pressure. The pressurized mortar annihilates the in situ soil structure. Therefore, the product is a stress-free mixture of soil and mortar.

Designed to prevent tunnel deformation ahead of the face, jet-grouting is typically penetrates a tunnel diameter ahead of the face, where the tunnel deformation initiates. Further, the tunnel excavation is resumed right after jet-grouting operation. Consequently, the jet-grouting umbrella is loaded when it is hardening. This issue requires the consideration of the jet-grouting hardening in the analysis of the tunnel.

The mathematical description of the hardening cemented materials, however, is still challenging for constitutive modelers (Ulm and Coussy, 1996). The simplest representation of the hardening behavior of the jet-grouting is elastic with time-dependent stiffness. This modeling assumption is typically used in approximate qualitative studies. In these models, the deformation modulus is updated over time. Within the first 24 hours, the stiffness and strength can be defined by

$$E(t) = 11000\sqrt[3]{f_c(t)} \quad ; \quad f_c(t) = \frac{t}{4.76 + 0.83\,t} f_c(28)$$

where E(t) is the Young's modulus at age t days, and $f_c(t)$ is the uniaxial compressive strength in MPa at age t days. In order to account for the creep deformation caused by permanent loads, the proposed elastic modulus is modified by ascaling factor (about three).

Einstein et al. (1991) proposed a relationship between the deformation modulus of shotcrete and its resistance to compression

$$E(t) = \frac{1306\, f_c(t)^{1.92}}{1 + 0.18\ f_c(t)^{2.283}}$$

In this approach, the evolution of the deformation modulus is directly determined by the concrete compressive strength. Sezaki et al. (1992) accounted for the hardening by updating the Young's modulus and Poisson's ratio as

$$E(t) = E(\infty)\,(1 - \exp(-\beta t)) \qquad \vartheta(t) = \vartheta(\infty) + 0.32\exp(-\alpha t)$$

In Chang and Stille (1993), the evolution of the Young's modulus and compressive strength is defined by a single function with different parameters as

$$F(t) = F(\infty)\ exp(\frac{c}{t^{0.7}})$$

where F(t) represents the Young's modulus or the uniaxial compressive strength at age t days. Parameter c is different for these quantities. In order to have more accuracy in the calculation of the jet-grouting response, the following plastic model may be used.

3.2. ELEMENT EMBEDMENT

This section describes a numerical method to represent the hardening of the jet-grouting in a finite element model. The hardening of cementitious linings is typically incorporated in the time-independent description of the lining mechanical behavior by considering the time variation of the material parameters (e.g., Cantieni and Anagnostou, 2011; Graziani et al., 2005; Oreste, 2003; Pottler, 1990).

The development of jet-grouting unconfined compressive strength (UCS) is selected from the results of experiments made by Coulter and Martin (2006). By assuming an exponential function for the growth of jet-grouting UCS with time and fitting the data, we obtain the variation of the jet-grouting UCS with time (Fig. 16):

$$UCS(t) = UCS_{ul} \cdot (1 - e^{-k_{ucs} \cdot t}) \quad ; \quad UCS_{ul} = 8\,MPa \quad ; \quad k_{ucs} = 0.036 \left(\frac{1}{\text{day}}\right)$$

where, and *t* is the jet-grouting age in days. In order to account for the jet-grouting stiffness growth with time, jet-grouting Young's modulus (E) is estimated by using the ACI relation between E and UCS:

$E=57000\sqrt{UCS}$; E and UCS in psi

By fitting an exponential curve to the values of E calculated for the UCS values in the data, we obtain the variation of jet-grouting Young's modulus (E) with time:

$$E(t) = E_{ul}\,(1 - e^{-k_s \cdot t}) \quad ; \quad E_{ul} = 13.5\,GPa \quad ; \quad k_s = 0.054\,(\frac{1}{day})$$

In the numerical model, the jet-grouting is assumed to behave according to Mohr-Coulomb model. Thus, the variation of jet-grouting cohesion is obtained from the UCS variation by

$$c(t) = \frac{UCS(t)}{2\sqrt{N}}; \qquad N = \frac{1 + sin\varphi}{1 - sin\varphi}; \quad \varphi = 20^o$$

Here, the internal friction angle is kept constant throughout the jet-grouting hardening.

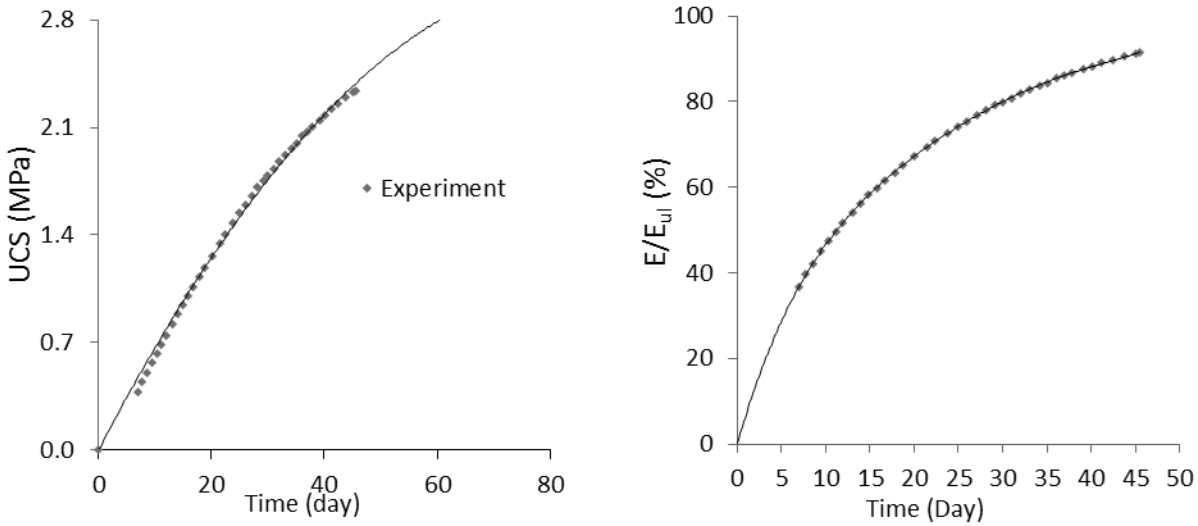

Figure 16: Evolution of the jet-grouting strength (c) and stiffness (E) with time

In order to incorporate the hardening of the jet-grouting in the finite element model, the notion of successive embedding of jet-grouting elements is utilized. The continuous development of the jet-grout stiffness and strength is discretized into a number of stiffness and strength increments (Fig. 17). Then, a number of parts with the same geometry as the jet-grouted zone is defined, and each increment of mechanical properties (E and c, here) is assigned to each of these parts. Each part will be embedded in the jet-grouted zone at the due time within the period of the jet-grouting hardening (Fig. 18). A similar concept was used by Cantieni and Anagnostou (2011) to model the time-dependent hardening of shotcrete. Successive embedding of the fictitious jet-grout elements provides for a realistic hardening mechanical behavior of the jet-grout because the increased stiffness and strength will be effective only for the superimposed loads. This implies an inelastic strain, commonly referred to as aging strain, which becomes evident after unloading (Boldini et al., 2005). On the contrary, using a single jet-grout layer and increasing its stiffness would unrealistically apply the new stiffness to the entire (current and superimposed) load on the

jet-grout. The proposed approach can be used without restrictions, i.e. for jet-grouting of any geometry.

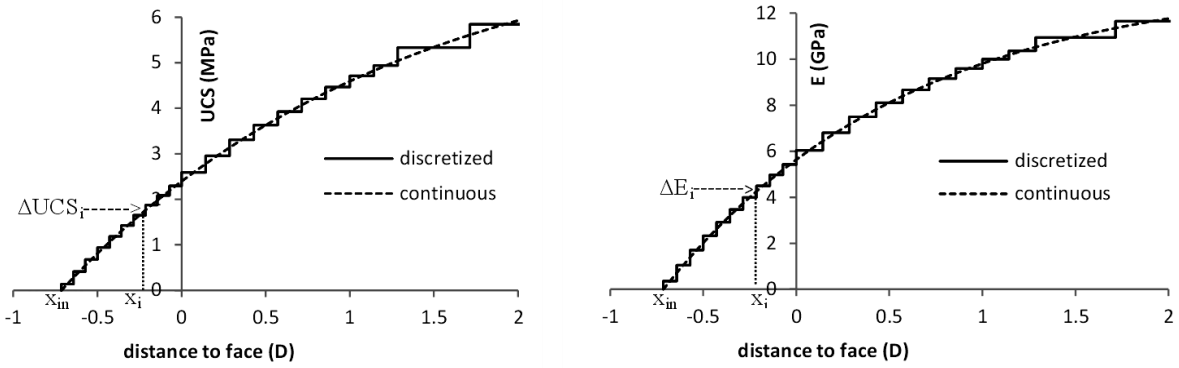

Figure 17: Discretization of jet-grout hardening: (a) strength; (b) stiffness

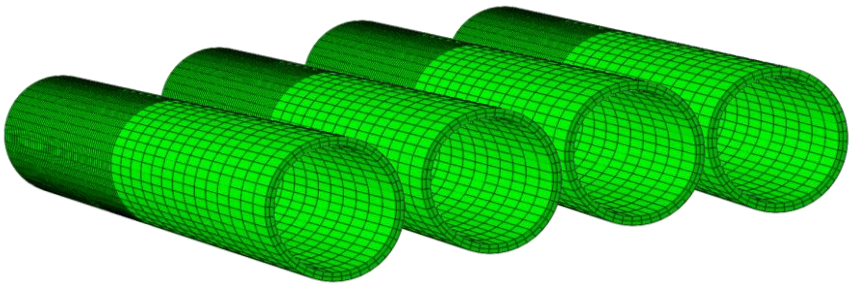

ID	E (MPa)	c (MPa)
1	1600	0.228
2	355	0.049
3	500	0.078
4	474	0.075
5	557	0.083
6	528	0.080
7	621	0.103
8	621	0.090
9	588	0.086
10	656	0.093

Figure 18: Geometry and properties of jet-grouting duplicates

3.3. CHEMOPLASTIC MODEL

In order to account for the hardening of the jet-grouting around the tunnel, a chemoplastic model developed by Hellmich et al. (1999) for shotcrete is used. This model is based on associated Dracker-Prager plasticity with isotropic hardening. The isotropic hardening depends on the accumulative shear plastic deformation. The hardening of the jet-grouting also depends on another hardening parameter which evolves with the age of the jet-grouting. As such, the size of the yield surface increases with both the plastic deformation and the material age. The elastic modulus of the jet-grouting also evolves with the age hardening parameter. In this model, the chemical hardening of the jet-grouting is not affected by the mechanical process. In order to use the model in conjunction with finite element software ABAQUS, it will be numerically integrated in a FORTRAN code.

The material parameters have been calibrated for the jet-grouting experimental results as given in Coulter and Martin (2006). By assuming an identical exponential function for the growth of the jet-grouting strength and stiffness with time, we obtain the following function for the variation of these quantities with time (Fig. 19):

$$\frac{UCS(t)}{UCS_{ul}} = \frac{E(t)}{E_{ul}} = 1 - e^{-k \cdot t}$$

where UCS_{ul}, E_{ul} , k, and t represent the ultimate strength, ultimate stiffness, growth rate, and the jet-grouting age in days.

In the chemoplastic model, parameter ξ stands for the ageing of the jet-grouting. This parameter grows over time according to the strength variation. As such, the strength and stiffness can be expressed by a linear function f(ξ).

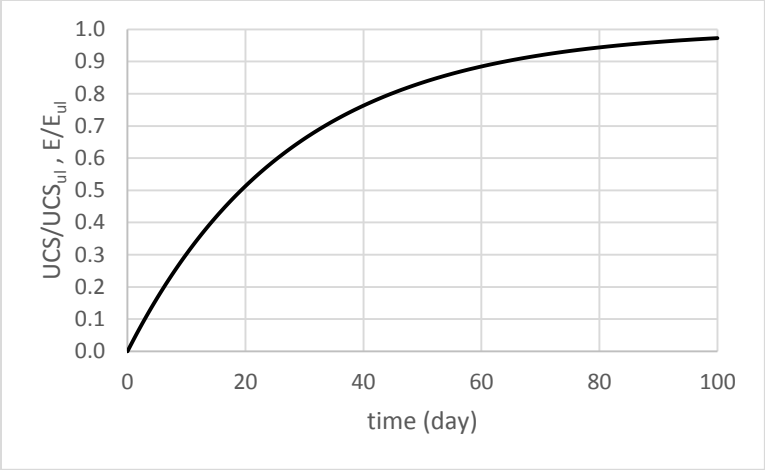

Figure 19: Ageing of the jet-grouting strength and stiffness

The yield function in this model is defined by

$$F(\sigma, p, \xi) = \sigma_{eq} + \alpha . I_1 - R(p, \xi)$$

where σ_{eq} and I_1 designate the equivalent shear stress and the confinement stress, respectively. Parameter α represents the slope of the yield locus in the meridional stress plane. Internal variable p is the accumulative equivalent shear strain defined by

$$dp = \sqrt{\frac{2}{3} de^p : de^p}$$

where de^p is the deviatoric part of the plastic strain.

The function R(p, ξ) represents the hardening of the material due to ageing and strain hardening. This function is defined as a quadratic function in p by

$$R(p) = \frac{\alpha\, \kappa}{\kappa - 1} [f(\xi) . \omega + f(\xi)(1 - \omega) \left[1 - \left(\frac{p}{p_{ult}} - 1\right)^2\right]]$$

In this function, parameter κ designates the ratio between the uniaxial and biaxial strength. Parameter ω designates the ratio between the initial and ultimate strength at p_{ult}, which is the value of p at the peak strength.

Fig. 20 shows the effect of age hardening on the uniaxial compressive response of the material. In loading at higher rates, the jet-grouting strength is developed less, and thus the jet-grouting performs weaker.

The material parameters given in Table 5 are used in the subsequent analyses. They have been calibrated with the data given in Coulter and Martin (2006) for jet-grouting.

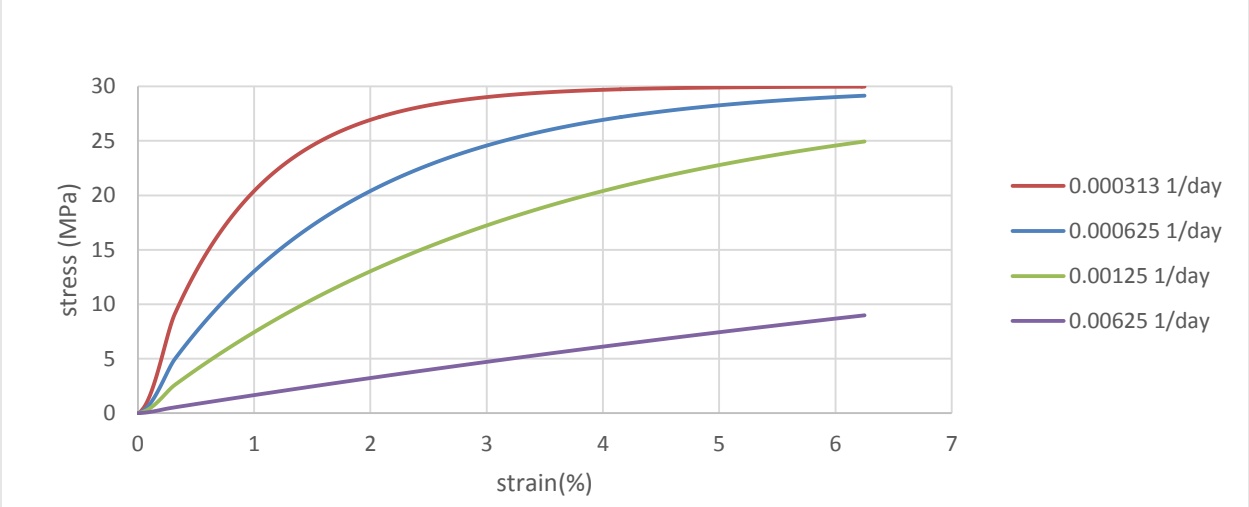

Figure 20: Rate-dependent strength as a result of age hardening

PARAMETER	SYMBOLE	JET-GROUTING	INVERT
Ultimate Young's modulus	E_{ult} (GPa)	13.5	27.0
Ultimate uniaxial compressive strength	UCS_{ult} (MPa)	8.0	32.0
Growth rate	k (1/day)	0.036	0.036
Biaxial/Uniaxial strength ratio	κ	1.16	1.16
Initial/ultimate strength	ω	0.25	0.25

Table 5: Properties of jet-grouting and concrete invert

THREE-DIMENSIONAL ANALYSIS

Chapter 4: Nonviscous Ground

This section studies the response of the tunnel in ground with time-independent behavior. This study is intended to obtain insight on the behavior of the tunnel by excluding the complexity of time-dependent mechanisms. Furthermore, the accuracy of the numerical model can be validated by comparing the model results with the available analytical solutions.

The frequent use of finite element analyses in tunneling relates to the complex characteristics of the tunneling problems. In tunnels, the ground-structure interaction strongly depends on the details of the excavation and construction methods and on the mechanical behavior of the ground and the support system. Analytical solutions cannot account for these factors. On the other hand, numerical analyses can treat these details with a degree of accuracy limited only to the computational power. Various excavation technologies have been analyzed numerically such as the use of shotcrete, compressed air, mechanical shields, soil freezing, ground jet-grouting (Pichler et al., 2003; Gioda and Swoboda, 1999).

Numerical analyses can also take consideration of geometrical complexities including the shape of the tunnel, the presence of discontinuities in the rock mass, the presence of non-homogenous or non-isotropic layers, etc. The numerical modeling can also treat tunnels in ground with non-homogeneous initial stress field, with non-linear, time-dependent or coupled multi-phase behavior, or with existing structures.

The analysis of the tunnel excavation and the support installation calls for three-dimensional finite element modeling. Two-dimensional models fail to provide information on the longitudinal variation of the tunnel response. This issue becomes particularly

important in the evaluation of longitudinal support measures such as jet-grouting or face dowels.

4.1. NO SUPPORT

In the simulations hereafter, the ground condition is similar to the clay ground condition in Cassia 2 tunnel constructed in Italy using the ADECO method (Tonon, 2011). All analyses are carried out assuming the ground and the supports as continuous media. The ground behavior is also assumed to be *rate-independent*. The tunnel is assumed to be situated in an infinite ground with an isotropic in situ stress. Given the low permeability of the clay ground, the tunnel is also assumed to be excavated in undrained conditions. Therefore, a total stress analysis is first carried out, using the elastic-perfect plastic model with the Tresca yield criterion (Mohr-Coulomb with a zero frictional angle). Then, an effective stress analysis is carried out using Cam-Clay model. In order to compare the results of the two models, the parameters of the models are calibrated with the same data: the undrained shear strength c_u, the undrained Young's modulus E_u=200 MPa, and the isotropic in situ stress p_0=1 MPa.

This part deals with the full-face excavation of a tunnel with no support and pre-confinement. For the sake of comparison of the model results with available analytical results, a circular tunnel is first analyzed. The tunnel radius R is 7 m (D=14 m) and the tunnel length is 200 m. In order, to simulate the infinite boundary conditions for the ground, a block of 100 m in depth and width is selected for the ground (Fig. 21).

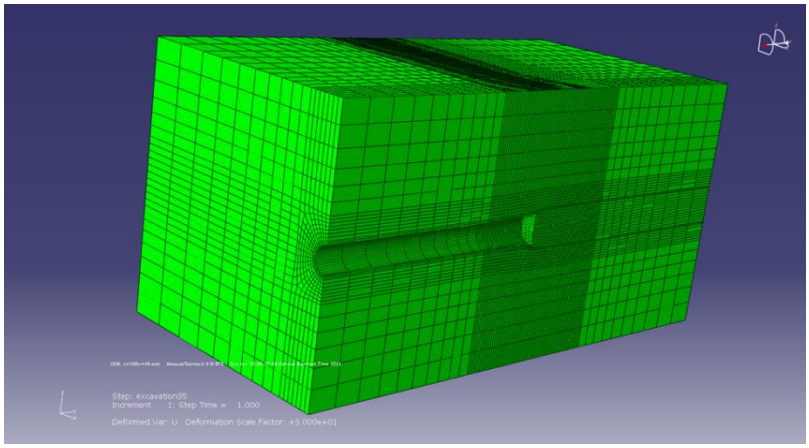

Figure 21: Model geometry and mesh

The tunnel is assumed to be excavated under undrained conditions. Accordingly, the ground is analyzed in total stress using a perfect-plastic model with Tresca yield criterion (Mohr-Coulomb with phi=0^o). The incompressibility of the ground response is accounted for by taking a Poisson's ratio very close to 0.5.

As opposed to fully constrained boundaries parallel to the tunnel axis, only one boundary surface in each direction is constrained and the other boundary surface is loaded with the in situ stress.

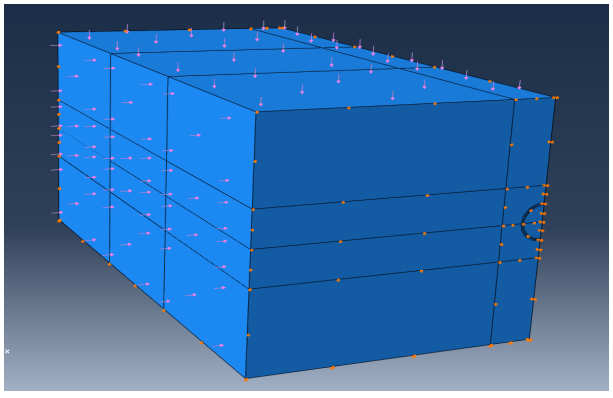

Figure 22: Far field boundary conditions

Given the incompressibility of the ground behavior, this setting for the boundary conditions prevents volume locking of the model (Fig. 22). In Fig. 23, the tunnel convergence u obtained from the model is compared to the analytical result for a range of Poisson's ratio ϑ up to 0.5 given by

$$\frac{u}{R} = \frac{(1+\vartheta)c_u}{E_u}\left\{e^{\left(\frac{p_0}{c_u}-1\right)} + (1-2\vartheta)\left(e^{\left(\frac{p_0}{c_u}-1\right)} - \frac{p_0}{c_u}\right)\right\}$$

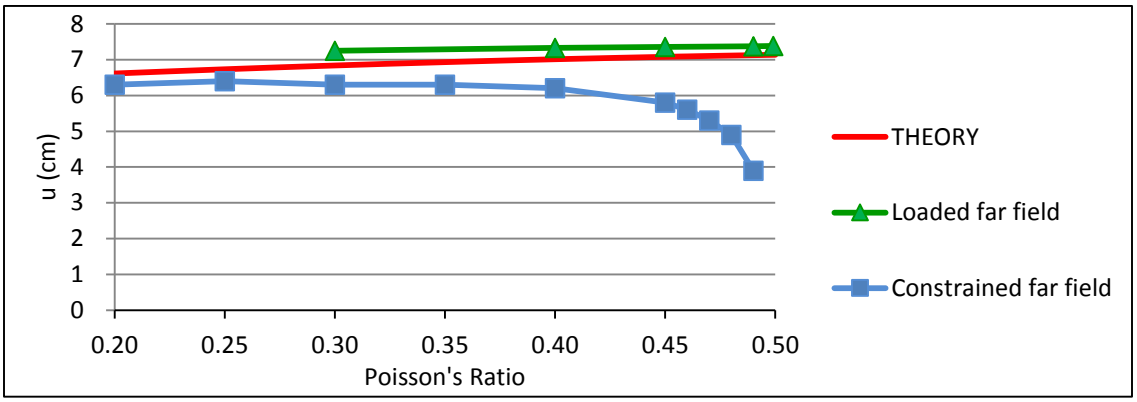

Figure 23: Analytical vs. numerical tunnel convergence

Fig. 23 clearly verifies the model results in terms of the tunnel convergence. It also shows the effect of volume locking in case of adopting fully constrained displacement boundary conditions for the ground block.

The convergence curve of the ground for different values of undrained shear strength is obtained by carrying out a two-dimensional plane strain analysis of the tunnel cross-section (Fig. 24).

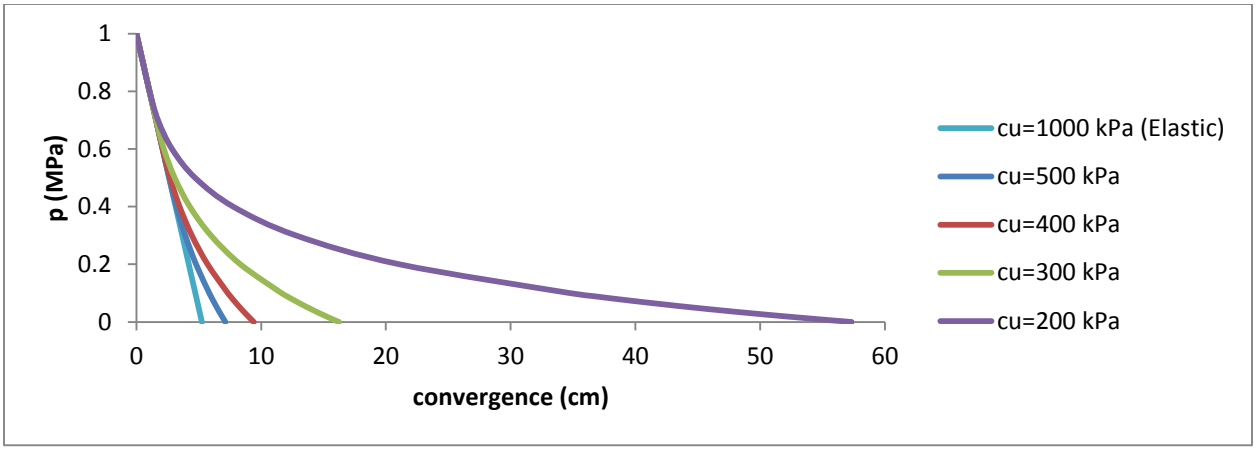

Figure 24: Ground convergence curve

Fig. 25 displays the variation of the tunnel ultimate convergence with the ground strength represented by the undrained cohesion c_u. It also shows that the tunnel convergence dramatically increases for the ground strength ratios below 0.2. This result agrees with the margin given by Hoek (2001) for squeezing ground conditions.

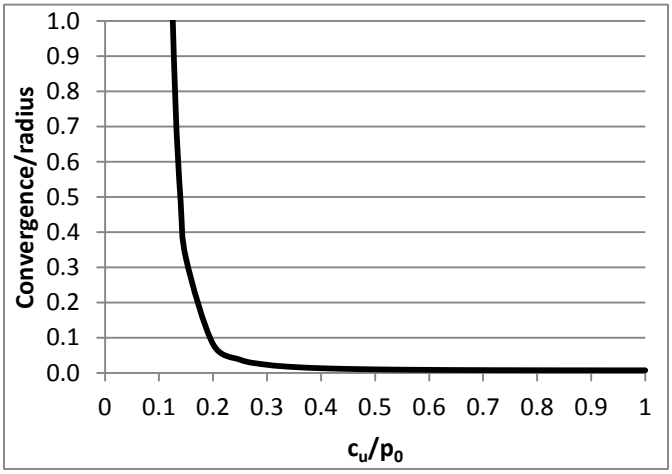

Figure 25: Tunnel convergence vs. ground relative strength

Other results of the tunnel with no pre-confinement will be shown along with the results of the pre-confined tunnel.

4.2. SUB-HORIZONTAL JET-GROUTING

Having validated the model with no pre-confinement against analytical results, the tunnel pre-confined with jet-grouting umbrella is simulated. In the simulations, hardening of the jet-grouting is considered by using the element embedment method described in chapter 2.

In order to interpret the responses of the ground and jet-grouting umbrella to excavation, the stress paths at two representing points, i.e. at the ground next to the jet-grouting umbrella and at the center of the tunnel face, are explored during the excavation of the tunnel (Fig. 26). The stress paths may also be used to evaluate the effect of jet-grouting on the deformation and stability of the tunnel.

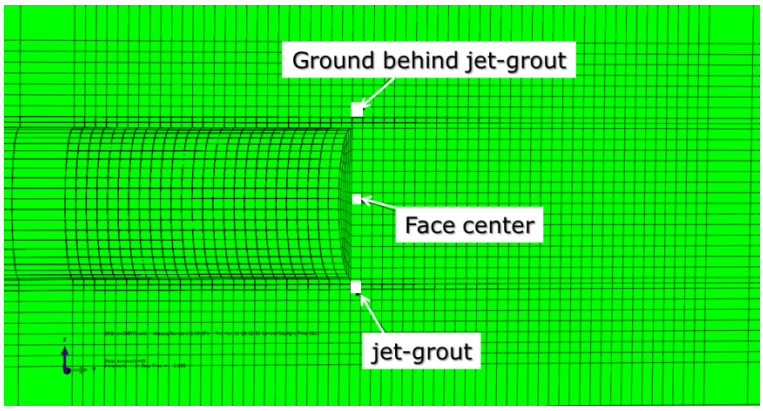

Figure 26: Location of points for stress paths

Fig. 27-37 show the variation of the maximum shear stress and mean pressure in ground, and circumferential and radial stress in the jet-grouting umbrella.

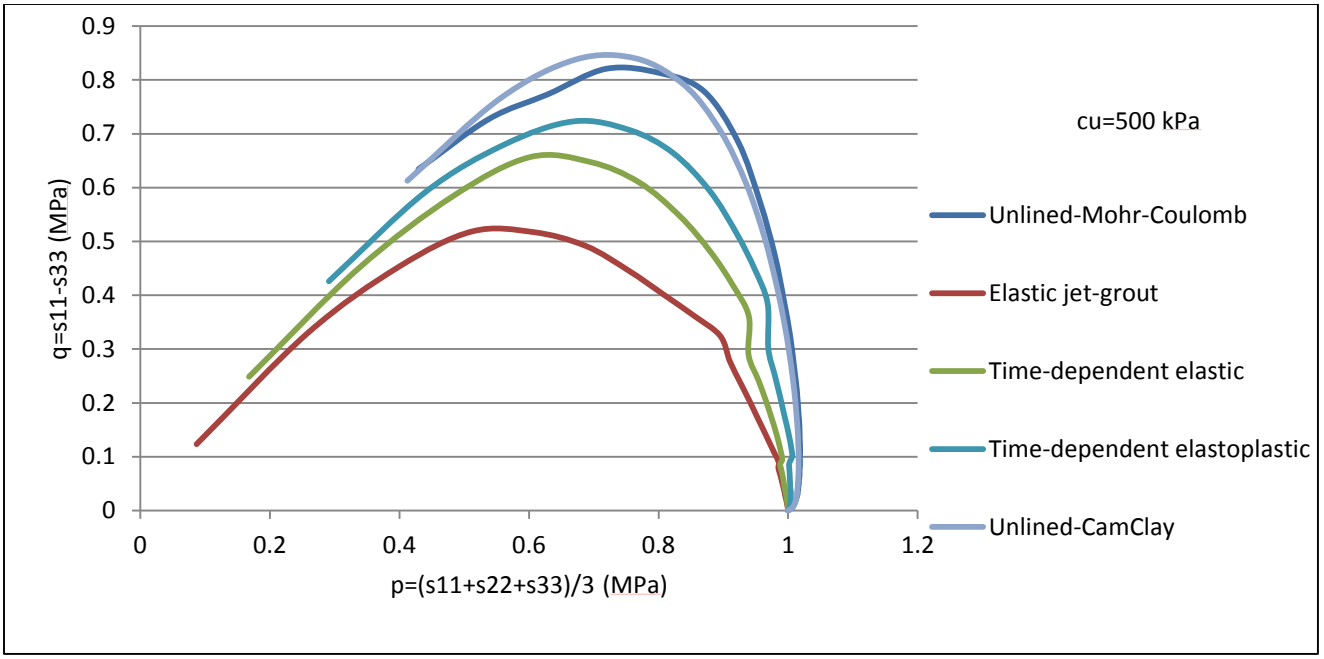

Figure 27: Stress trajectories in core

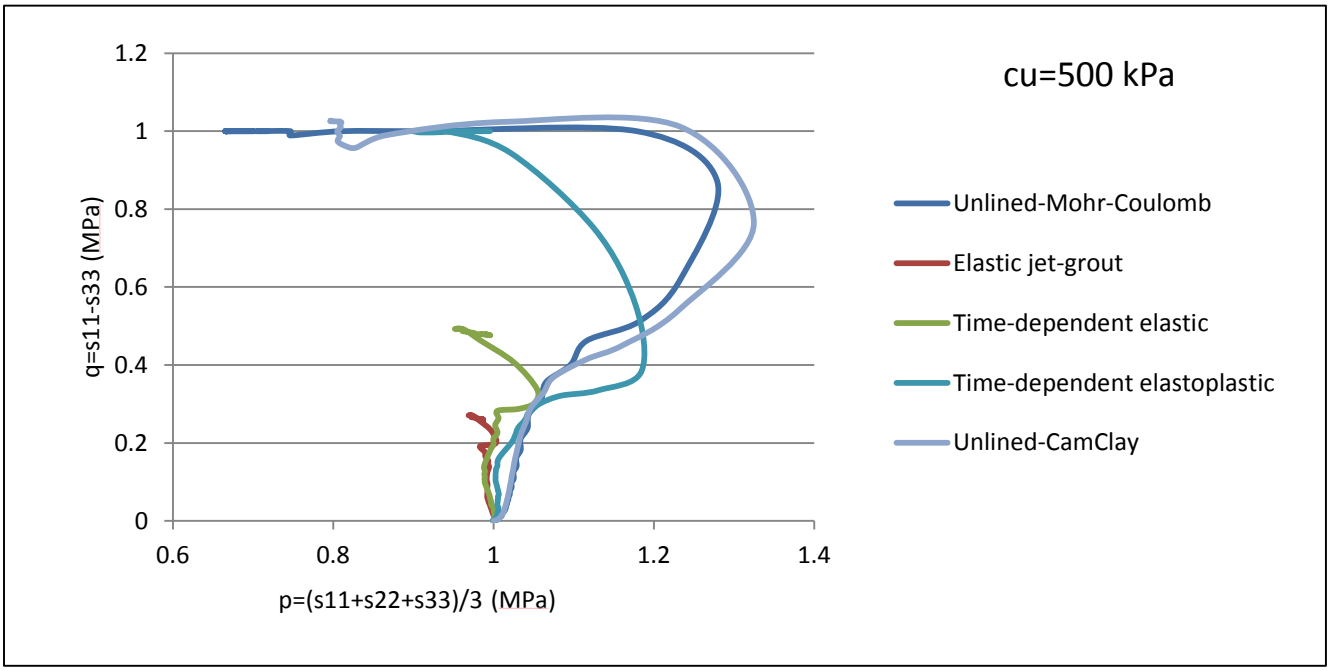

Figure 28: Stress trajectories at cavity

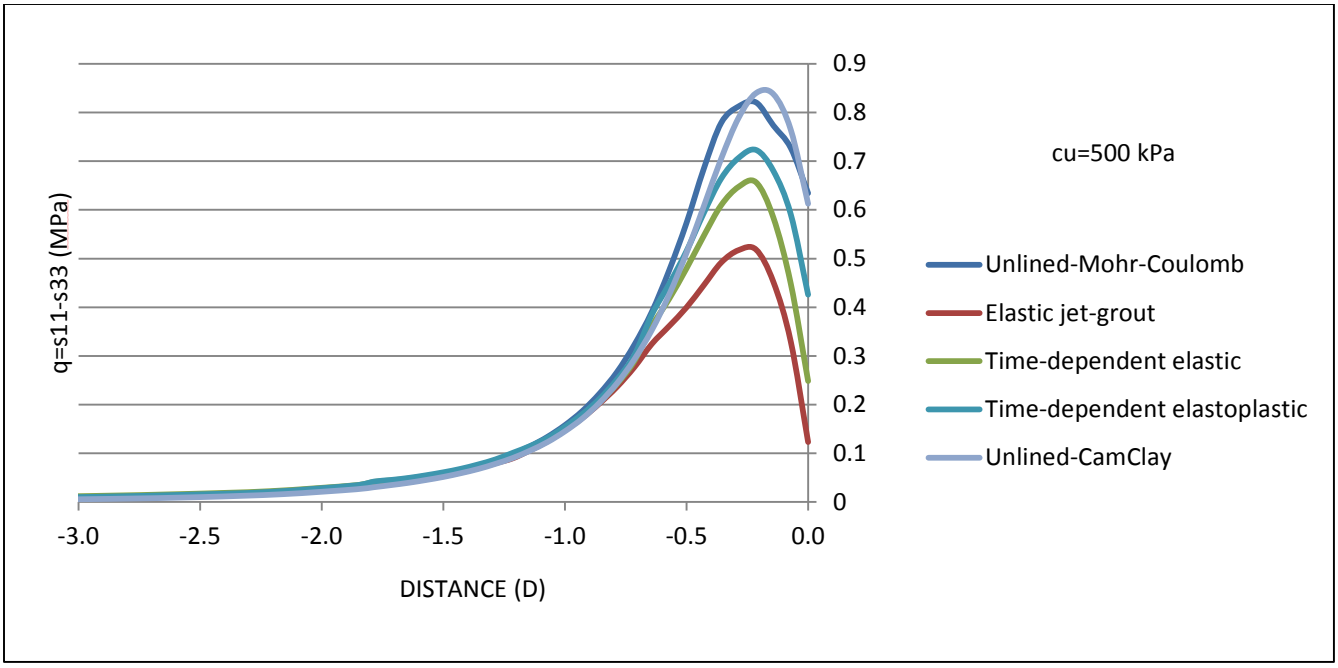

Figure 29: Shear stress in core

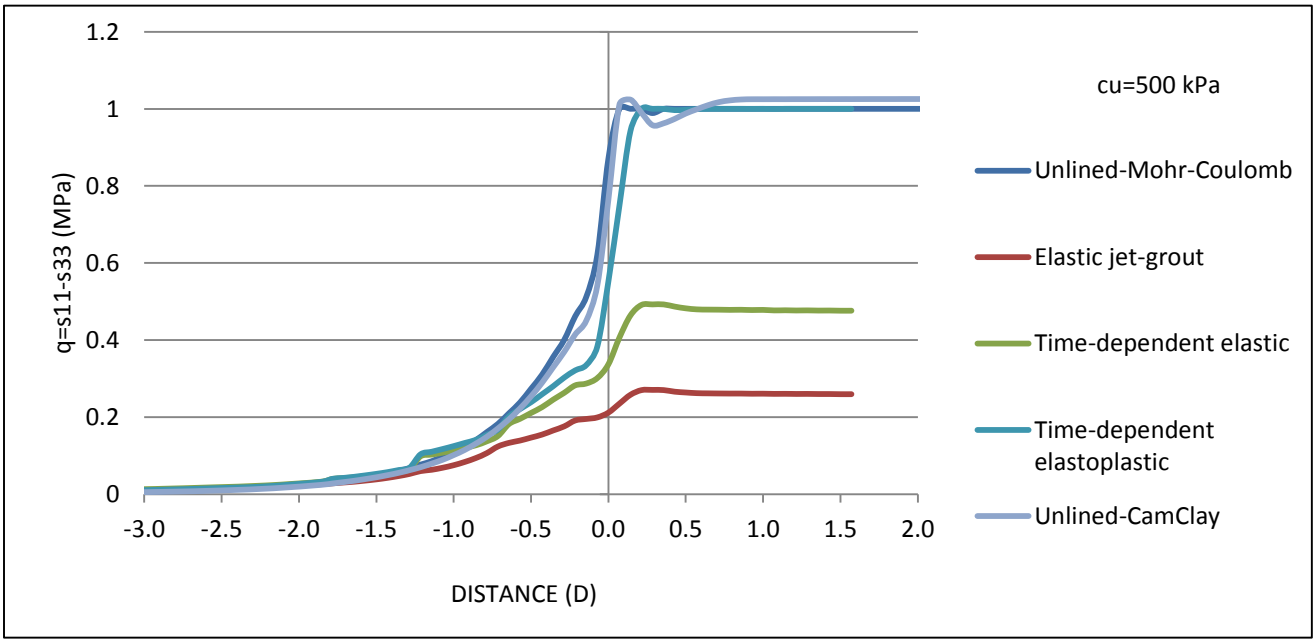

Figure 30: Shear stress at cavity

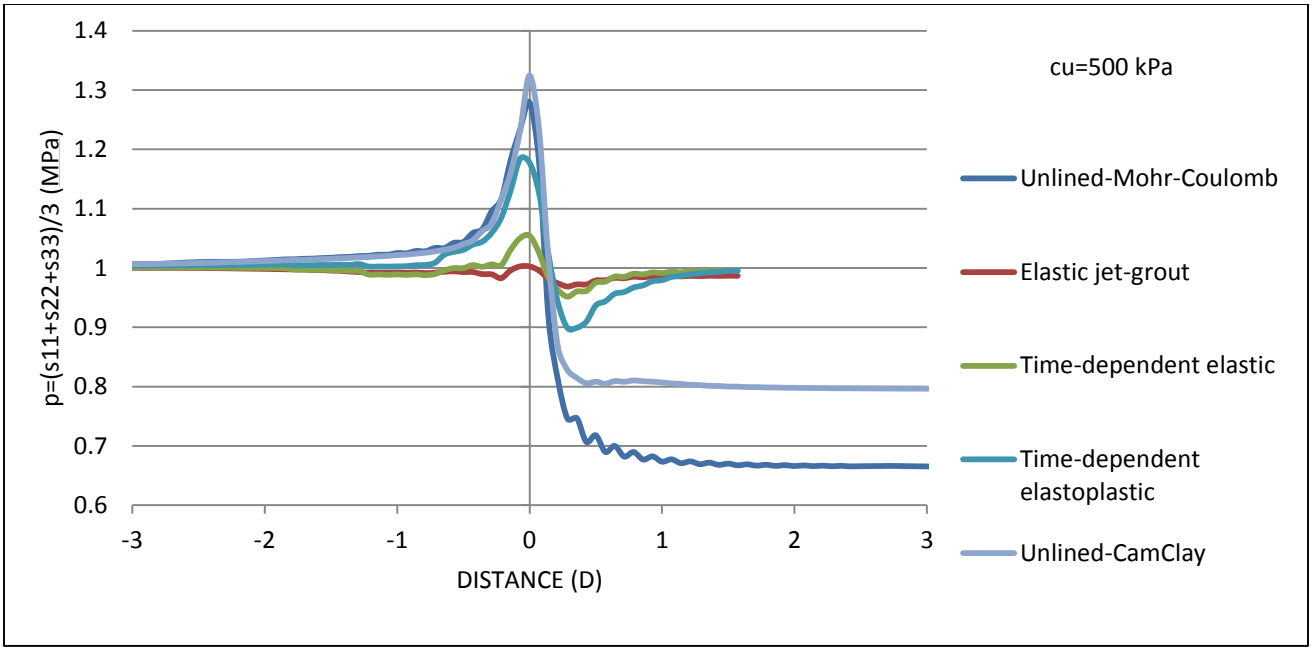

Figure 31: Mean pressure at cavity

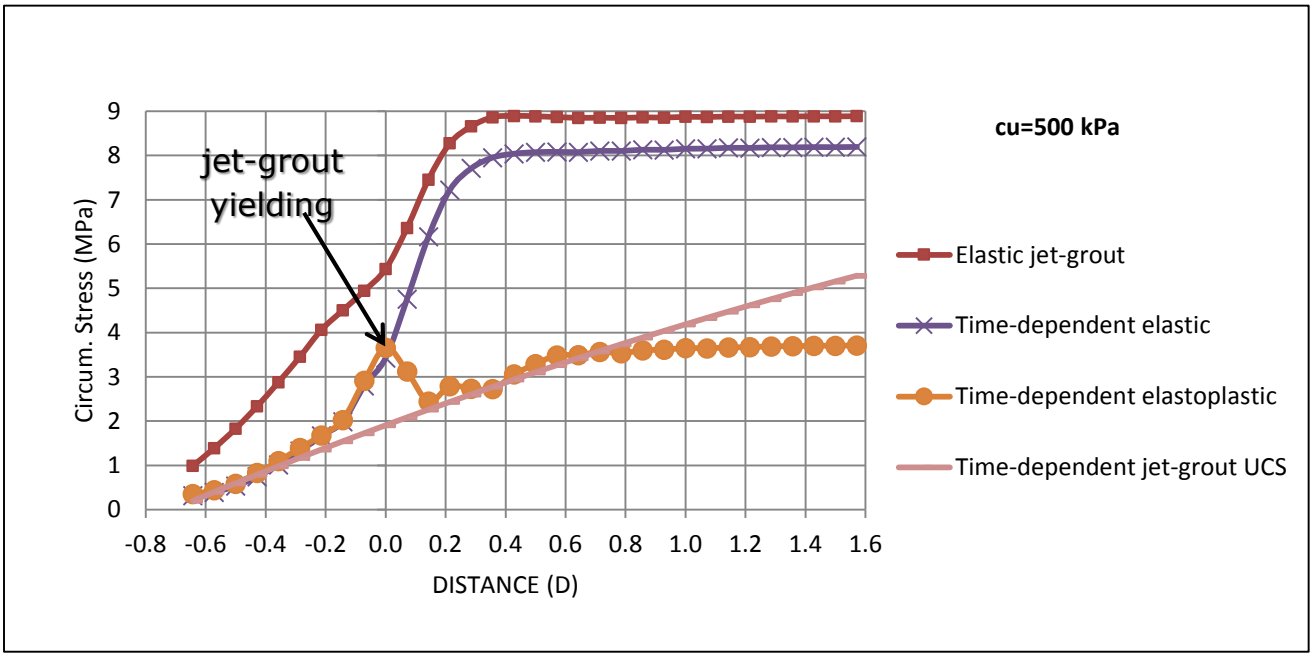

Figure 32: Hoop stress in jet-grouting

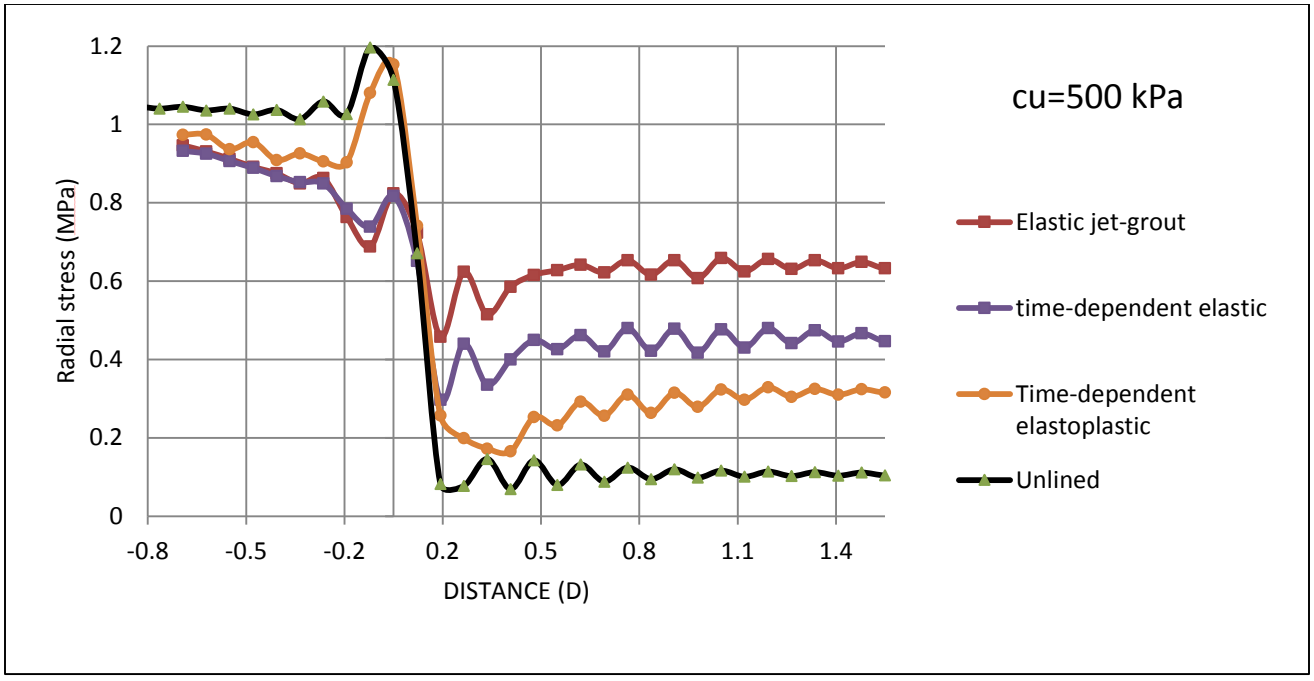

Figure 33: Radial stress in jet-grouting

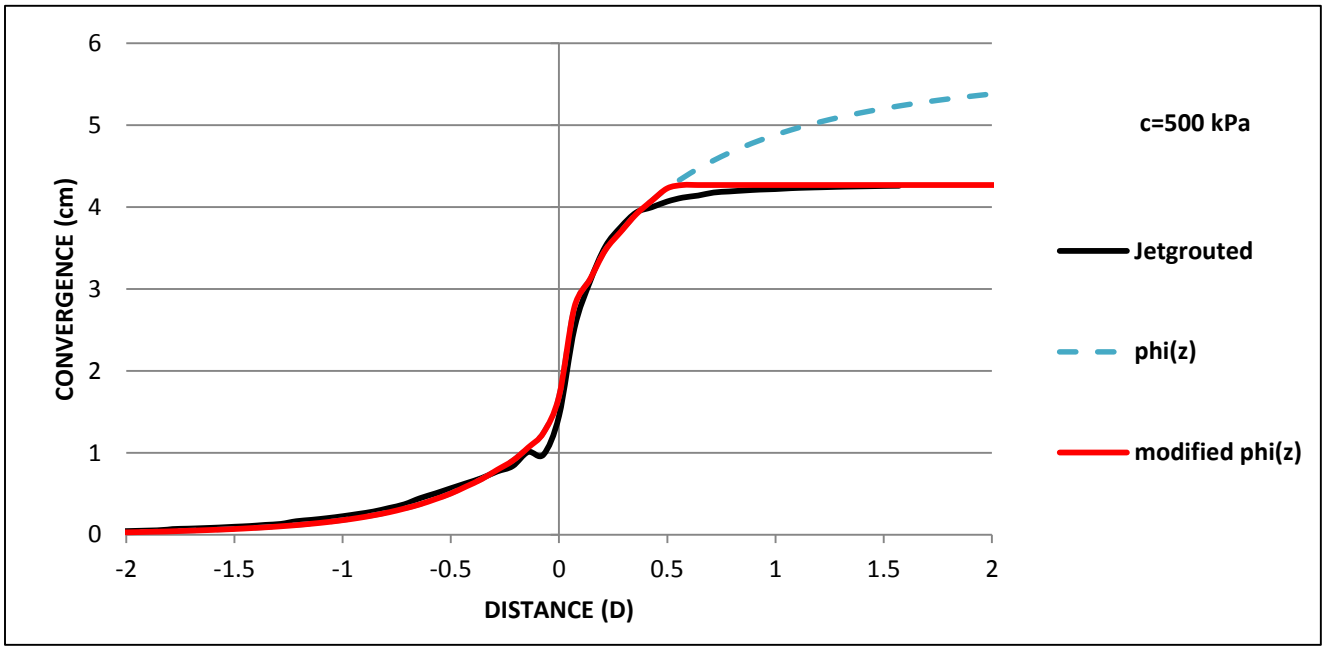

Figure 34: Convergence along tunnel

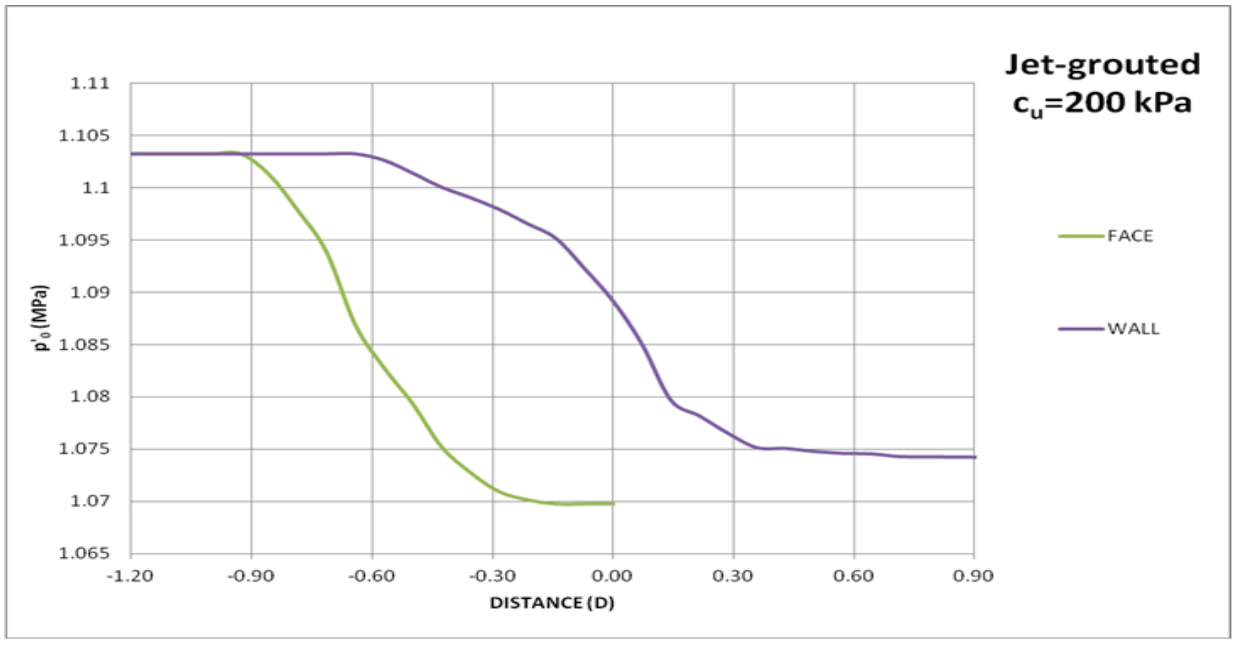

Figure 35: Yielding at face and wall indicated by change in the size of yield locus

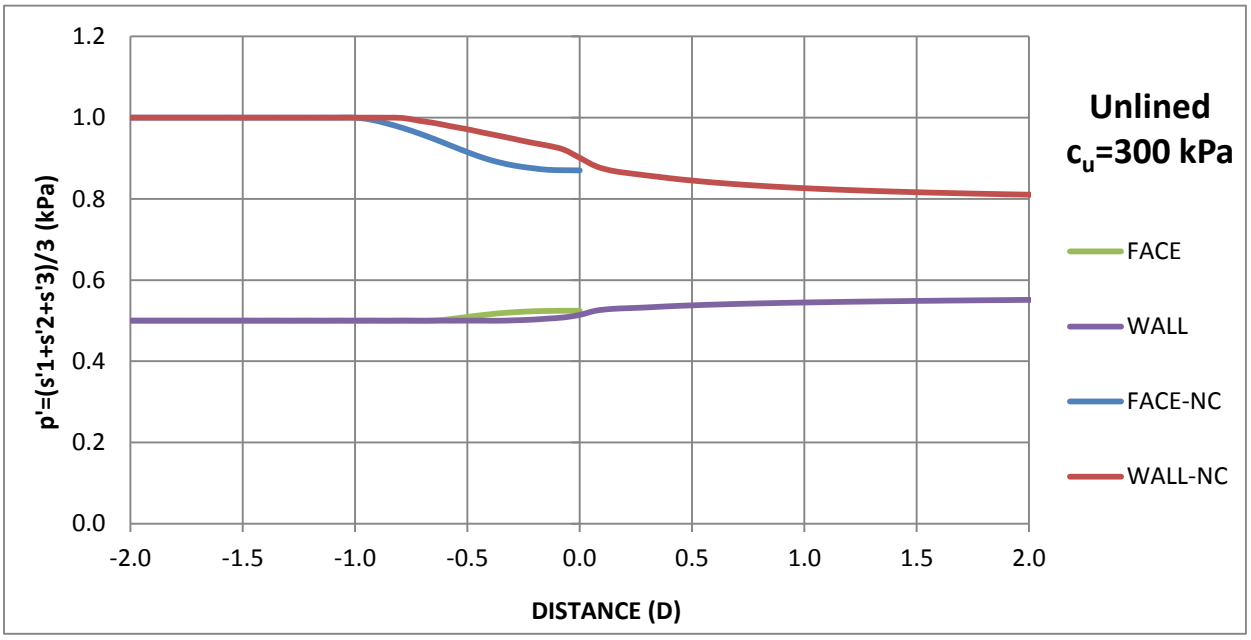

Figure 36: Effective mean stress in high vs. low OC clay (identical undrained strength and stiffness)

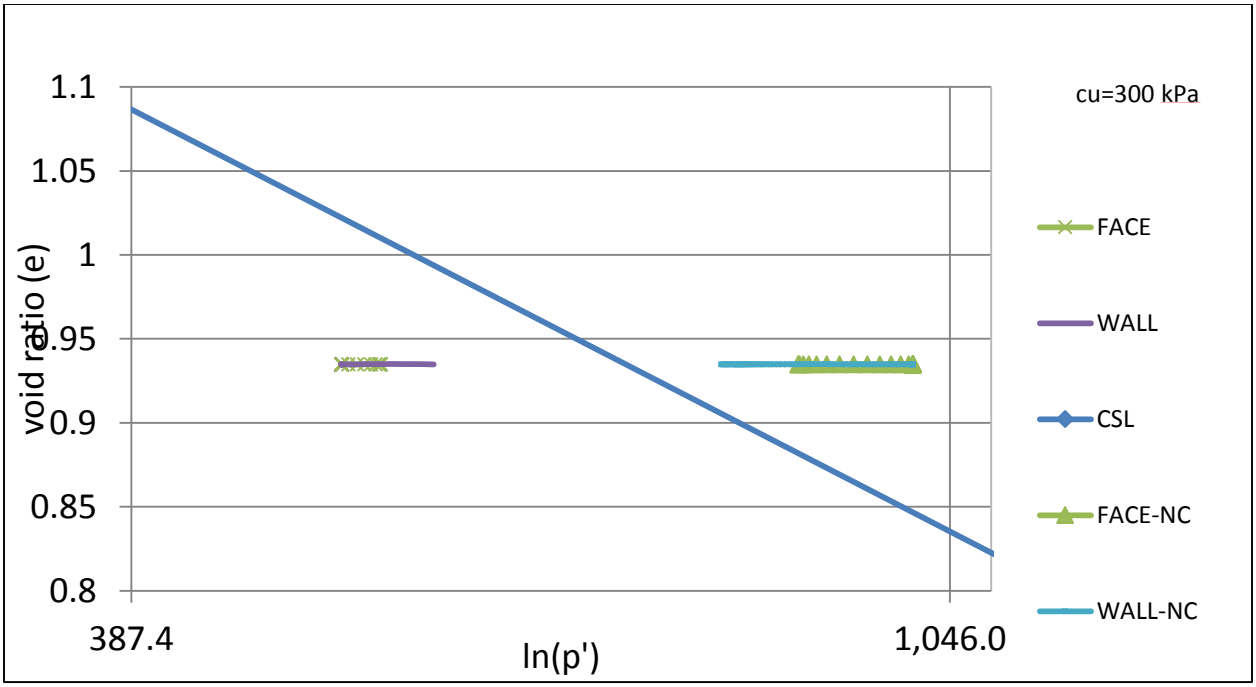

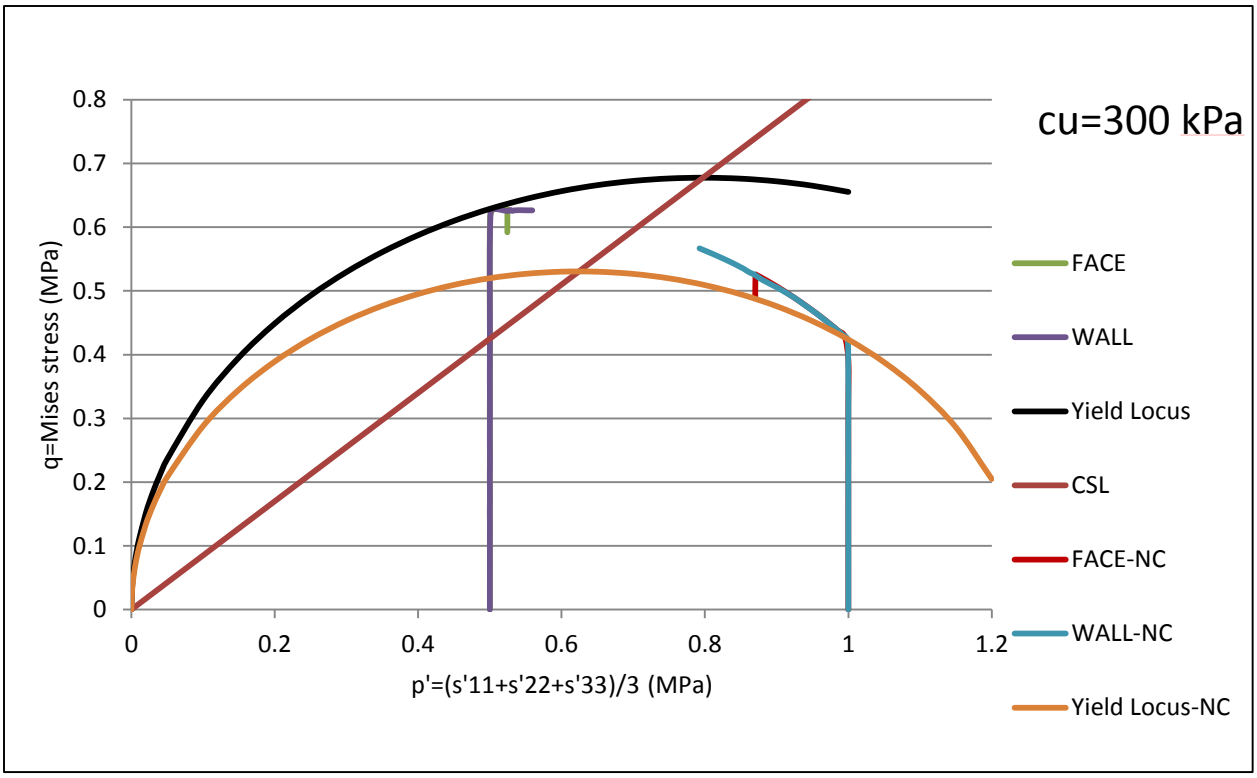

Figure 37: High vs. low OC clay with identical c_u and E_u

The stress variations for unlined and jet-grouted tunnel are in good agreement. Furthermore, the following conclusions can be observed in the figures shown:

Core

1) Jet-grouting causes a reduction of 20% in load on core.
2) Loading on core starts about 1.5D ahead of face.
3) Maximum shear stress occurs at 1/3D ahead of face.
4) Jet-grouting *negligibly* reduces confinement.
5) Decrease in confinement starts 1D ahead of face.
6) Decrease in effective confinement in NC ground: less dowel-ground bond strength
7) Increase in effective confinement in OC ground: elevated dowel-ground bond strength

Cavity

1) Stronger jet-grouting umbrella => Less decrease in confinement => Less shear load on cavity.
2) Yielding starts 1/4D behind the face => Cavity supports should be added within this distance.
3) Confinement varies within 2D across the face.

Jet-grouting

1) Yielding starts 1/5D behind the face => Cavity support at face to compensate loss of core confinement.

4.3. FACE DOWELING

Bolting is a widely used technique in the construction of tunnels. Bolts are usually embedded either radially in the tunnel wall or horizontally into the face (fiberglass dowels). Wall bolting influences the convergence while face bolting influences the pre-convergence.

The density and installation rate are most influential in the performance of rock bolts to control the tunnel convergence.

In face doweling, the embedded dowels are bonded to the ground over their entire length by means of a resin or cement sealant (Fig. 38). In order to provide adhesion between the dowel and the sealant, jagged rods or frictional bolts are used. Unlike steel rods, fiberglass dowels allow for the excavation of the reinforced ground. These rods are embedded in the ground using high pressure injections, chemical or concrete sealants. The length of these bolts can reach up to 50 m and the maximum tensile strength can reach up to 1800 kN. They are typically used in reinforcing the tunnel excavation face. The overburden typically controls the density of face doweling. The length of the dowels is also controlled by extrusion of the face. Stabilizing the face is central in the full-face excavation method suggested by ADECO-RS (Lunardi, 2000).

Figure 38: Face doweling

Different approaches are used to represent rock bolts in tunnel analyses. In semi-empirical methods, a potential failure surface and limit state conditions are usually assumed. However, based on three-dimensional analyses, Peila (1994) pointed out that a shear failure surface does not necessarily develop and only face extrusion happens, as confirmed experimentally by Broms and Bennermark (1967). He proposed a fictitious confining pressure to represent the tunnel face reinforcement. This pressure is limited to the minimum of the reinforcement tensile strength and the reinforcement-ground bonding strength. Lunardi (1998) proposed an extrusion laboratory test to determine the internal pressure required to limit the extrusion of a cylindrical hole made in a sample of the ground. The homogenization approach is used to represent a dense array of rock bolts. Bernaud et al. (1995) derived improved properties of the reinforced ground along the reinforcement (anisotropic material properties). In the study conducted by Pellizza et al. (1994), the reinforcement is represented by an augmentation in the ground cohesion.

A variety of finite element approaches, with different degrees of complexity, may be used to account for the reinforcement in the analysis of the ground response. These approaches vary by the elements chosen for the reinforcement, by the type of the interaction between the ground and the reinforcement, and by the mechanical behavior chosen for the reinforcement (as well as the sealant).

The reinforcement may be most conveniently represented by one-dimensional bar elements completely embedded in the ground continuum elements. The use of bar elements, however, may lead to disproportionate representation of the reinforcement relative size and stiffness, ignoring the effect of ground confinement and the shear strength of the interface. These issues impair the results obtained by making use of bar elements. In most general case, the reinforcement may be represented by solid elements interacting with the ground elements through most general contact elements (friction, slip, separation).

In tunnels excavated in difficult ground conditions, jet-grouting pre-confinement is typically accompanied by reinforcement of the core with fiberglass dowels. In this simulation, the core is reinforced by 90 dowels (1 dowel per 1.7 m^2), being 24-m long with 12 m overlapping. Fig. 39 displays the configuration and mechanical properties of the dowels in the tunnel face.

Fig. 40 depicts the tunnel convergence after reinforcing the face. Because the face reinforcement is removed during excavation, it does not affect the ultimate tunnel convergence. However, the temporary reduction of convergence across the face is of importance for jet-grouting or shotcrete to harden and thus function. In the vicinity of the face, core dowel pre-confinement delays loading on the fresh jet-grouting umbrella by increasing the contribution of the core in carrying the loads. The same advantage may be employed in cases where cavity supports are to be installed rather far from the face.

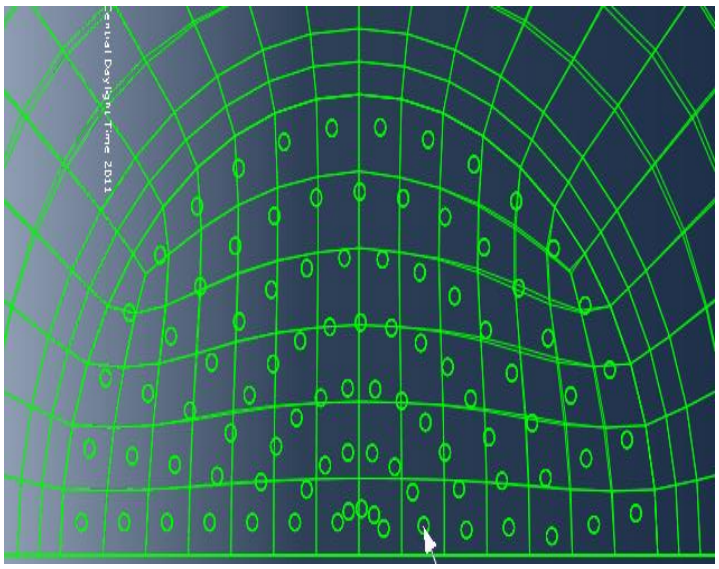

Dowel Mechanical Properties	
A (m^2)	0.0005
E (MPa)	40,000
Capacity(kN)	440
Capacity(MPa)	880

Figure 39: Face dowel configuration and properties

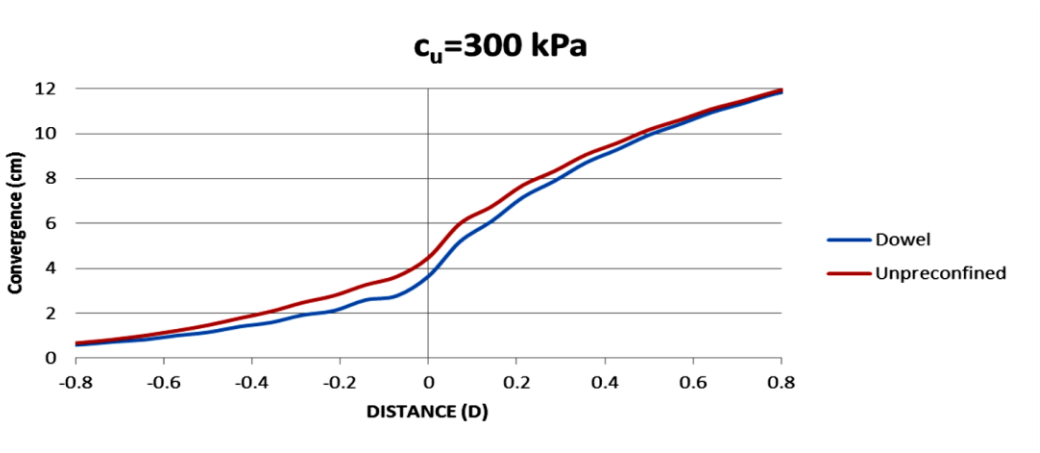

Figure 40: Effect of face reinforcement on the tunnel longitudinal convergence profile (LCP)

Chapter 5: Viscous Ground

In chapter 4, the spatial effects of tunnel excavation were investigated. We observed the variation of the convergence and the pressure on linings as the distance from the working face increases. However, these quantities do not change solely as a result of face advancement. Due to temporal mechanisms such as ground consolidation and viscous behavior, they may vary with time, as indicated by convergence increase in case of no face advancement (Boidy et al., 2002).

Time-dependent deformation in a tunnel may generally be associated with support time-dependent behavior, ground consolidation, or ground viscous behavior. The first case was explored in chapter 4, where hardening of jet-grouting was taken into account. Here, the effect of ground consolidation on the tunnel delayed deformation is first examined. Then, introducing a constitutive model for the ground viscous behavior, the effect of ground viscous behavior on the tunnel delayed deformation is studied.

5.1. GROUND CONSOLIDATION

The ground consolidation is referred to the change in the stress and deformation field in the ground due to the dissipation of the excess pore water pressure. Induced by the excavation of the tunnel, the excess pore water pressure dissipates by the diffusion of the pore water pressure through the ground pores. The rate of the pore water diffusion depends primarily on the ground local characteristics such as permeability and bulk behavior, and on the ground hydraulic boundary conditions such as the pore pressure at the tunnel periphery, the permeability of the tunnel supports, the level of the ground water table, etc.

The analysis of the tunnel construction may be conducted assuming undrained conditions when the tunnel consolidation rate is markedly lower than the tunnel advance rate. The analyses made in the previous sections were made in the undrained conditions.

This was realized by assuming an artificially low permeability coefficient for the ground and jet-grouting zone, and also no flow boundary conditions for the tunnel periphery. A series of sensitivity analyses proved k=5E-13 m/day to be sufficiently low to reproduce undrained conditions.

For tunnels with a consolidation rate comparable to the tunnel advance rate, the coupled analysis of the tunnel construction is necessary. Consolidation is a coupled phenomenon which requires considering the ground as a two-phase medium of water and porous soil skeleton. In this section, we will analyze the same tunnel but with a realistic permeability coefficient, k=5E-4 m/day. The pore water inflow through the tunnel periphery is also allowed using the same permeability coefficient for the jet-grouting as for the ground. The results shown hereafter are obtained right after the end of the tunnel excavation. Hence, the results are signified by "End of Construction" (EoC). In order to illustrate the effect of consolidation on the tunnel behavior, the results of the consolidation analysis will be compared to those obtained in the undrained conditions.

From Fig. 41-46, we may draw the following conclusions on the possible consequences of excess pore water pressure dissipation as a result of seepage in ground and through the tunnel wall and face:

- Advantages of excess pore water pressure dissipation:
    - Decrease in yielding at ground behind jet-grouting
    - Decrease in lateral convergence
    - Decrease in pore water pressure at wall
- Disadvantages of excess pore water pressure dissipation:
    - Increased yielding at unsupported floor ground
    - Increased vertical convergence
    - Increased yielding in core

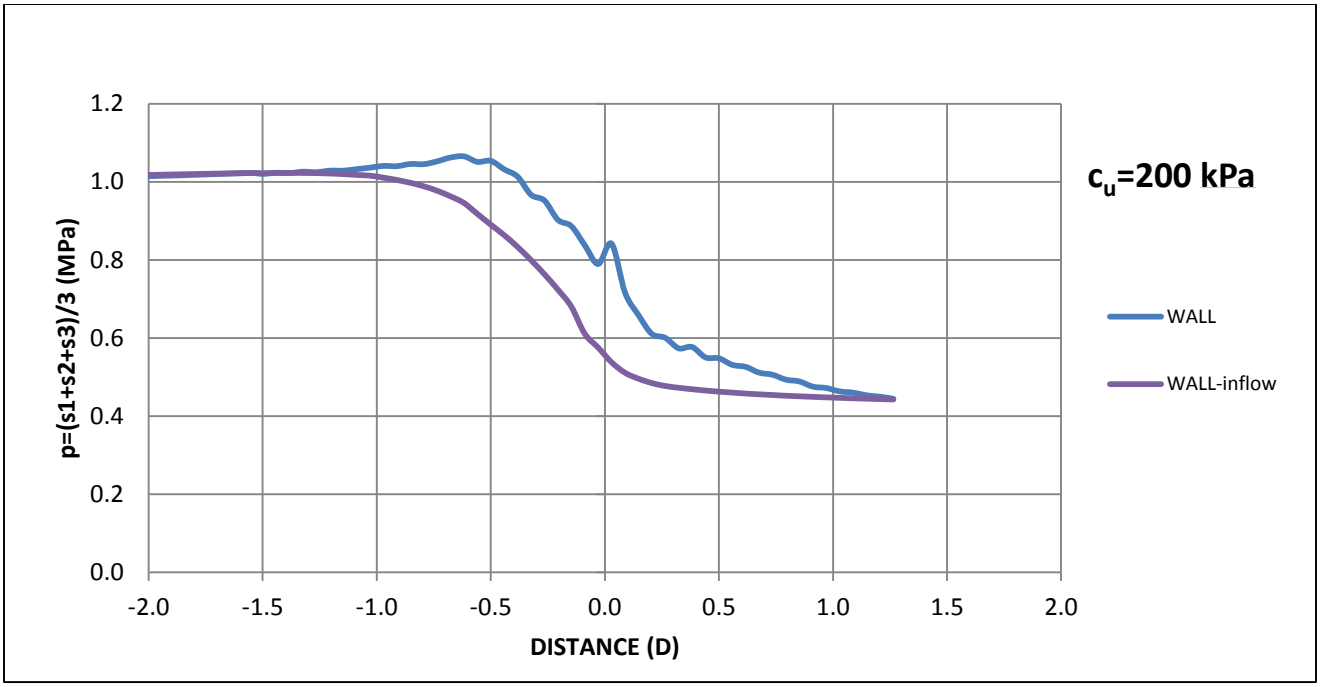

Figure 41: Total pressure in undrained vs. EoC conditions

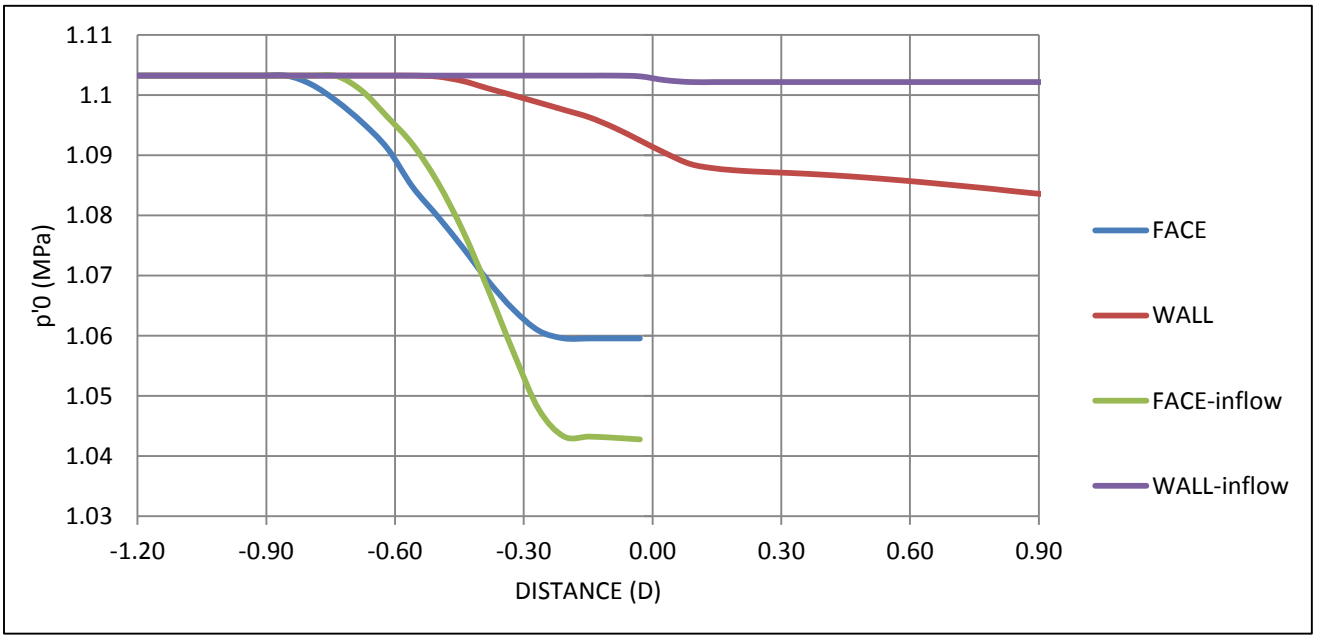

Figure 42: Reduction of yield surface size in undrained vs. EoC conditions

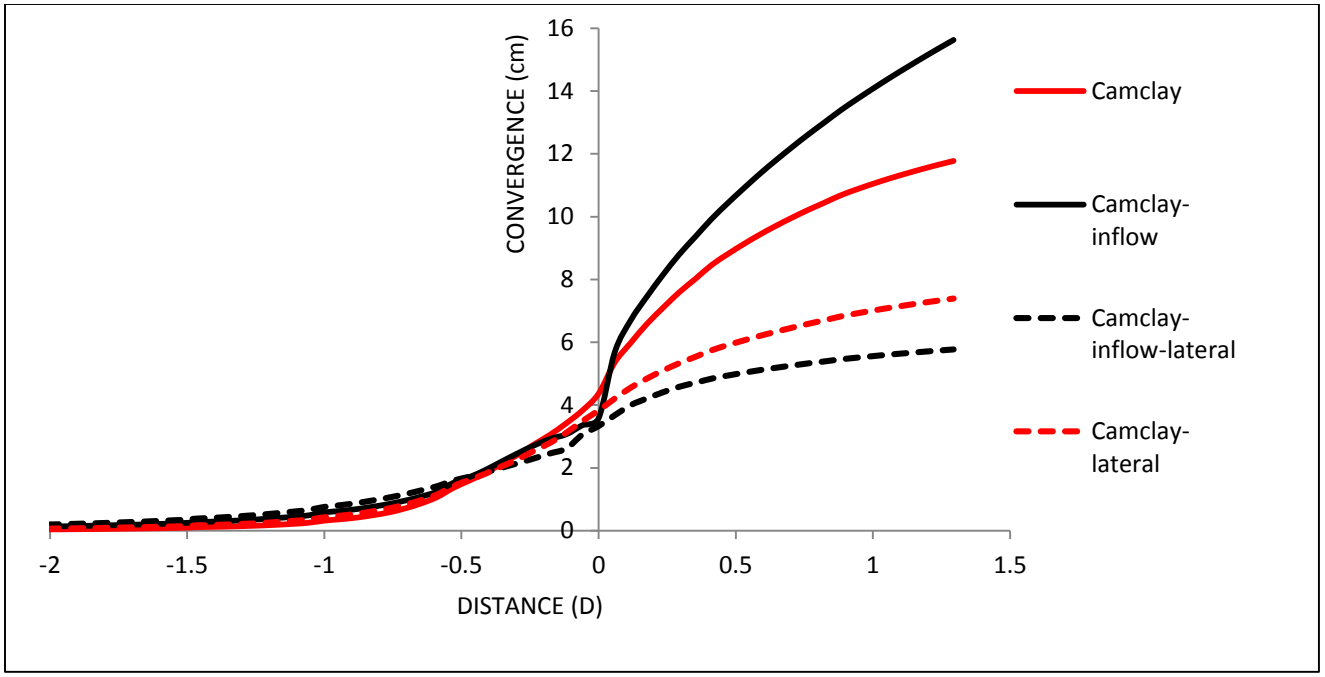

Figure 43: Vertical and lateral convergence in undrained vs. EoC conditions

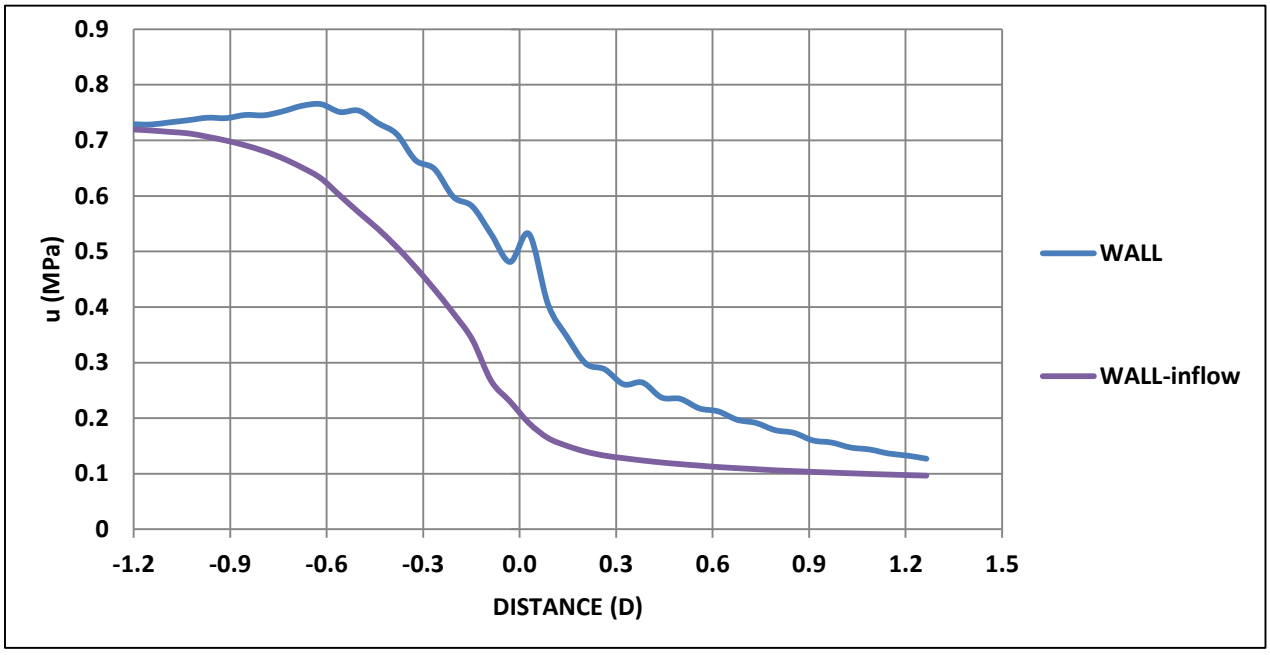

Figure 44: Pore pressure in undrained vs. EoC conditions

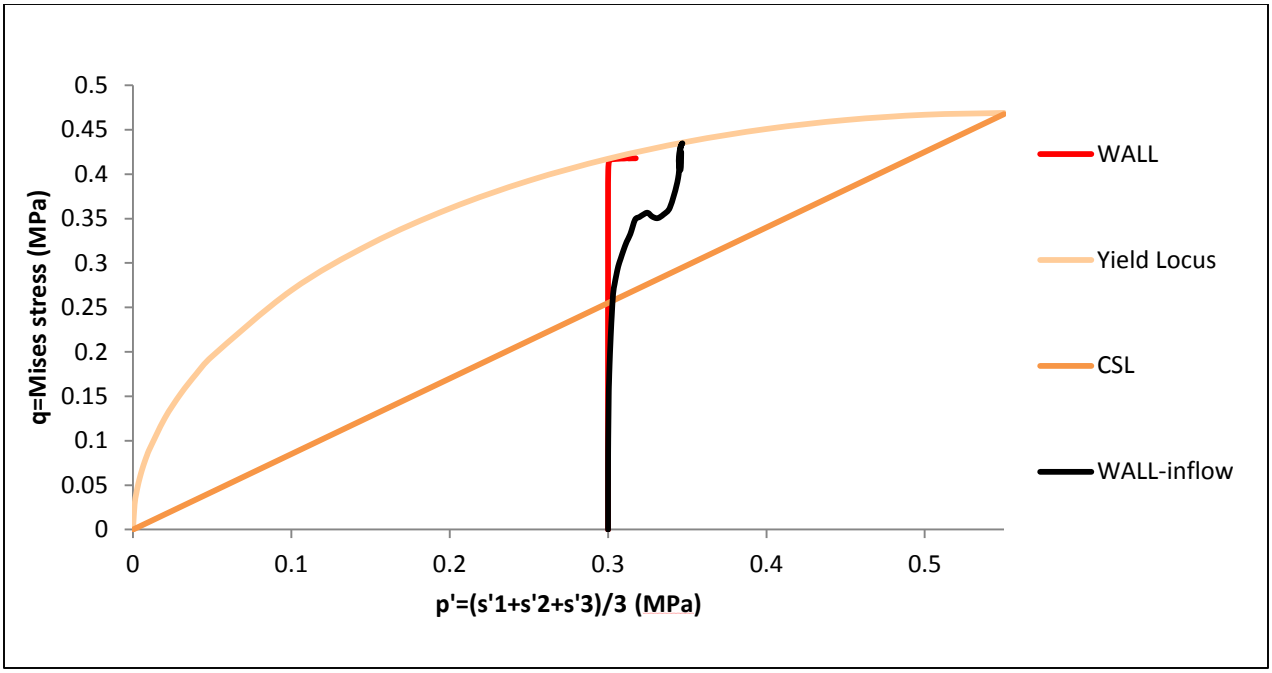

Figure 45: Stress path in undrained vs. EoC conditions

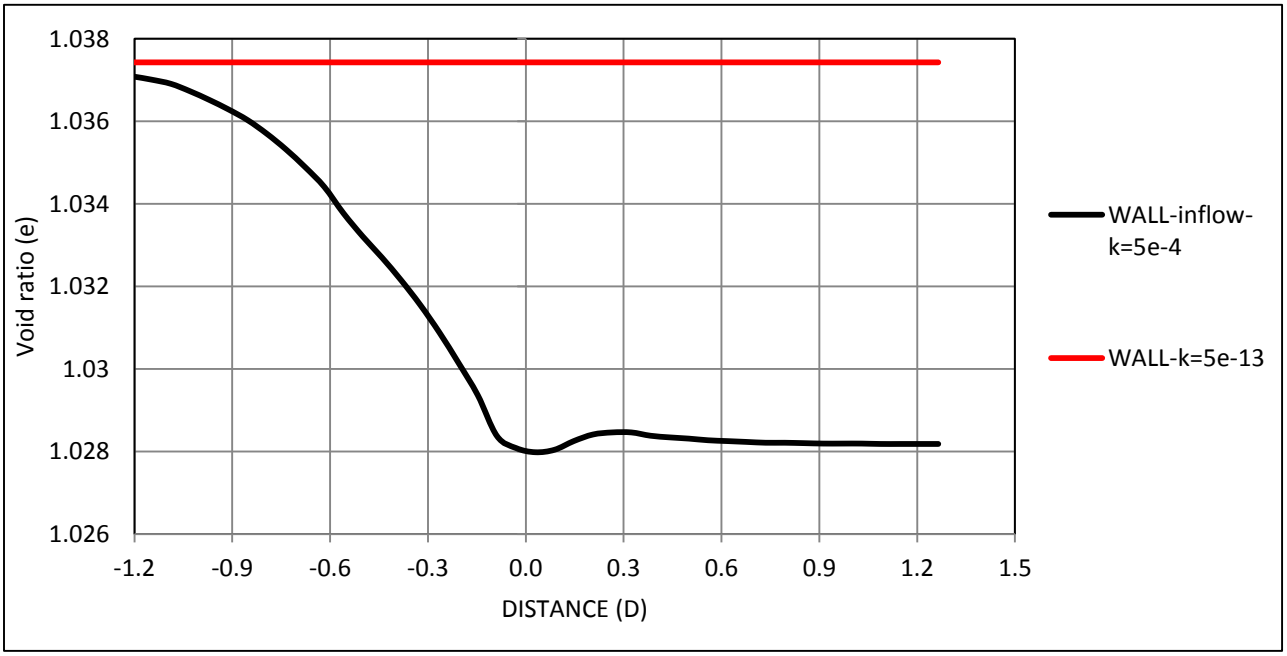

Figure 46: Void ratio in undrained vs. EoC conditions

5.2. CASE STUDY: TARTAIGUILLE TUNNEL

Located on the new high-speed train line between Valence and Montelimar, France, Tartaiguille tunnel was constructed in 1998. This tunnel is a double track single tube with 180 m^2 cross-section. It crosses fractured limestone on its north end, stiff marls and sandstones on its south end, and Stampien clays on the middle section (Fig. 47).

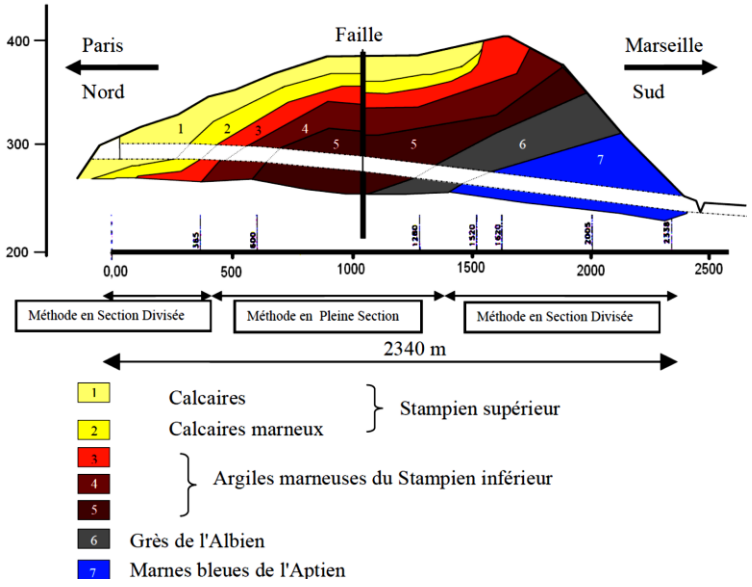

Figure 47: Geology and location of Tartiguille tunnel (after Purwodihardjo, 2004)

As shown in the tunnel cross-section in Fig. 48, the tunnel is actually supported first by shotcrete and steel hangers and finally by CIP reinforced concrete. In this work, the tunnel is assumed to be supported by jet-grouting umbrella and the final concrete invert.

The tunnel was excavated using two different methods of excavation. According to the tunnel design, the tunnel was excavated using the sequential excavation method, but this method was replaced by the full-face excavation method following significant failures encountering difficult ground conditions at the middle section of the tunnel (Fig. 47). The

next sub-section describes these two methods. Hereafter, the focus will be on tunneling in the challenging middle section.

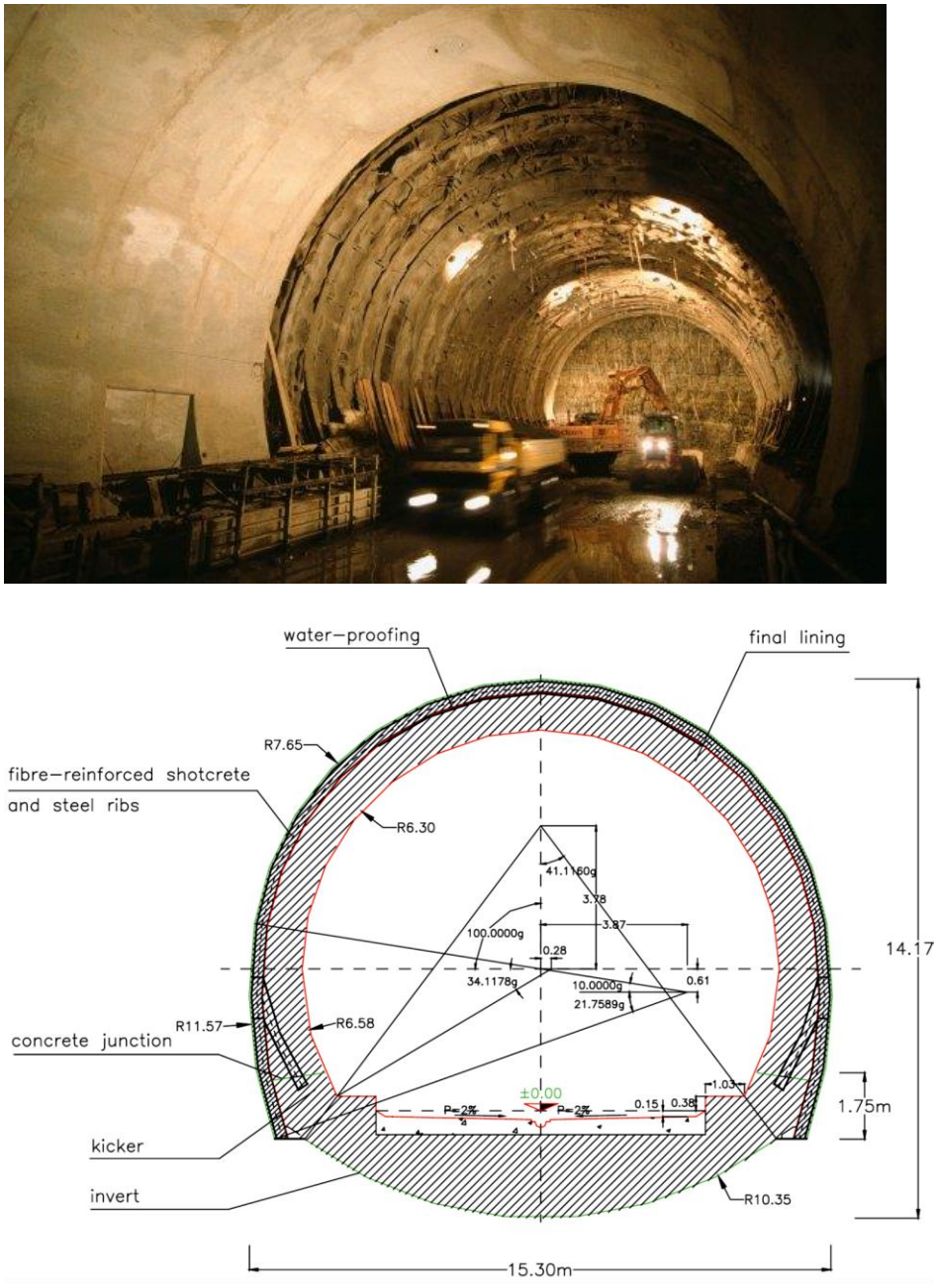

Figure 48: Dimensions and supports in Tartaiguille tunnel

The ground surface and water table at the middle section are nearly 100 m above the tunnel. The ground consists of alternating levels of stratified marl, clay and silt with the presence of limestone (5-10%). Clay and marl are extremely compact, being consistent like a rock. The ground is moderately fractured. According to the ground consistency, field tests, and laboratory tests, the ground is strongly consolidated. Clay and marl materials are extremely sensitive such that the rock loses its consistency in exposure to tunnel environment, and behaves like a highly plastic clay. Table 6 gives the basic geotechnical information from laboratory tests on the shale rock at this section.

PROPERTY	SYMBOLE	VALUE
Density	γ (kN/m3)	22.15
Water content	w (%)	10
Void ratio	e	0.27
Saturation	Sr (%)	100
Permeability	k (m/s)	10-7
Young's modulus	E (MPa)	200
Poisson's ratio	ν	0.3
Undrained friction angle	φ_u (degrees)	0
Undrained cohesion	cu (MPa)	0.8
Drained friction angle	φ' (degrees)	20
Drained cohesion	c' (MPa)	0.2

Table 6: Geotechnical properties

5.3. SEQUENTIAL EXCAVATION METHOD

The sequential excavation is a conventional method used in all ground conditions. In this method, the tunnel is excavated consecutively. In each step, a segment of the tunnel cross-section is excavated (Fig. 49).

Figure 49: Sequential excavation

The method is based on the notion that the stability of a smaller tunnel can be provided with considerably less effort. The tunnel support demand is determined by the extension of the ground failure zone, and the latter strongly depends on the excavation size. Accordingly, the recommended number of segments increases for ground with poor mechanical properties (Rabcewicz, 1969) (Fig. 50).

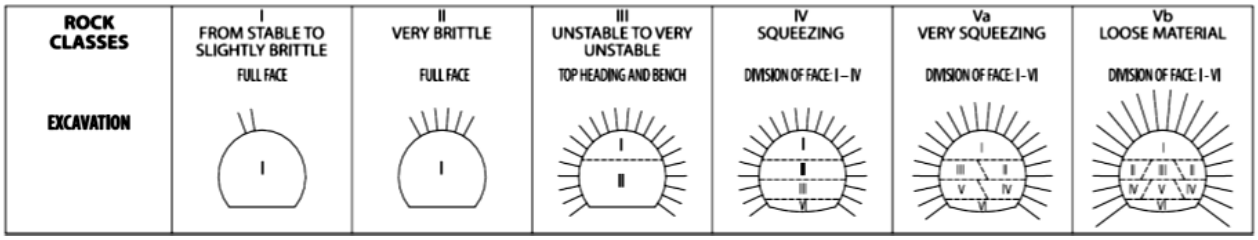

Figure 50: Excavation sequences recommended by Rabcewicz (1969)

Variations of the method have been applied over the world (Tonon, 2010). The variations differ essentially in the configuration and sequence of the excavations. The followings give the details of the method as applied in the case study of Tartaiguille tunnel. Fig. 3 shows the cross section of the tunnel divided in heading (100 m^2) and bench (80 m^2) segments. The tunnel is excavated in heading and bench (Fig. 51). The bench is excavated nearly 100 meters behind the heading face, and a concrete invert is implemented nearly 50 m behind the bench face (Fig. 52).

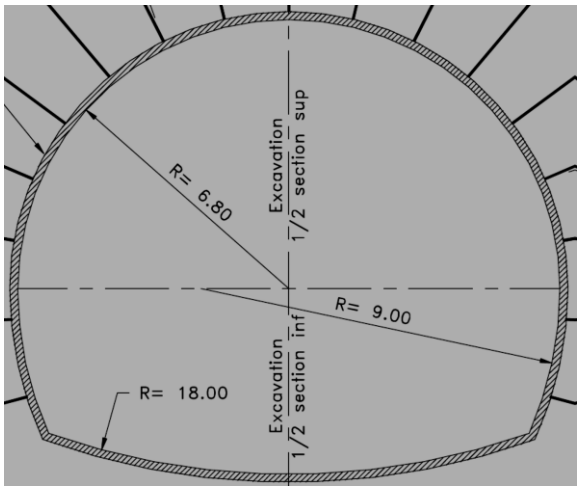

Figure 51: Head and bench segments in Tartaiguille tunnel sequential excavation

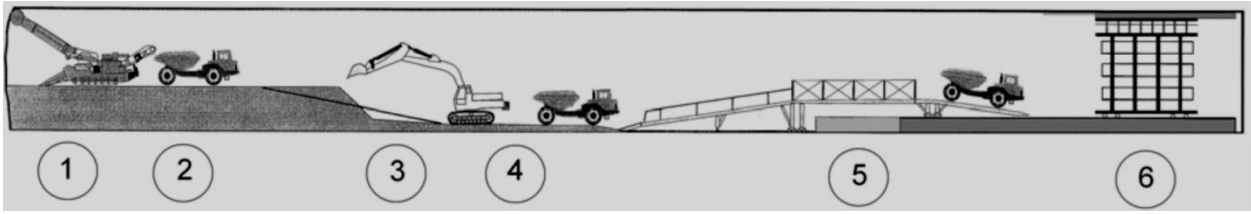

Figure 52: Construction sequence in sequential excavation (after Purwodihardjo (2004))

The sequential method failed when the tunnel penetrated the difficult ground conditions. An extensive crack divided the shotcrete shell at the tunnel crown along the entire excavation length. The cracking indicated delayed tunnel deformation.

5.4. FULL-FACE EXCAVATION METHOD

In the full-face excavation method, almost the entire tunnel cross-section is excavated at once. Although the method advantages have been long acknowledged, its application was delayed by the lack of competent construction and design technology in the past decades (Tonon, 2010). A single working face in this method allows for employment of modern machinery, which leads to higher efficiency and advance rate, less labor intensity, and better control over operation area, to mention a few. Further, the systematic excavation and support installation allows for more reliable analysis and thus design of the tunnel. Nonetheless, a main concern in this method is the stability of the large face, which is provided in this method by face reinforcement. Design and construction details for full-face tunnel excavation may be found in Lunardi (2008).

In the full-face method, the control of the tunnel deformation is of primary importance. Accordingly, the completion of the tunnel support is accelerated by the implementation of the tunnel invert adjacent to the face (Fig. 53). As such, a complete support structure becomes effective immediately after the excavation.

While the use of full face excavation under the most difficult conditions seems paradoxical at first sight because of the potential instability of the face, which may even reach a height of 9–12 m, it is in fact often found to be very reliable giving good performance, provided the stability of the face is ensured (the only critical zone with this type of advance) with appropriate ground reinforcement and improvement.

Following the failure of the sequential method in controlling the tunnel excessive deformation, the full-face method was adopted. In this method, the heading and bench segments are excavated simultaneously (full-face) in 6 m/day advance rate. The excavation stops every four meters for the implementation of the invert in 3.5 days. The concrete invert is cast adjacent to the face.

Figure 53: Invert installation adjacent to face in full-face method (after Lunardi (2008))

5.5. FULL-FACE VS. SEQUENTIAL EXCAVATION: NUMERICAL RESULTS

This section investigates the performance of the full-face method and the sequential method in Tartaiguille tunnel. To this end, the analysis of the tunnel takes into consideration the important mechanisms in difficult conditions.

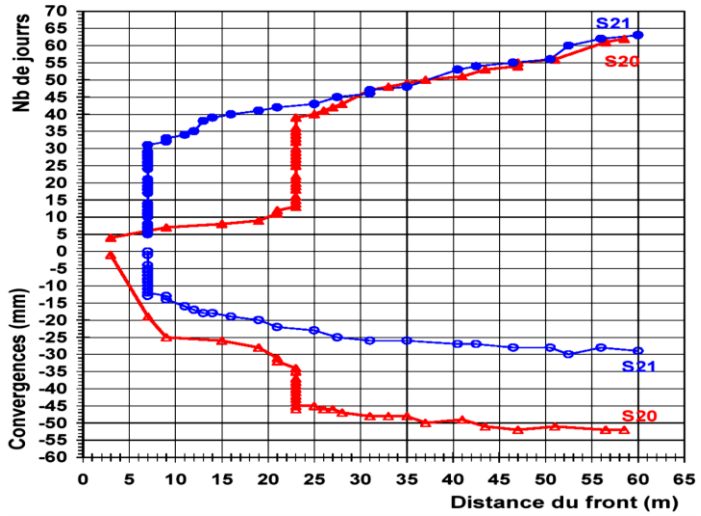

Figure 54: Face advance and convergence at a cross-section measured in Tartaiguille tunnel

The tunnel analysis accounts for the ground viscous behavior. Fig. 54 displays the schedule of the tunnel face advance and the convergence measured at a cross-section of the tunnel. The delayed ground response is clearly indicated by the significant increment of the tunnel convergence during the face stoppage. Hence, the ground viscous behavior would be an important factor in the response of the tunnel to the different excavation methods.

The model also probes the effect of the invert installation time. A major difference between the two methods is the time (distance) of the invert implementation. The full-face method emphasizes accelerated installation of the invert. On contrary, the sequential

method allows for delayed installation of the invert so as to maximize the use of the ground capacity in the stability of the tunnel. In order to assess the importance of this fundamental difference, the tunnel is analyzed with the invert installed at different distances to the face.

Full-face and segmented-face excavation of Tartaiguille tunnel are simulated using a block of ground, extending 200 m in each direction (Fig. 55). The block includes the tunnel in its center. Due to the vertical symmetry of the problem, only the left half of the model is analyzed.

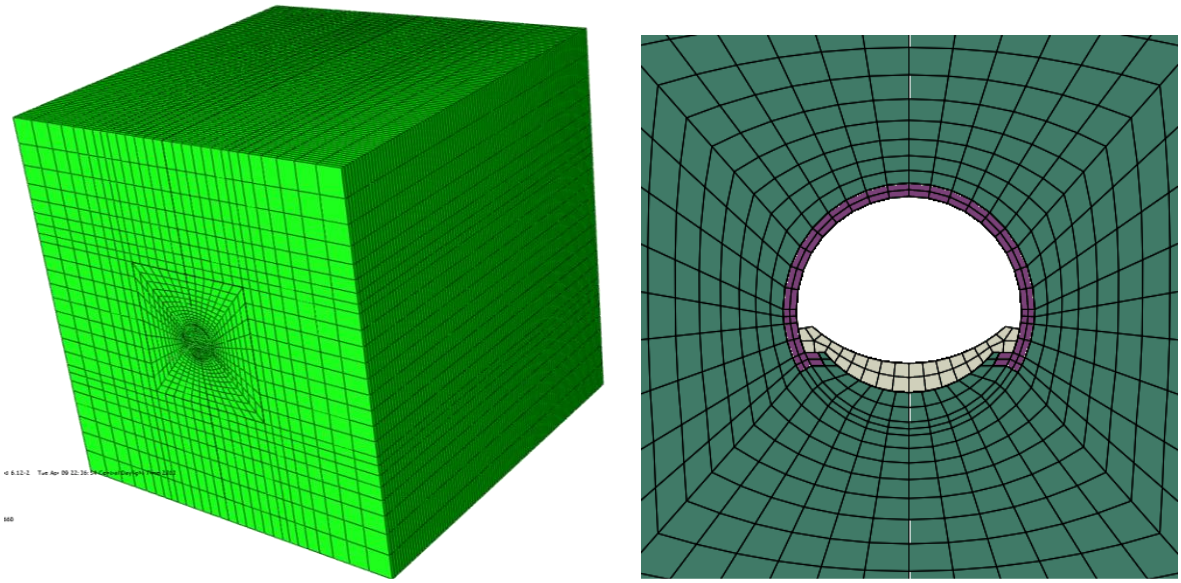

Figure 55: Three-dimensional model; tunnel cross-section; jet-grouting (red); invert (yellow)

In order to exclude the time-dependent effects of ground consolidation, the analyses are conducted in the undrained conditions. The undrained analysis can be accomplished by using a general uncoupled analysis scheme. In this scheme, the ground can be represented by ordinary solid elements. The response of these elements is defined by the effective stress response of soil skeleton superimposed by the bulk response of the pore water. The use of

the ordinary elements significantly reduces the computational demand for time and memory by eliminating the additional degree of freedom for the pore water pressure.

The model takes into account the total weight of the ground and the supports. Hence, a pressure is applied on the lateral side of the model to represents the far field boundary conditions. This pressure increases linearly with depth to equilibrate the total weight of the ground. As in Tartaiguille tunnel, the tunnel is 100 m below the model top surface, which bears no pressure to represent the very ground surface. The water table is also at the ground surface.

The in situ ground stress field is introduced in the model by defining initial stresses which increases linearly in equilibrium with the ground total weight. The in-situ stress field is assumed isotropic, although in-situ measurements indicate a lateral earth pressure coefficient of about 1.2. The initial equilibrium conditions are checked by the Geostatic analysis step before beginning the actual analysis steps.

The ground at the tunnel is composed of black and grey marl with a narrow interlayer of calcareous marl. In the analyses, the ground is assumed to be composed entirely of the black and grey marl. The viscoplastic CJS model is used to account for the ground viscous behavior. The parameters of this model are identified for the black and grey marl in section 2.4.7.

The hardening of the jet-grouting and the concrete invert are also accounted for in the analyses using the element embedment, described in section 3.2. The ultimate strength (UCS) and Young's modulus (E) of the jet-grouting umbrella are 8 MPa and 13.5 GPa, respectively. These values are respectively 32 MPa and 27 GPa for the cast-in-place invert concrete. Hardening of the invert concrete is accounted for by using the same hardening curve as used for the jet-grouting.

The excavation of the tunnel is simulated by eliminating the elements representing the core of the tunnel. In the full-face excavation, the heading and bench segments are excavated simultaneously and with no distance along the tunnel in 1 m advance steps. The invert is installed adjacent to the tunnel face after every 4 m excavation. Fig. 56 shows a sequence of the construction steps in the full-face method.

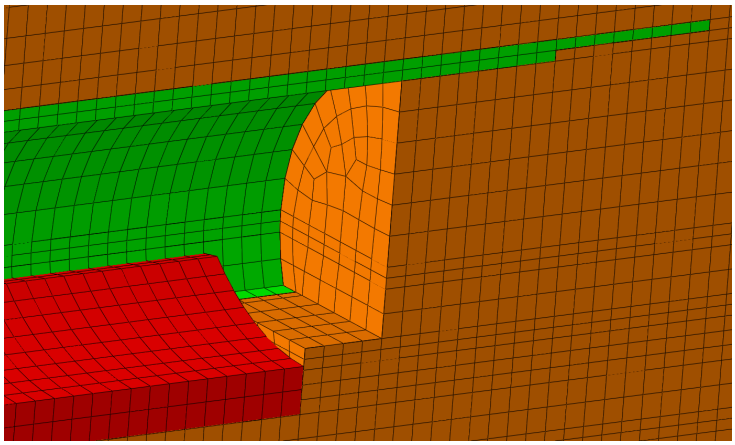

Figure 56 (a): Jet-grouting (green); length=16 m; duration=84 hours

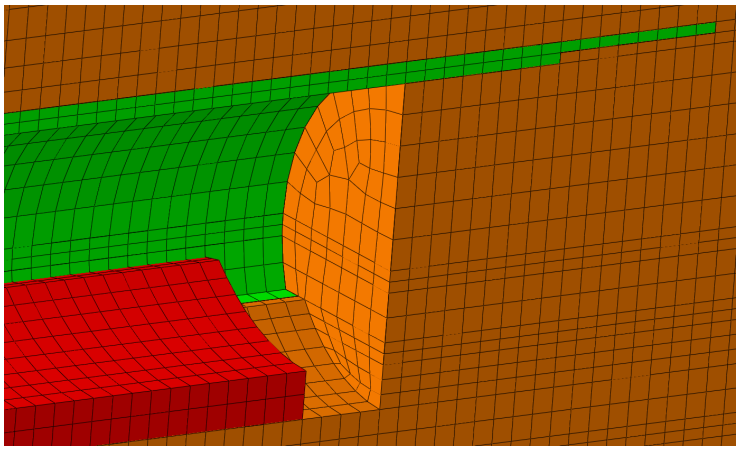

Figure 56 (b): Invert excavation (and installation) (red); length=4 m; duration=12 hours

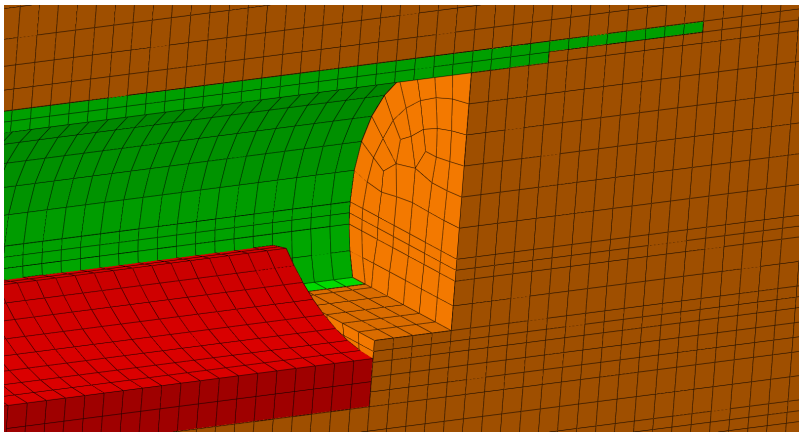

Figure 56 (c): Full-face excavation for 4 m in 1 m/4 hours

In the sequential excavation mehod, the heading, bench, and invert are excavated simultaneously *but* with some distance along the tunnel. Accordingly, the top and bottom jet-grouting are carried out simultaneously but with the same distance along the tunnel. Herein, the tunnel is analyzed for the distance between the heading, bench, and invert excavation faces chosen 8 m, 24 m, and 48 m. Fig. 57 shows the tunnel construction steps in the sequential excavation method with 8 m distance between the excavation faces.

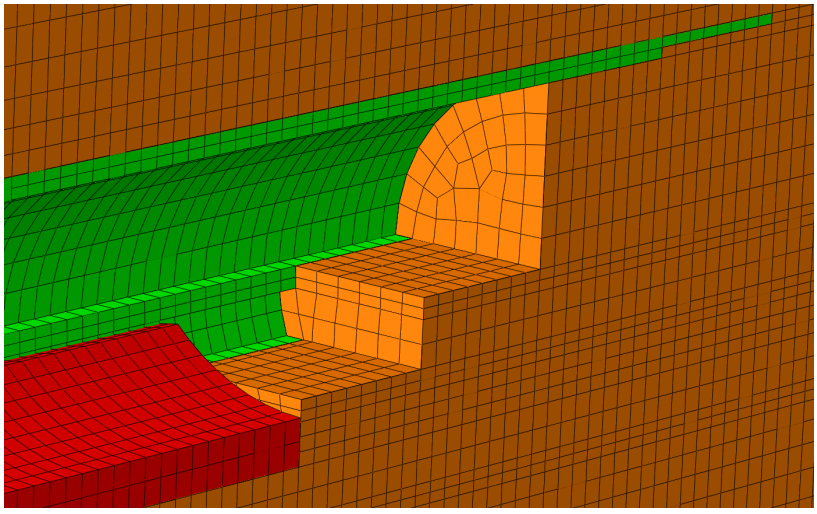

Figure 57 (a): Jet-grouting of heading and bench; length=16 m; duration=72 hours

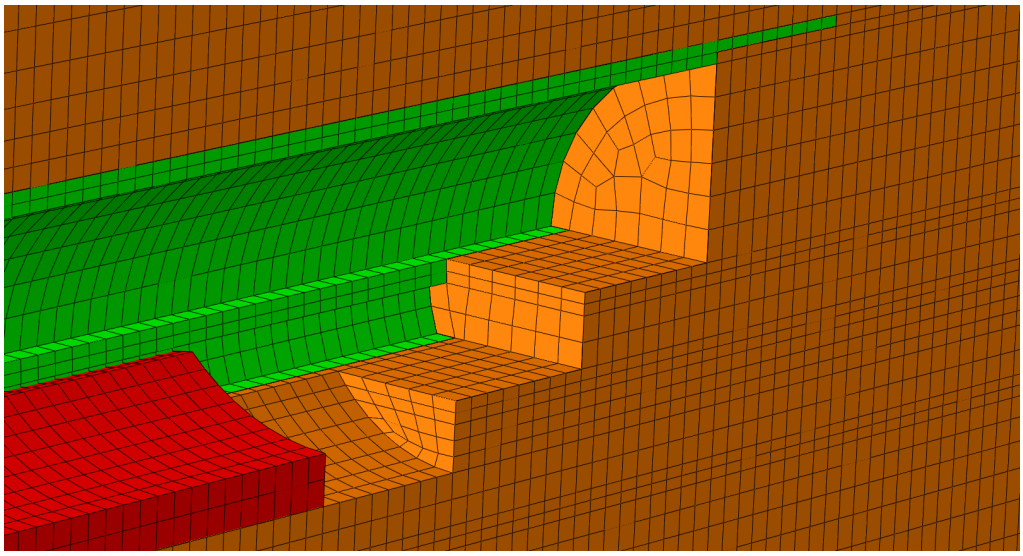

Figure 57 (b): Excavation of heading, bench, and invert for 8 m in 1 m/3 hours

Fig. 58 shows the materials assigned to the jet-grouting and invert sections installed at different times. These sections have different properties because their properties depend on time and thus age of these materials.

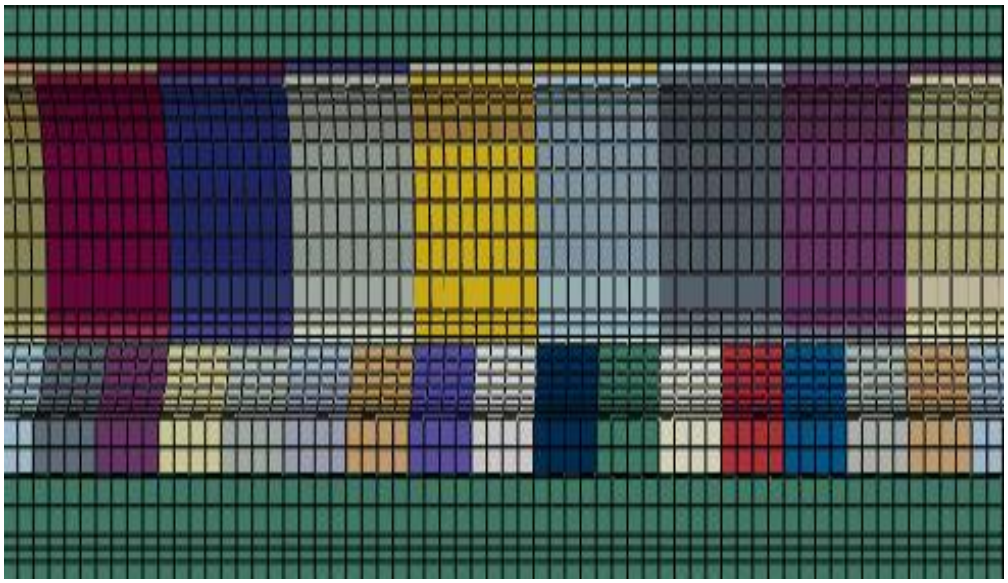

Figure 58: Materials assigned to jet-grouting and concrete invert with different ages

Fig. 59 (a) shows the deformed cross-section of the tunnel. The invert with a different curvature from the jet-grouting causes concentration of out-of-plane shear loads in the jet-grouting around their connection point. This issue may cause shear failure of the jet-grouting, as indicated in Fig. 59 (b). This issue may impair the in-plane function of the jet-grouting shell, which is the principal function of the jet-grouting arch. In Tartaiguille tunnel, in order to avoid this problem, the connection between the shotcreted shell and the invert was strengthened by steel arms (Fig. 59 (c)).

Fig. 60 (a) shows the transversal distribution of the equivalent shear stress in the tunnel invert. A significant stress concentration develops at the point where the benches connect to the arch invert. This issue occurs because of bending of benches due to the eccentricity of the load from the jet-grouting with respect to the arch invert. This issue may impair the invert's function, which is axial resistance. Again, this problem was precluded by diverting the load path from the jet-grouting to the invert through additional arms.

Fig. 60 (b) shows the longitudinal distribution of the equivalent shear stress in the invert. The top of the invert shown is closer to the tunnel face. The intensity of the load is higher at points closer to the face. These points are of the same age, and thus have the same properties. This observation agrees with the fact that supports with the same properties installed closer to the face take higher loads.

Fig. 61 displays the deformation of the tunnel excavated in the full-face and sequential method with different distances between the excavation faces. As shown, the convergence of the tunnel increases with the increase in the distance between the excavation faces.

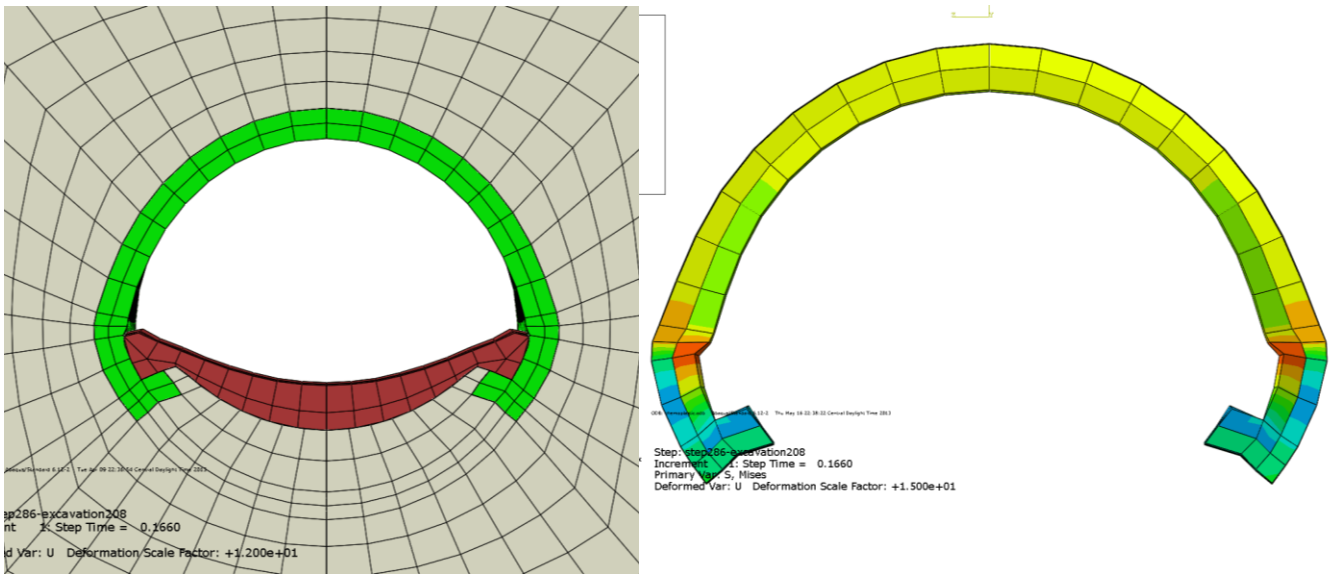

Figure 59: (a) Tunnel deformed cross-section; (b) Equivalent shear stress in jet-grouting

Figure 59 (c): Supporting arms in Tartaiguille tunnel

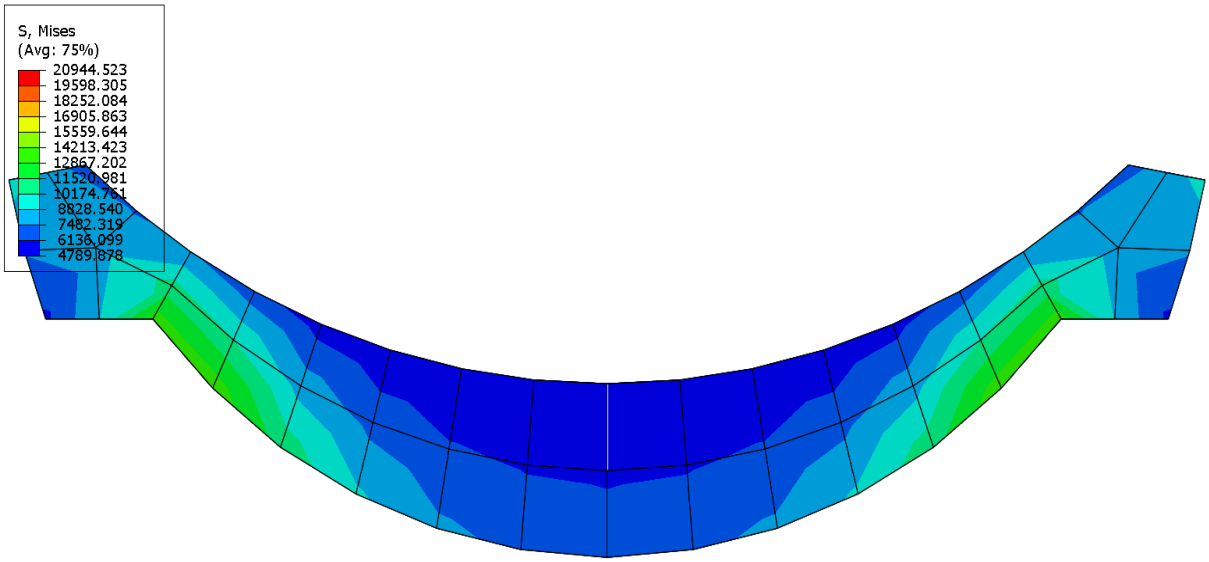

Figure 60 (a): Transversal distribution of shear stress in invert

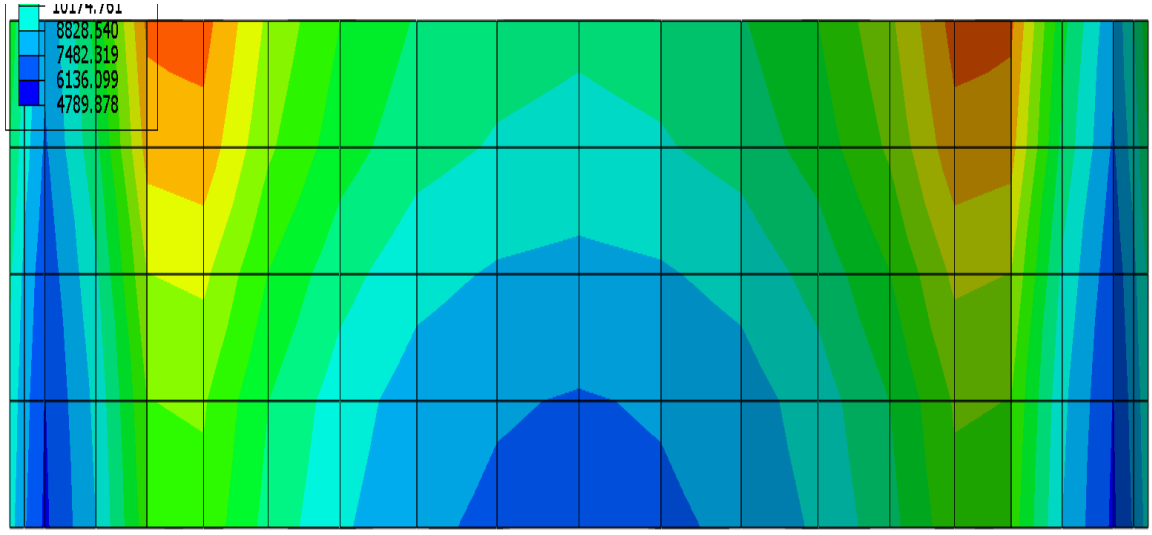

Figure 60 (b): Longitudinal distribution of shear stress in invert

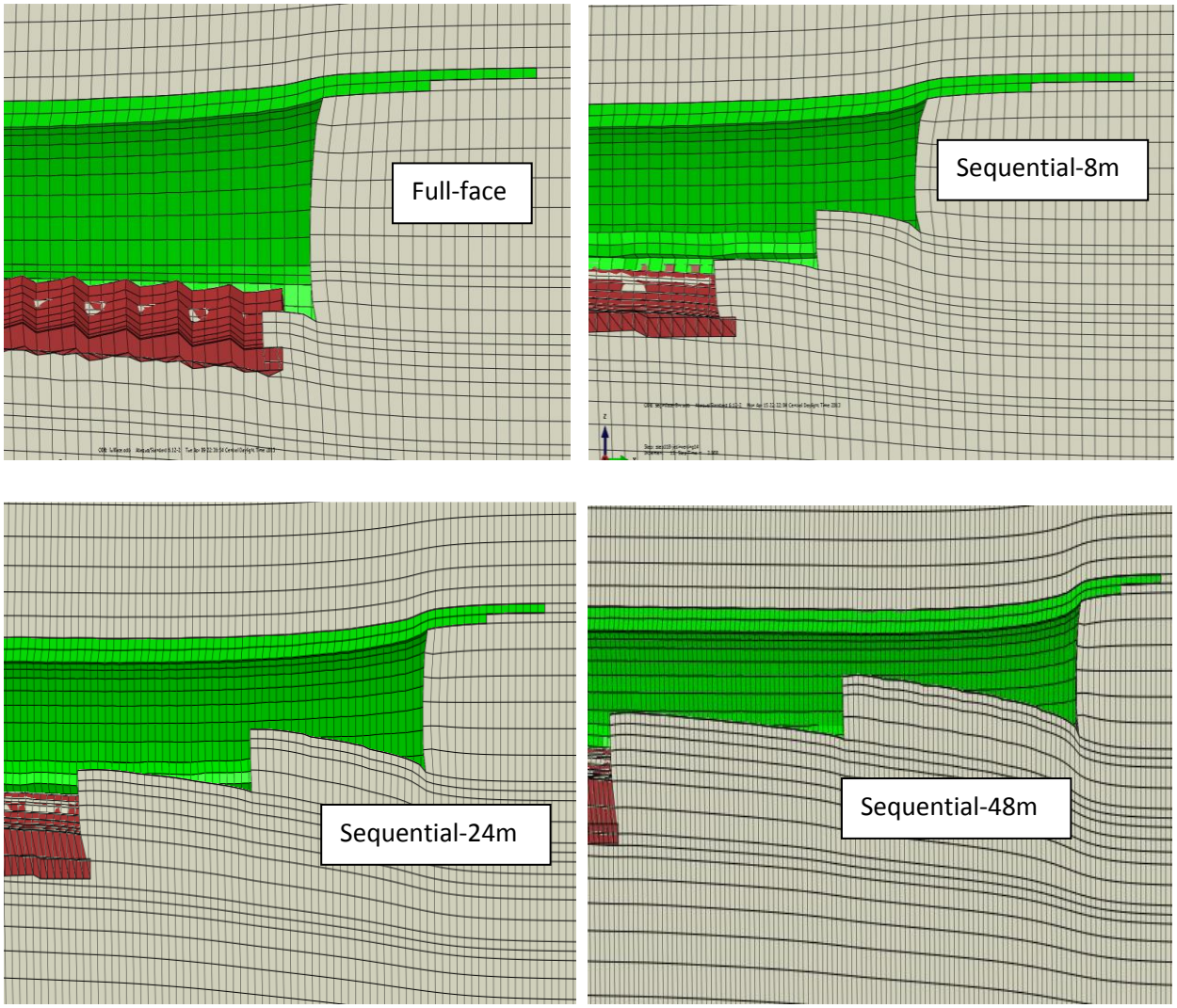

Figure 61: Tunnel longitudinal convergence in full-face and sequential methods

Fig. 62 shows the plastic zone developed around the tunnel cross-section in full-face and sequential methods. The disturbance of the ground virgin state extends in excavations with increased distance between the excavation faces.

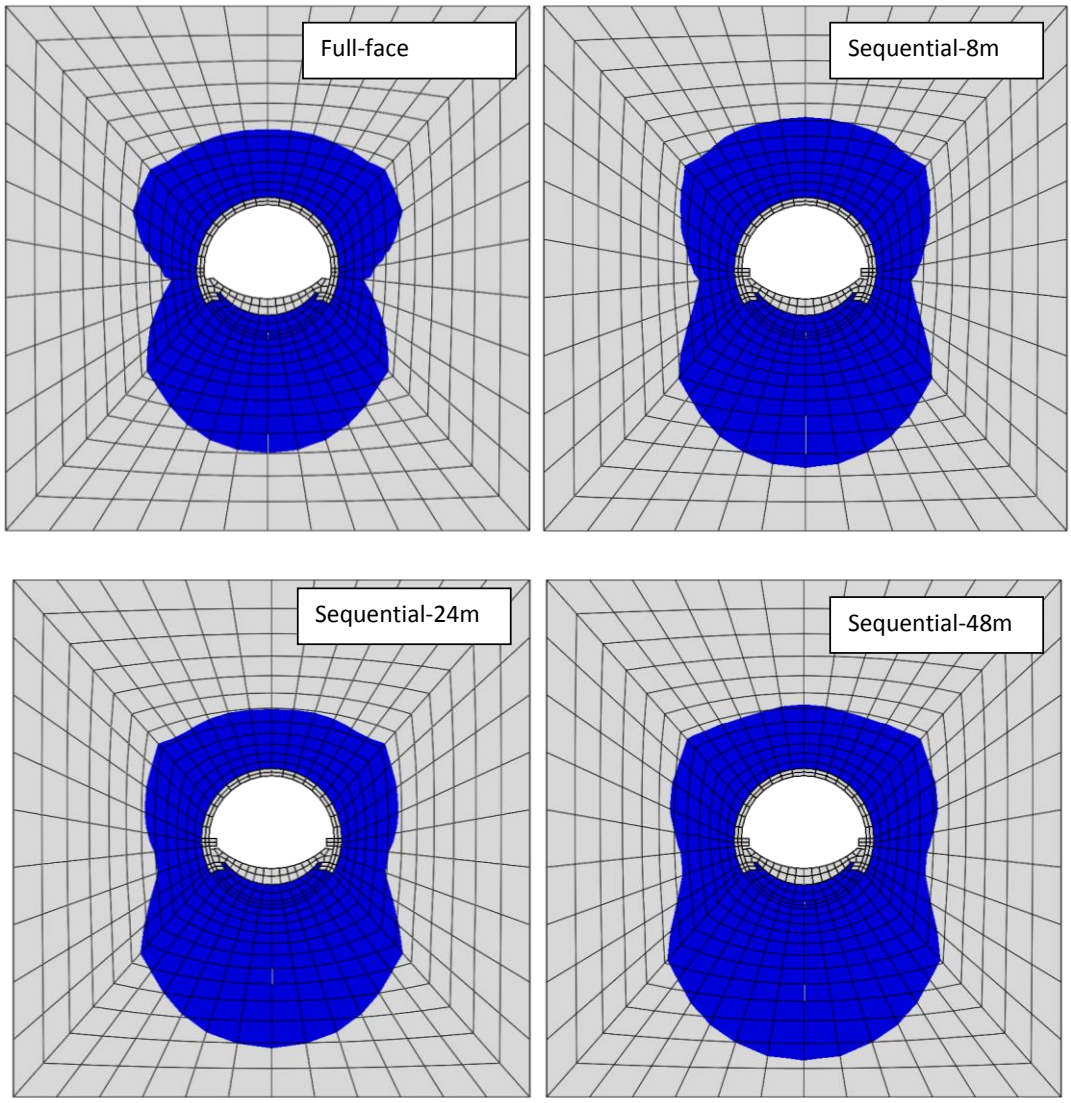

Figure 62: Ground plastic zone in full-face and sequential methods

Fig. 63 displays the softening zone around the tunnel cross-section excavated in full-face and sequential methods. By increasing the distance between the excavation faces, the softened zone enlarges at the footings of the jet-grouting arch.

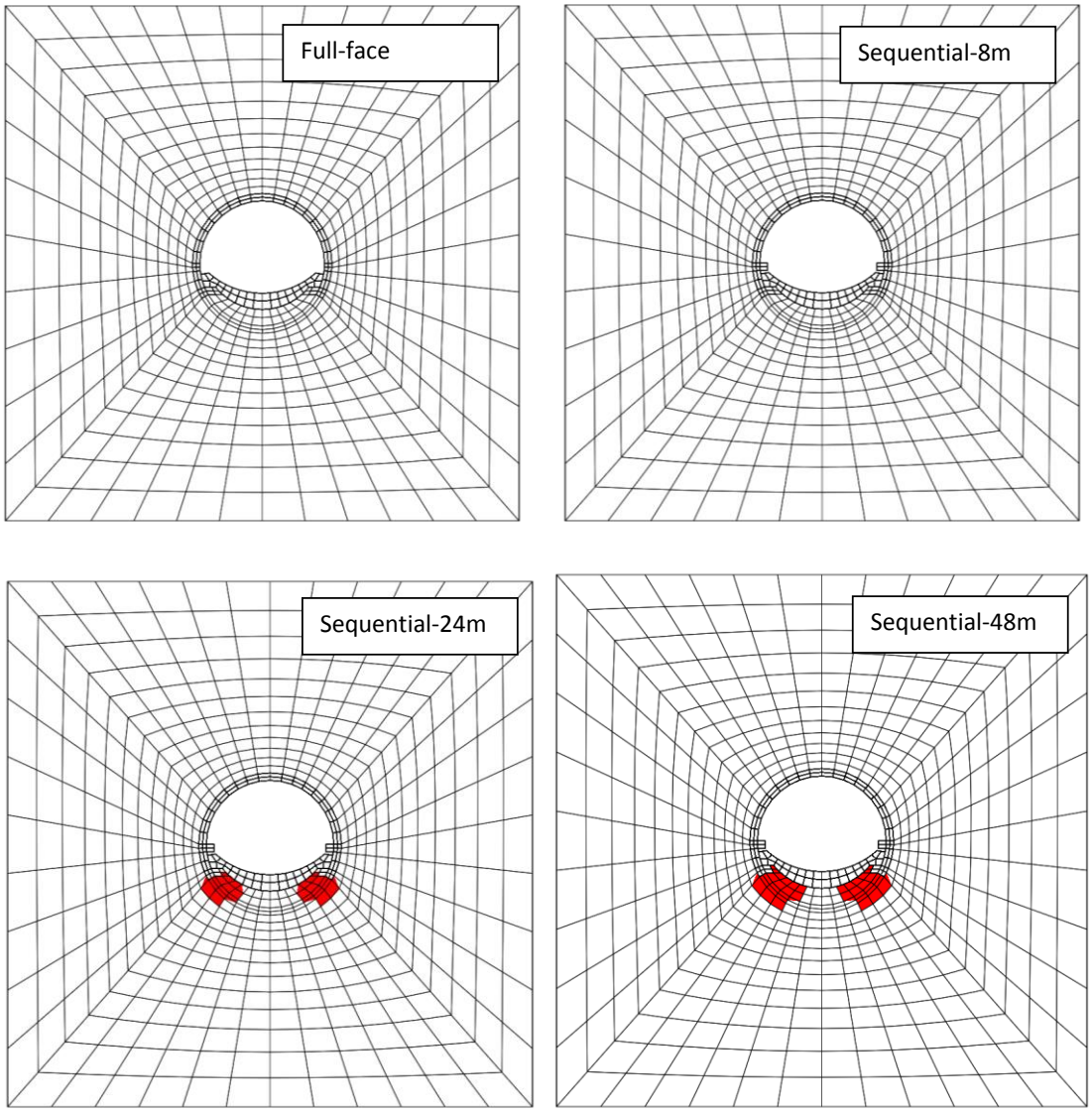

Figure 63: Ground softened zone in full-face and sequential methods

Fig. 64 shows the distribution of the excess pore water pressure in the tunnel cross-section. The negative excess pore pressure under the tunnel invert results from ground unloading due to the lack of jet-grouting and delayed implementation of the invert. The latter also leads to an increased pressure on the tunnel sides leading to the positive excess pore pressure at the tunnel sides.

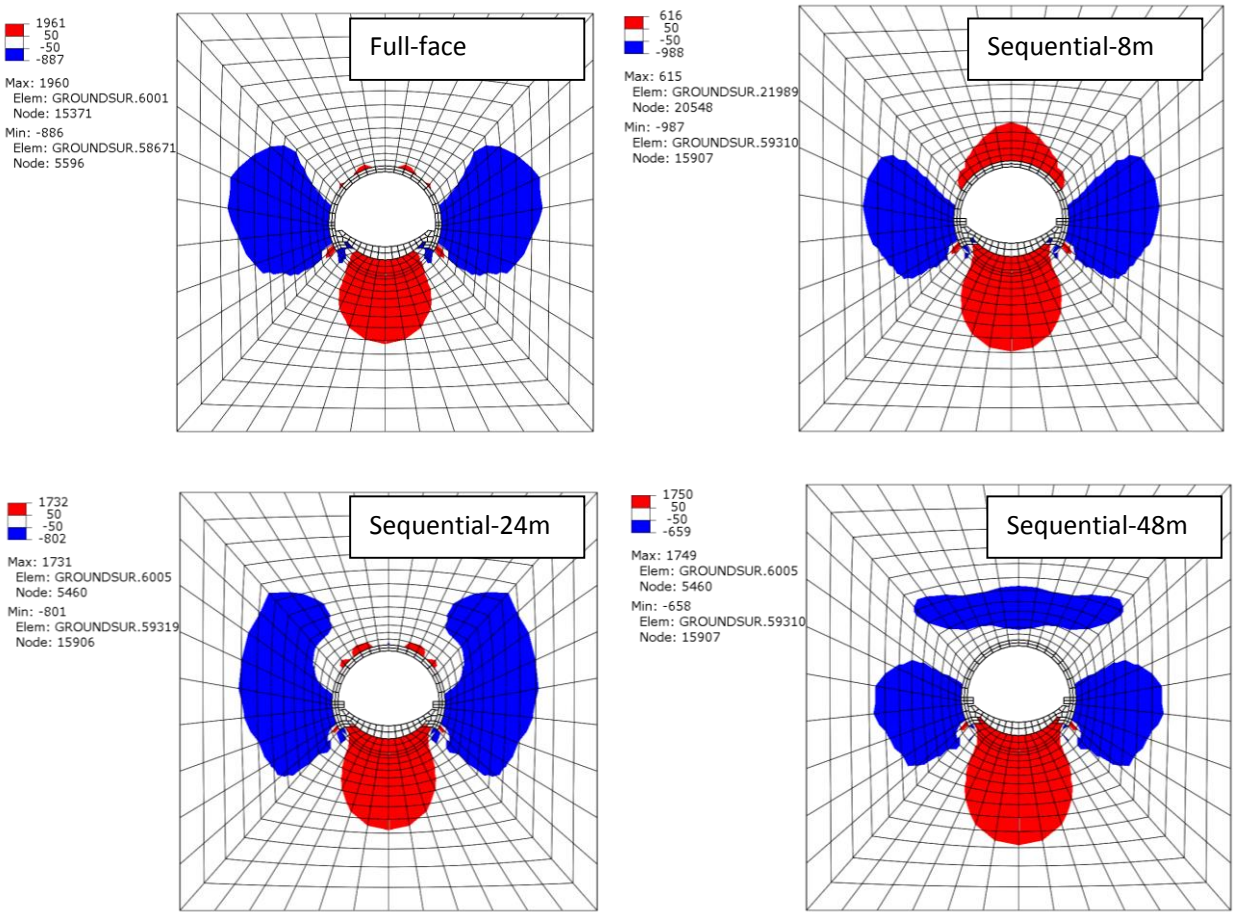

Figure 64: Distribution of excess pore pressure in full-face and sequential methods

Fig. 65 displays the displacement bulb around the tunnel. By increasing the excavation distance between the excavation faces, the displacement bulb enlarges. This enlargement may indicate the performance of the methods in controlling the tunnel deformations.

The plot in Fig. 66 shows the variation of the tunnel vertical closure in terms of the face distance and time. The tunnel closure increases by increasing the distance between the excavation faces. Because the invert is implemented earlier and closer to the face, the full-face method can control the tunnel deformation in a shorter length (and time) behind the

face. The tunnel deformation increases by a third when the sequential method with 50 m distance replaces the full-face method. A larger deformation increase may be expected for Tartaiguille tunnel, which was excavated sequentially with 100 m distance between the excavation faces.

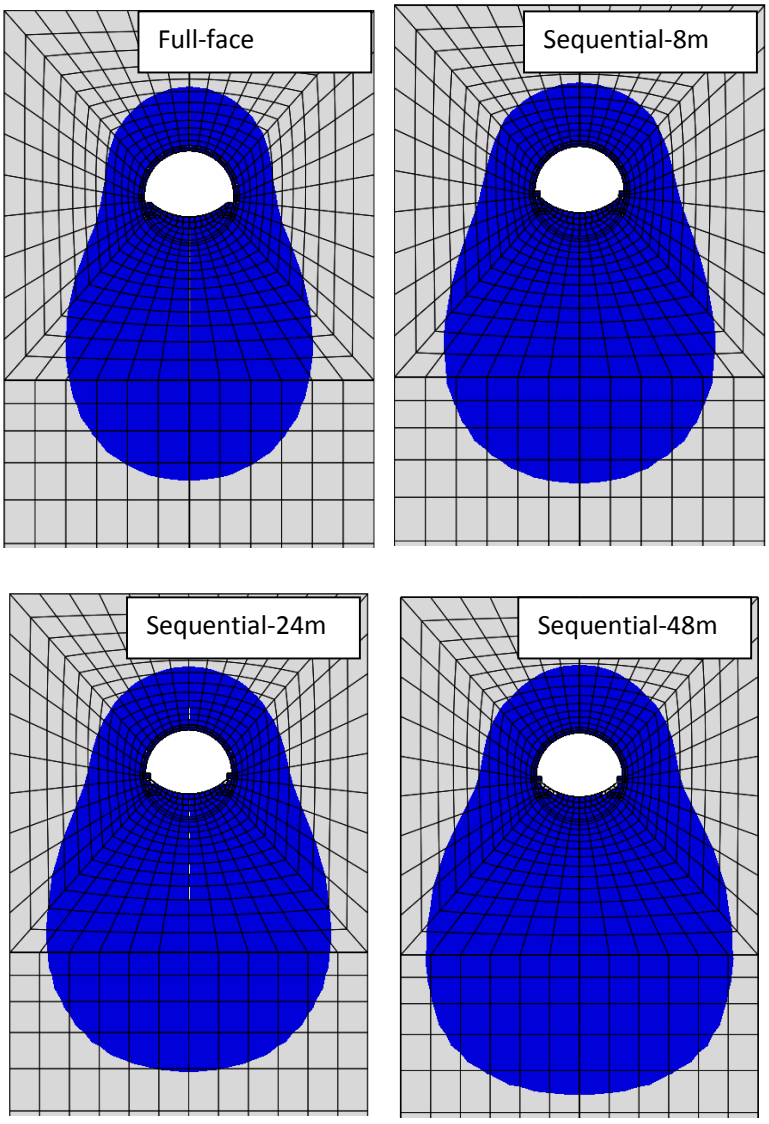

Figure 65: Displacement bulb in full-face and sequential methods

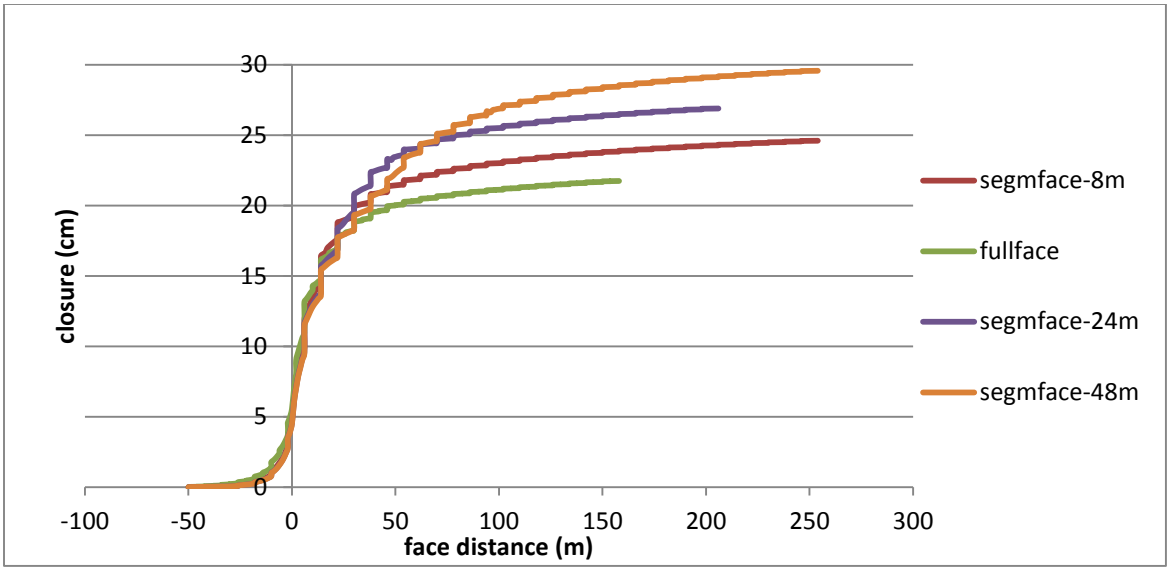

Figure 66 (a): Tunnel vertical closure vs. face distance in full-face and sequential method

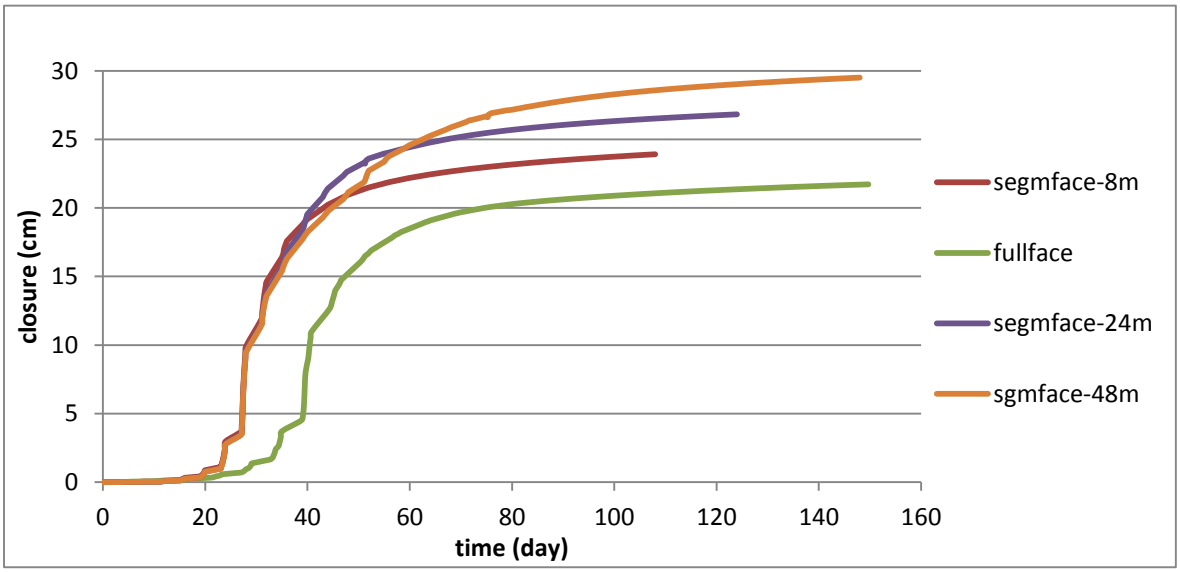

Figure 66 (b): Tunnel vertical closure vs. time in full-face and sequential method

The invert in fact integrates the structure of the supports installed at the cavity by replacing the ground at the foundation of the supports with the invert. The low bearing

capacity of the ground in difficult ground conditions would impair the capacity of the supports. This augmentation in the rigidity of the supports is crucial in the difficult ground conditions. The distance of the invert implementation to the face is important as well. Closer installation to the face would result in less tunnel convergence.

As shown in Fig. 67 (a), the face extrusion increases after the excavation of the ground at the face toe for casting the invert in the full-face method. This implementation is associated with the adverse effect of removing the longitudinal support for the face by the ground at the invert. As shown in Fig. 67 (b), a significant part of the resisting shear surface against the face instability passes through the ground at the invert.

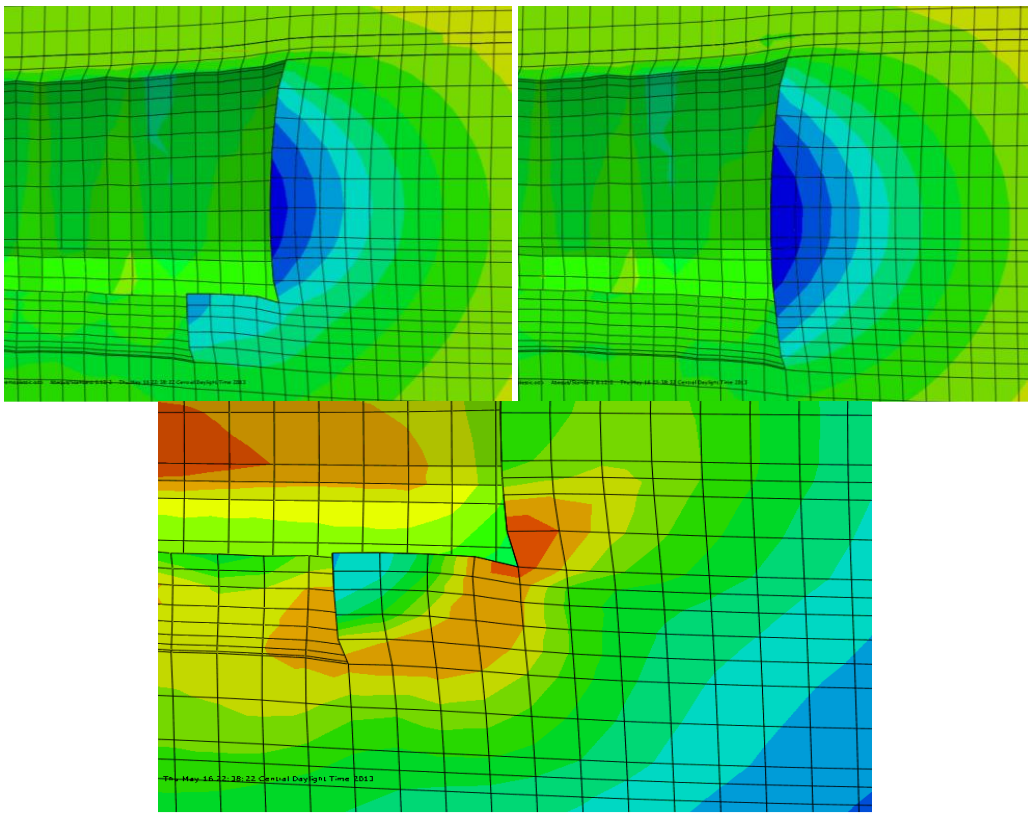

Figure 67: (a) Face extrusion before and after invert excavation in full-face method; (b) location of the shear resisting surface through the ground at tunnel invert

TWO-DIMENSIONAL ANALYSIS

Chapter 6: Two-dimensional Tunnel Analysis Methods

The analysis of tunnels is still challenging in geotechnical engineering. The complexity of the ground-support interaction in tunnels does not allow for the separation of ground action and support reaction, as is widely used in geotechnical engineering. In many cases, the analysis and design of tunnels is still based on empirical methods which have been successful in similar geological conditions. However, this analogical approach is defined in qualitative factors that are not clearly identified, and thus not consistently interpreted.

The followings cause more difficulties in the analysis of tunnels:

- Complex ground characteristics: inhomogeneity, anisotropy, time-dependency, etc.
- Inadequate knowledge of in situ values of analysis quantities: in situ stress, pore pressure, etc.
- Three-dimensional nature of tunnel deformation: longitudinal effects near the face.

6.1. EMPIRICAL CLASSIFICATION SYSTEMS

The empirical methods are based on ground classification systems. In this method, no analysis is in fact carried out. The tunnel supports are determined by identifying the category of the tunnel in one of the classification systems. Several classification systems have been proposed, of which Bieniawski's RMR method (1979) and Barton's Q method (1974) are widely used in practice. The recommended support system is defined in terms of a lumped score which is based on several quantified parameters.

These empirical methods are not intended to use universally as the basis for a complete design and construction of the tunnel, but as a simple support tool for tunnel designers. They are difficult to apply in difficult ground conditions, give insufficient

consideration to the effects of the in situ stress state, the dimensions and geometry of the tunnel, and the deformation response of the tunnel.

Because these methods are founded on correlations calibrated with real tunnel case histories, they may result in more realistic designs of specific tunnels. However, the tunnel relevancy to these cases through a single score quantity is hard to justify. Therefore, the applicability of these methods is limited to tunnels with very similar conditions as the case history tunnels, and these methods may not be used in tunnels constructed with advanced construction methods.

6.2. LIMIT STATE METHODS

In the second approach of tunnel analysis, the ground load on the support is estimated by the limit equilibrium of the ground block above the tunnel under its weight, the reaction of the support and the mobilized ground strength along the failure section. Different failure zones have been suggested in the literature (Caquot, 1966). Fig. 68 displays the failure zone proposed by Terzaghi.

A failure zone can develop in cases where the ground load is quite independent of the support response. The ground wedge between the ground surface and tunnel in shallow tunnels, and a pending rock block are instances in this regard (Fig. 69). In deep tunnels, however, a failure zone would develop at exceedingly high deformations, which may not be justified at service conditions.

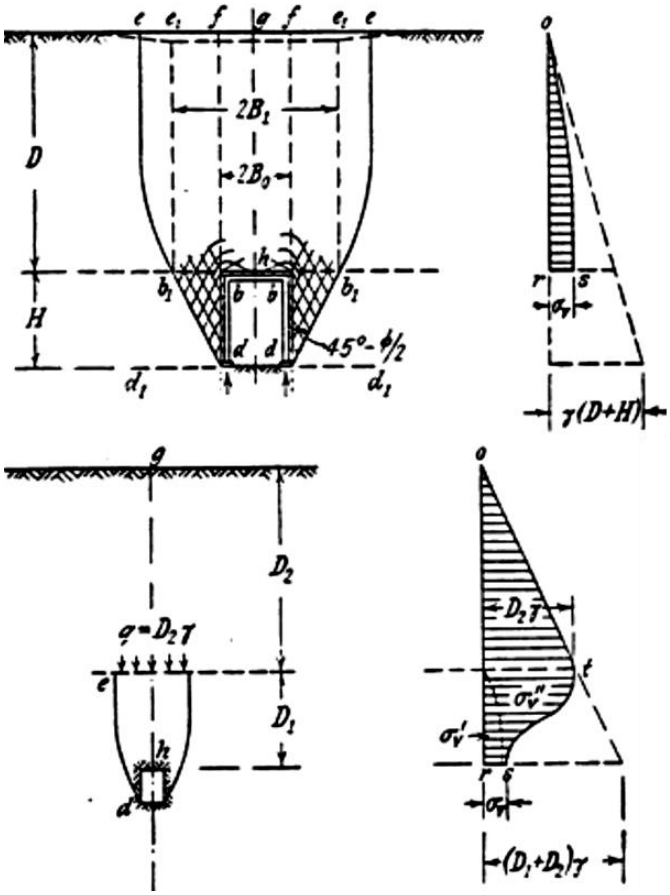

Figure 68: Terzaghi's limit state method for shallow and deep tunnels

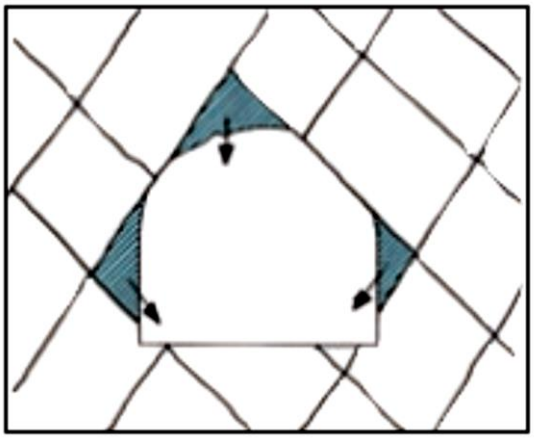

Figure 69: Impending rock blocks supported by tunnel linings

6.3. ANALYTICAL SOLUTIONS

Analytical solutions have also been derived to estimate the response of tunnels in ground with variety of behaviors. These methods are analytical solutions developed for tunnels using continuum mechanics. They can estimate the order of magnitude of the ground-support interaction forces and displacements.

In general, these solutions hold under certain simplifying assumptions. Kirsch's solution is the analytical solution for an unlined deep circular tunnel in an infinite ground with linear elastic behavior (Hoek et al., 2000). The analytical solution for an elliptical tunnel can be found in Poulos and Davis (1974). Detourney and Fairhurst (1987) proposed an analytical solution for an unlined circular tunnel in an infinite ground with Mohr-Coulomb elastoplastic behavior. They derived the solution in terms of the radius of plastic zone around the tunnel. These analytical solutions furnish an estimate of the displacements and stresses around deep tunnels within order of magnitude. Based on Mindlin's solution, Sagaseta (1988) obtained analytical solutions for the stress distribution around the tunnel as well as the ground surface settlement for unlined circular tunnels in a semi-infinite medium with homogeneous and isotropic linear elastic behavior. An analytical solution was derived in plane strain by Einstein and Schwartz (1979) for a cylindrical tunnel supported by a linear elastic shell which is applied instantly after excavation in an elastic infinite ground with homogeneous anisotropic initial stress state.

Analytical methods are very insightful because they feature the underlying mechanisms and their contribution to the global response of the ground to the tunnel excavation. However, because of simplifying assumptions made in these methods, they cannot describe the response of tunnels with complex geometry and or ground conditions in details.

6.4. HYPERSTATIC REACTION METHODS

In another type of approaches, the ground-structure interaction is accounted for more rigorously. In these approaches, the ground is represented by pre-loaded springs fixed at one end and supported by stress-free tunnel lining at the other end (Fig. 70). The loads on the tunnel lining are obtained after the interaction between the support and the springs are complete.

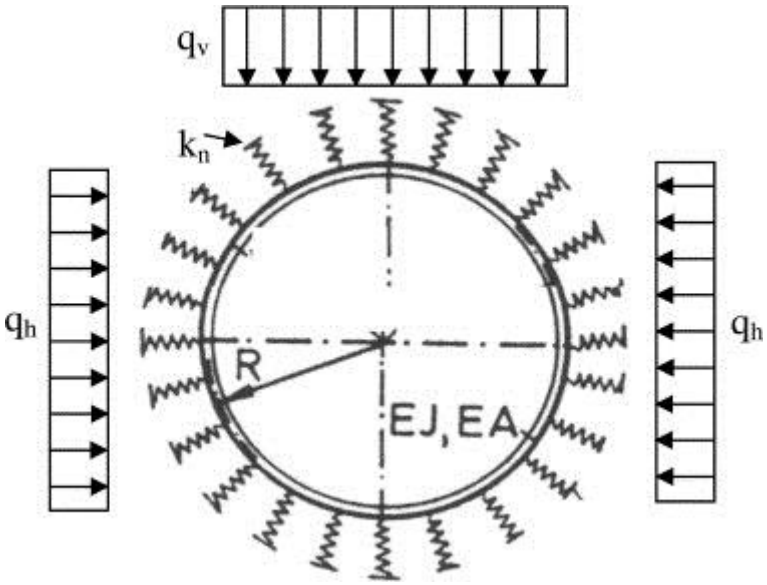

Figure 70: Ground action represented by springs and in situ stresses in hyperstatic reaction method

The concept is rather simple. Hence, this analysis is frequently used in practice. However, specification of the spring rigidities requires decent engineering judgment.

6.5. NUMERICAL MODELING

Numerical simulation is the most rigorous method of analysis. This method allows for the analysis of tunnels with any support material and geometry, any ground material

and conditions, different behaviors for the support-ground contact, and different tunnel excavation and support installation methods.

The aforementioned aspects are accounted for only in three-dimensional analyses. However, these analyses are used mainly for very complex underground facilities where the application of simplified methods is questionable (Fig. 71), for research on particular subjects, and for research on new construction methods (Shin et al., 2002). In practice, these analyses are seldom used because the calculations are demanding in terms of computational cost and time, particularly for models with nonlinear material behavior and interactions. The extensive amount of details in the obtained results needs decent skill and knowledge to interpret. Hence, they are not favorable in practice, where a number of sensitivity analyses are necessary because of the uncertainty in the geotechnical parameters.

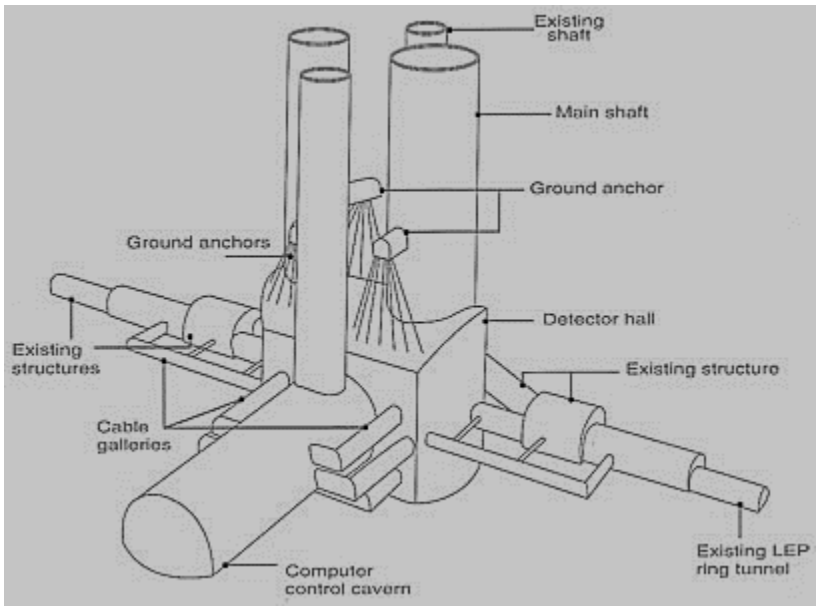

Figure 71: CERN underground facilities

Two-dimensional modeling, on the other hand, is generally more convenient for implementation and less time consuming in computation and interpretation of results. In many cases, two-dimensional plane strain analysis suffices to calculate simple tunnel geometry using certain simplifications to account for the three-dimensional face effect. When tunneling process is analyzed with plane strain finite element analysis, assumptions are typically made on the deformations prior to the installation of structural elements. Thus, these models account for the actual three-dimensional state of stress and deformation in the vicinity of the face area in an approximate manner.

The available two-dimensional approaches include the convergence-confinement method (Panet, 1995), gap method, disk calculation method, progressive softening method, volume loss control method, and hypothetical modulus of elasticity (HME) soft lining method. In the convergence-confinement method, which is the focus of this work, the longitudinal face effect is represented by a loss factor. The factor takes into account the amount of the ground stress release before the installation of the support. The next chapter addresses this method in more details.

Chapter 7: Convergence-confinement Method

Simplified two-dimensional methods are still typically used in practice to analyze the three-dimensional interaction between the ground and the supports of tunnels (Karakus, 2007). Convergence-confinement method (CCM) is a two-dimensional method, in which the tunnel cross-sections are assumed to deform in plane strain conditions throughout the excavation process. The plane strain analysis is motivated by predominantly transversal deformation of the tunnel. In order to simplify the ground-support interaction in one dimension, the tunnel is analyzed in axisymmetric conditions as well. Thus, CCM makes the following simplifying assumptions:

- Circular tunnel
- Infinite ground
- Plane strain conditions in tunnel cross-section
- Homogeneous ground and support
- Isotropic ground and support
- Uniform hydrostatic in situ stress state

As such, a single radial deformation (convergence) or its conjugate pressure at the tunnel locus can characterize the deformation and stress in the ground and in the support. This conjugate pressure accounts for the actual support pressure and a fictitious pressure representing the supportive effect of the ground ahead of the face (self-support). The self-support reduces from the in situ stress far ahead of the face to zero far behind the face. A longitudinal profile may be conceived for the self-support variation along the tunnel. It would decrease monotonically from the in situ stress far ahead of the face to zero far behind the face.

The reduction of the self-support is concomitant with an increase in the tunnel convergence (Fig. 72). The variation of the convergence along the tunnel is characterized by the longitudinal convergence profile (LCP) (Vlachopoulos and Diederichs, 2009). It would increase monotonically from zero far ahead of the face to the stabilized tunnel convergence, u, far behind the face. As depicted in Fig. 5, the net support convergence would be different from the ultimate ground convergence, u, by the tunnel pre-convergence at the support installation, u_0. The ultimate ground and support pressure, however, would be identical due to the vanishing self-support pressure.

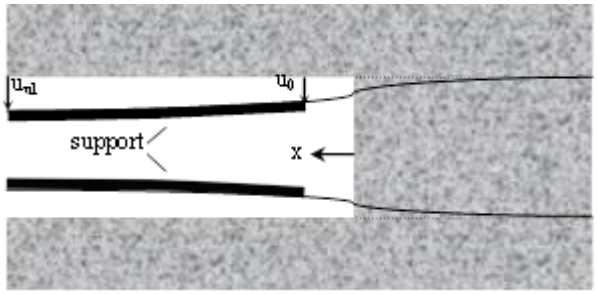

Figure 72: Longitudinal convergence profile (LCP)

The ultimate tunnel convergence and pressure can thus be calculated given the tunnel pre-convergence and the ground and support behavior at the ultimate state, as is shown schematically in Fig. 73. The ground and the support behavior are demonstrated by convergence curves. These curves are calculated by characterizing the ground and the support response to the tunnel convergence or the pressure. The pre-convergence is estimated by evaluating the longitudinal convergence profile at the support installation point. The ultimate condition may be represented by the intersection of the support and ground convergence curves.

As such, CCM is based on three characteristic curves, ground convergence curve (GCC), support convergence curve (SCC), and longitudinal convergence profile (LCP). Given the high level of certainty in the material properties of the support, SCC could be well constructed. GCC and LCP, however, require identification of the ground properties and response, which is quite complicated. The pre-convergence has also a significant effect on the calculated ultimate condition (Cantieni and Anagnostou, 2011). Small variations in the magnitude of the pre-convergence may lead to large variations in the resulting ultimate pressure, particularly in ground of highly nonlinear behavior.

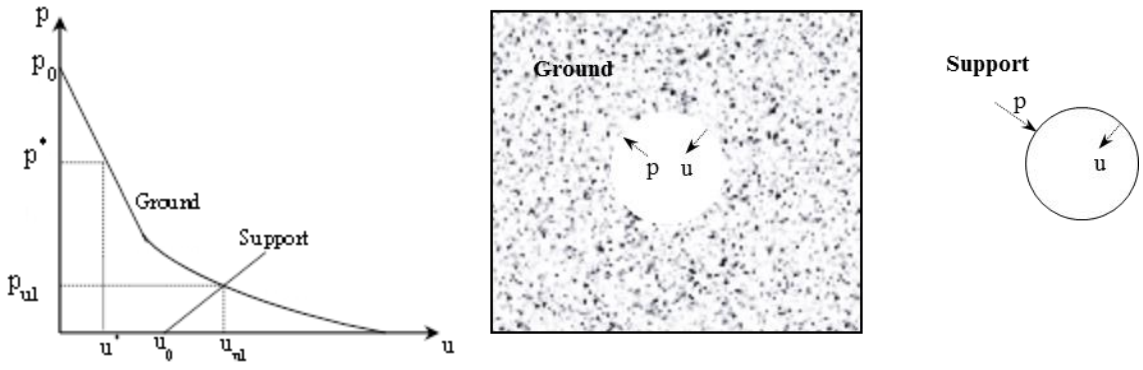

Figure 73: Convergence-confinement method (CCM)

The followings address the two approaches to assess the ground response and the pre-convergence.

7.1. CONVENTIONAL APPROACH

The convergence curve is conventionally constructed by calculating the tunnel convergence conjugate to the pressure at the tunnel locus (Panet, 1995).

In order to construct the ground convergence curve, a plane strain model of the tunnel under in situ conditions is created (Fig. 74). The in situ condition at the tunnel locus

is fulfilled by applying a pressure equal to the in situ stress p_0 on the tunnel locus. To find a point on GCC denoted by (u*, p*) in the plot in Fig. 6, the pressure at the tunnel locus is reduced from the in situ pressure p0 to pressure p*. The convergence u* is the convergence of the tunnel obtained at the end of this process. This approach has been followed in the variety of analytical and numerical calculation of the ground convergence curve in the literature (Jaeger and Cook, 1976; Panet, 1995; Carranza-Torres and Fairhurst, 1999). A pressure loss also accounts for the decrease in the face supporting effect before the support installation.

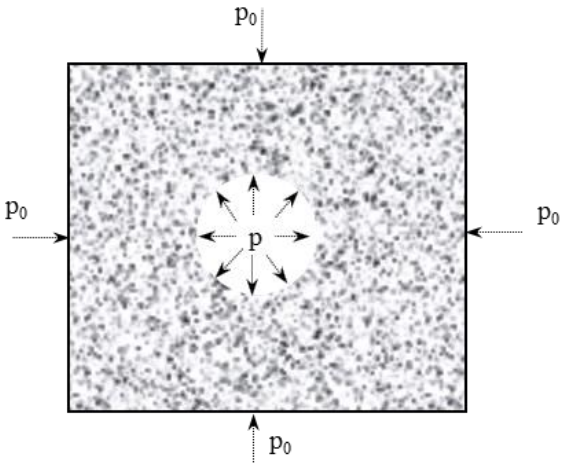

Figure 74: Conventional approach to calculate GCC

This pressure loss is obtained essentially by calculating the pre-convergence from LCP and then its conjugate pressure from GCC. Panet (1995) derived a pressure loss factor for tunnels in elastic ground following this approach. The loss factor increases from 0 to 1. A zero loss factor corresponds to a support installation far ahead of the face. Unit loss factor corresponds to a support installation far behind the face.

Determination of the pre-convergence, however, is not trivial. Indeed, it depends, in addition to the installation distance, on the ultimate convergence as well. Hence, the solution of a tunnel would lead to an implicit set of equations because the pre-convergence and the ultimate convergence are mutually dependent.

7.2. NEW APPROACH

This approach constructs the ground convergence curve by probing the ground response in terms of the tunnel convergence (Heidari and Tonon, 2013). To this end, a plane strain model of the tunnel under in situ conditions is created. As shown in Fig. 75, here, the in situ condition at the tunnel locus is fulfilled by constraining the radial displacement (convergence) of the tunnel locus. The tunnel convergence will be controlled by identical displacement of the constraints in the radial direction.

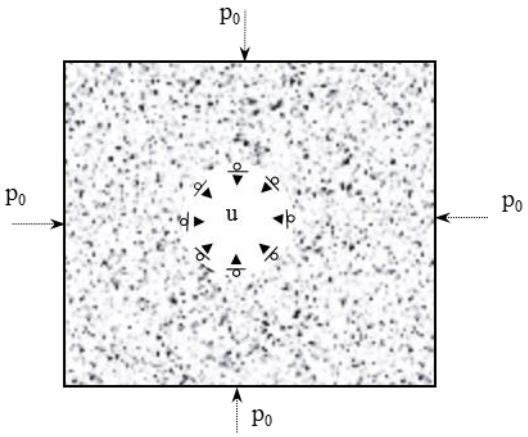

Figure 75: New approach to calculate GCC

To find a point on GCC denoted by (u*, p*) in Fig. 6, the tunnel convergence is increased from zero up to u* displacing the constraints. The pressure p* is the pressure between the constraints and the tunnel obtained at the end of this process. The support

installation instant can also be directly represented by allowing for a convergence equal to the tunnel pre-convergence. For tunnels in time-independent conditions, the calculated GCC will be the same as the GCC constructed by using the conventional approach. Accordingly, the approach will allow for a direct consideration of the pre-convergence, emphasizing the importance of LCP in CCM.

Considerable research has been performed to find accurate relations for LCP carrying out costly 3-D numerical analyses of incremental excavation and support installation (Panet and Guenot, 1982; Corbetta and Nguyen-Minh, 1992; Unlu and Gercek, 2003; Vlachopoulos and Diederichs, 2009; Pilgerstorfer and Radoncic, 2009). In order to utilize LCP for a tunnel in the elastic ground for a tunnel in the ground with elastic-plastic behavior, Corbetta (1990) made use of the notion of self-similarity: the profile for the elastic-plastic medium is produced by projecting the profile for an elastic medium from the origin (face) and with a projection scaling factor equal to the ratio between the elastic and elastic-plastic ultimate convergence (Fig. 76). Accordingly, he suggested the following single relation for the convergence profile along an unsupported tunnel.

$$u(x) = u_{un}\left[0.29 + 0.71\left(1 - e^{-1.5\left(\frac{2x}{\alpha D}\right)^{0.7}}\right)\right] \quad ; \quad \alpha = \frac{u_{un}}{u_{eun}}$$

where D is the tunnel diameter, and x designates the position of the cross-section along the tunnel axis (it is positive for cross-sections in the cavity and negative for the sections in the core ahead of the face). u_{un} and u_{eun} are respectively the elastic-plastic and elastic convergence for the unsupported tunnel. Recently, accounting for the extent and interaction of the plastic zones around the tunnel wall and face, Vlachopoulos and Diederichs (2009) proposed separate relations for convergence profile across the face. The LCP established for the unsupported tunnel may then be used as the basis for the LCP of the supported

tunnel, where the supports significantly affect the ultimate convergence as well as the whole profile along the tunnel.

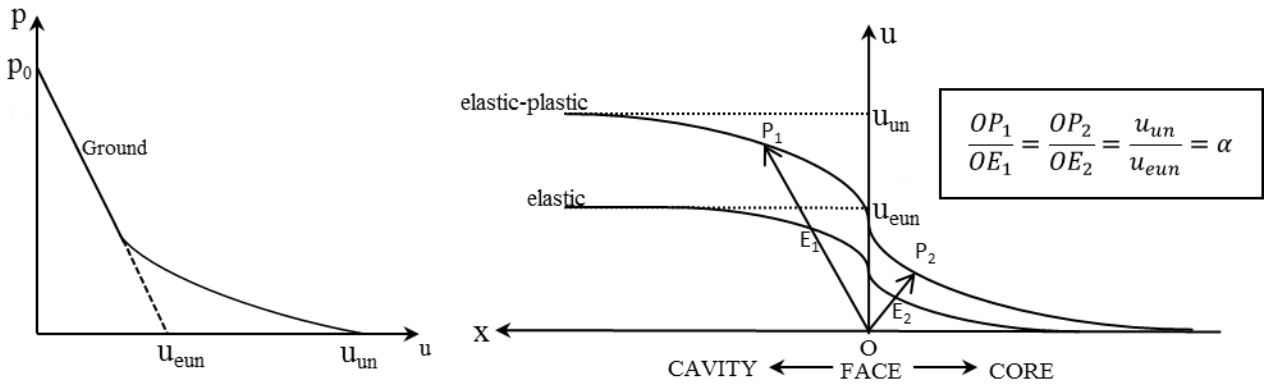

Figure 76: Similarity concept in estimation of LCP

In the presence of tunnel supports, the use of the same relation proposed for the unsupported tunnels would overestimate the LCP and thus underestimate the ultimate support pressure (A.F.T.E.S., 2001; Bernaud and Rousset, 1996). This observation prompted a new implicit refinement made by Nguyen-Minh and Guo (1998): on the basis of extensive numerical analyses, carried out with different support stiffness, installation distance from the face, and *in situ* stress, the authors incorporated the effect of the supports by scaling the convergence profile of the unsupported tunnel. Scaling factor $\varphi(z)$ is a function of the ratio between the ultimate convergence of the supported and the unsupported tunnel:

$$\frac{u_{sup}(x)}{u_{free}(x)} = \varphi(z) \leq u_{eq} \quad , \quad \varphi(z) = 0.55 + 0.45\, z - 0.42\,(1-z)^3 \quad , \quad z = \frac{u_{ul}}{u_{un}} \qquad (1)$$

where $u_{sup}(x)$ and $u_{free}(x)$ represent the convergence along the supported and unsupported tunnel, respectively (Fig. 77). Bounding the value of function $\varphi(z)$ to u_{ul} was

appended by Heidari and Tonon (2013). They demonstrated that the original relation may predict values greater than the supposed ultimate convergence for distances far from the face. In this implicit method, calculation of the initial convergence requires implicit solution of a non-linear equation because of the mutual dependence of the ultimate convergence and the initial convergence.

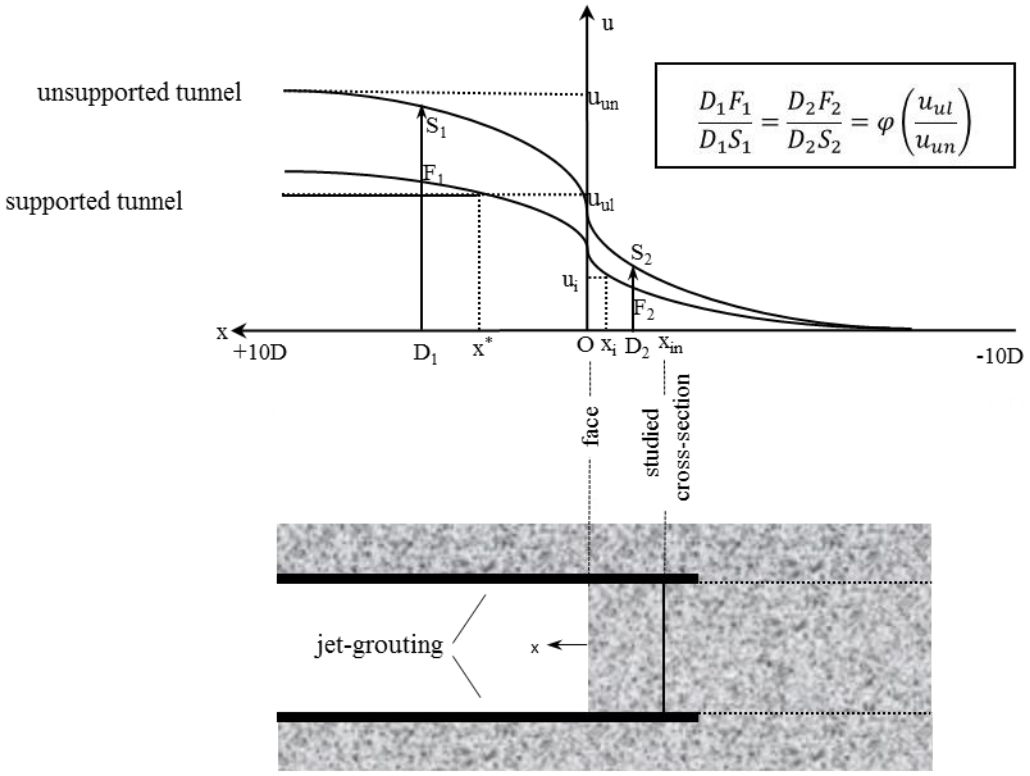

Figure 77: LCP for supported vs. unsupported tunnel (excavation face is at the instant of jet-grouting installation at the studied section)

Chapter 8: Ground Convergence Curve for Time-dependent Conditions

8.1. INTRODUCTION

Adequate estimation of ground deformation and support loads is central in modern tunnel design methods (Lunardi, 2008). With the advent of modern tunneling technology, more tunnels are driven in difficult ground conditions and supported by unconventional reinforcements. The ground and support behavior in these conditions are highly time-dependent due to a variety of time-dependent mechanisms. In the vast majority of practical cases, the time-dependent analysis of the ground-support interaction is simplified by assuming short- and long-term limit steady state conditions for the tunnel (AFTES, 2001). This assumption, however, may not be justified in general, particularly for mechanisms with a characteristic rate comparable to the tunnel construction rate.

Time-dependent mechanisms with a variety of characteristic rates may influence the tunnel response. Rheological ground behavior, pore water pressure redistribution (consolidation), and hardening of concrete-type reinforcements are time-dependent mechanisms that can have a rate comparable to the tunnel advance rate. In such circumstances, the ground-support interaction is strongly time-dependent during tunnel construction. This issue is manifested through the dependency of the tunnel response on the tunnel advance rate, as evidenced in a number of tunnel cases (Peck, 1969; Adachi et al., 1988, Sulem et al., 1987; Boidy et al., 2002). On the other hand, mechanisms such as ground or support weathering or accumulating damages due to successive ice and frost action or due to tunnel service (ageing) take place after the tunnel completion or with a rate significantly lower than the tunnel construction rate (Sandrone and Labiouse, 2010). These mechanisms may be disregarded in the analysis of ground-support interaction during tunnel construction, which is the focus of this work.

A number of models and approaches have been used to study the effects of ground viscous response on the tunnel. Panet (1979), Ladanyi (1980), Critescu (1985), to name a few, use viscoelastic rheological models to represent the ground delayed response in tunnels. Analytical solutions may be derived for these viscoelastic models. However, experimental studies show that the ground delayed deformation is almost plastic, and the delayed deformation appears for loadings beyond a specific limit. Accordingly, Berest and Nguyen-Minh (1983), Fritz (1984), Sulem et al. (1987), and Rousset (1990), Cristescu (1988), Boidy et al. (2002), Purwodihardjo and Cambou (2005), Debernardi and Barla (2009), Sterpi and Gioda (2009) used viscoplastic models for the ground time-dependent behavior. The solution of these models generally calls for numerical calculation methods. Based on in situ convergence measurements and a viscoplastic ground behavior, Sulem et al. (1987) showed that the delayed and immediate convergence due to tunnel excavation could be separated.

Several authors have studied the time-dependent effects of ground consolidation on the tunnel response. The change in the stress conditions at the tunnel boundaries generally induces volumetric deformation of the ground. This deformation entails the diffusion of the pore water, which is essentially a time-dependent process. The pore water diffusion can also be caused by the change in the ground hydraulic conditions at the pervious boundaries of the tunnel. A number of these studies pertains uncoupled analysis of the tunnel in drained steady state for different flow conditions at the tunnel boundaries (Bobet, 2003; Kolymbas and Wagner, 2007; Carranza-Torres and Zhao, 2009; Fahimifar and Zareifard, 2009). The results of these studies would be valid only for highly permeable ground conditions. In fact, several authors have shown that the response of the tunnel, in particular with pervious boundaries, is highly history dependent, and the uncoupled drained solution, by violating the actual coupled process in other ground conditions, may lead to inaccurate unsafe results

(Ohtsu et al., 1999; Graziani and Boldini 2012; Ramoni and Anagnostou, 2011). Several authors have performed coupled analyses accounting for the entire process of pore pressure dissipation around the tunnel (Carter and Booker, 1983; Giraud and Rousset, 1996; Li and Flores-Berrones, 2002).

Hardening of cast-in-place (CIP) cementitious supports is another source for the time-dependency of the tunnel response (Gschwandtner and Galler, 2012). Tunneling industry has long used CIP supports such as shotcrete, concrete lining, mortared rock bolts. Sub-horizontal jet-grouting is another type of CIP supports where an arch made up of a series of overlapped jet-grouted columns is implemented at the tunnel profile ahead of the tunnel face (Pelizza and Peila, 1993; Pichler et al., 2003; Heidari and Tonon, 2013). The arch controls the tunnel deformation since its very initiation ahead of the face (no pre-deformation). The progressive hardening of the mechanical properties of cement-based supports over time is well-established. Typically casted as the primary supports at or ahead of the tunnel face, the intense primary hardening of these supports is coincident to the evolution of the tunnel profile due to the face advancement. However, their mechanical response is still typically characterized by models with constant average properties (Pottler, 1990; Stille et al., 1989). In order to account for the time-dependent effects of support hardening, elastic behavior with evolving constants have been used in the literature (Pan and Huang, 1994; Oreste, 2003). Nonetheless, the high rate of tunnel deformation across the face typically causes loading of the support in excess of its premature low strength. Accordingly, elastoplastic models with hardening parameters have been developed in the literature (Hellmich et al., 1999; Lackner et al., 2002; Ulm and Coussy, 1995). In addition to the identification of the involved time-dependent mechanisms, the tunnel design in the preliminary phase calls for a simple yet representative analysis framework.

The convergence-confinement method (CCM) is widely used in the preliminary design of tunnels. CCM can reasonably characterize the three-dimensional ground-support interaction in tunnels by making use of less demanding two-dimensional plane strain models. The ground-support interaction is described in the method by the ground convergence curve, the support convergence curve, and the longitudinal convergence profile (Brown et al., 1983; Panet, 1995). The method has been well developed and applied for the tunnel response in time-independent conditions or in limit steady state conditions (Fahimifar and Zareifard, 2009; Alejano et al., 2010; Fang et al., 2013).

The method has also been applied to describe the coupled effects of different time-dependent mechanisms on the ground-support interaction during tunnel excavation. CCM was used for tunnels in ground with viscous behavior by Sulem et al. (1987), Pan and Huang (1994), for tunnels in consolidating ground by Callari (2004), and for tunnels with hardening supports by Oreste (2003), Graziani et al., 2005. Because of the time-dependency of the analysis, the results depend on the time variation of the quantity that controls the analysis. Accordingly, the removal rate of the fictitious confinement pressure is also determined in all these coupled analyses.

This chapter presents an approach to calculate the convergence curve of tunnels in time-dependent conditions. In the approach, the convergence curves are still calculated by analyzing the plane strain model of the tunnel. The analysis, however, is alternatively conducted by controlling the tunnel convergence and calculating the fictitious confinement pressure. Accordingly, the time variation of the controlling quantity is determined by the provided longitudinal convergence profile of the tunnel. The approach is employed to calculate the convergence curve of a tunnel in the time-dependent conditions, in particular with characteristic rates comparable to the tunnel advance rate. To this end, a finite element plane strain model of the tunnel is constructed, where the time-dependent behavior of the

ground and the jet-grouting is represented by a viscoplastic and chemoplastic model, respectively. The calculated convergence curves show the capability of the approach to characterize the importance of the time-dependent mechanisms in the response of the tunnel.

GCC has been derived for tunnels in time-dependent conditions following the conventional pressure-based approach. The ground response to a load depends on the rate of the loading process as well. As a result, to calculate the convergence for a magnitude of pressure, the rate of the process of pressure reduction must also be determined. To this end, the reduction rate of the self-support pressure, which together with the support pressure comprise the fictitious pressure, need be determined. This rate is typically estimated by first establishing a correlation between the self-support pressure and the face distance. Then, the self-support pressure is expressed in time by taking consideration of the face advance rate. The self-support correlation with the face distance is essentially estimated from the longitudinal convergence profile. Panet and Guenot (1982) derived a correlation for elastic ground behavior based on the longitudinal convergence profile of the ground.

Different correlations have been used in the literature between the self-support pressure and the face distance. In order to account for shotcrete hardening in CCM, Oreste (2003) used the correlation suggested by Panet and Guenot (1982). To calculate GCC for a tunnel in viscoelastic ground, Pan and Huang (1994) used a correlation which was suggested for the convergence variation by Sulem et al. (1987). Callari (2004) used a linear variation for the self-support pressure to construct GCC for a tunnel in consolidating ground. The conventional approach used in these calculations, however, does not account for the effect of the support and the time on the loss factor.

In view of the proposed convergence-based approach, the pressure conjugate to a magnitude of convergence also depends on the rate of convergence increase process.

However, the new approach can readily provide us with the rate of the convergence increase.

The rate of the convergence increase can be readily derived based on the LCP and the advance rate of the tunnel face. If LCP and the advancement of the tunnel face is expressed by *u(x)*, *x(t)*, respectively, then

$$\frac{du}{dt} = \frac{du(x)}{dx} \cdot \frac{dx(t)}{dt}$$

The effect of support on LCP is well characterized by implicit methods (Nguyen-Minh and Guo, 1998). These improvements can be readily exploited in the calculation of GCC in time-dependent conditions to account for the support effect on LCP.

In order to characterize the effect of the ground time-dependent behavior on LCP, the concept suggested by Sulem et al. (1987) may be used. They suggested the following empirical relation for the convergence of tunnels in viscous ground.

$$C(x,t) = C_1(x)\,[1 + m\,C_2(t)]\ ;\ C_1(x) = C_{\infty x}\left[1 - \left(\frac{X}{X+x}\right)^2\right];\ C_2(t) = 1 - \left(\frac{T}{T+t}\right)^n$$

where $C_{\infty x}, X, T, m, n$ are parameters that need to be calibrated. In this relation, $C_1(x)$ represents the LCP for the tunnel excavated infinitely fast (excluding delayed deformation). Preserving the notion of separation between the temporal and the spatial contributions, function $C_1(x)$ may be replaced by possibly more appropriate LCP's in the literature. Parameter 1+*m* represents the ratio between the ultimate tunnel convergence obtained in an infinitely fast and infinitely slow excavation. Function $C_2(t)$ represents the tunnel convergence variation over time after the tunnel is excavated infinitely fast. As such, functions $C_1(x), C_2(t)$ and the parameter m can all be obtained from simple plane strain test or analysis of the tunnel.

The ensuing sections will give in detail the procedure to construct GCC for a tunnel in time-dependent conditions. In order to characterize the importance of each individual

time-dependent mechanism, we first consider only the hardening of the jet-grouting by calculating the GCC of a jet-grouted tunnel in ground with time-independent behavior.

8.2. JET-GROUTED GROUND CONVERGENCE CURVE

This section calculates GCC for a tunnel with a sub-horizontal jet-grouted umbrella. The calculated GCC accounts for the time-dependency due to the jet-grout progressive hardening (increase of strength and stiffness with time). The GCC is computed point by point by analyzing a plane strain finite element model. In the analysis, the de-confinement process is applied by a controlled increase of the tunnel convergence. The hardening of the jet-grouting is also simulated by successive embedding of jet-grouting elements. The section concludes with an example and a comparison with the result of a progressively excavated 3-D finite element analysis. By computing the tunnel GCC for two advance rates, the importance of the approach is shown in the selection of the excavation rate.

The use of jet-grouting in the construction of tunnels is becoming increasingly common as an effective pre-confinement action to control surface settlement, tunnel convergence (pre-convergence in particular), face extrusion, and hence provide stability in tunnels excavated in difficult stress-strain conditions (Lunardi, 2008) (Fig. 78).

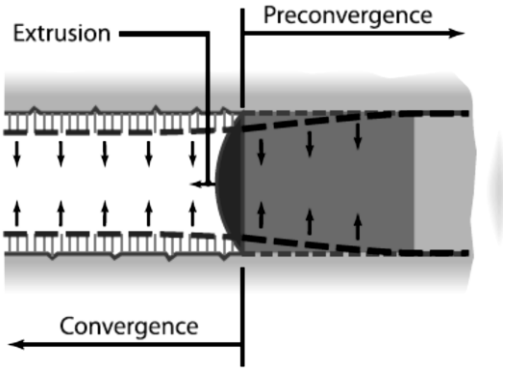

Figure 78: Different types of tunnel deformations (after Lunardi (2008))

Used for the first time in Italy in 1985, the technique involves installation of a set of sub-horizontal jet-grouted columns *ahead* of the tunnel face in order to form an arch effect *ahead* of the tunnel face in conditions where such an arch would not develop naturally (pre-confinement). Jet-grout columns are usually installed using the single-fluid technique, each column being 0.3–0.7 m in diameter. As shown in Fig. 79, in order to provide sufficient overlapping, the jet-grouted arches are installed in partial cone sections (umbrellas).

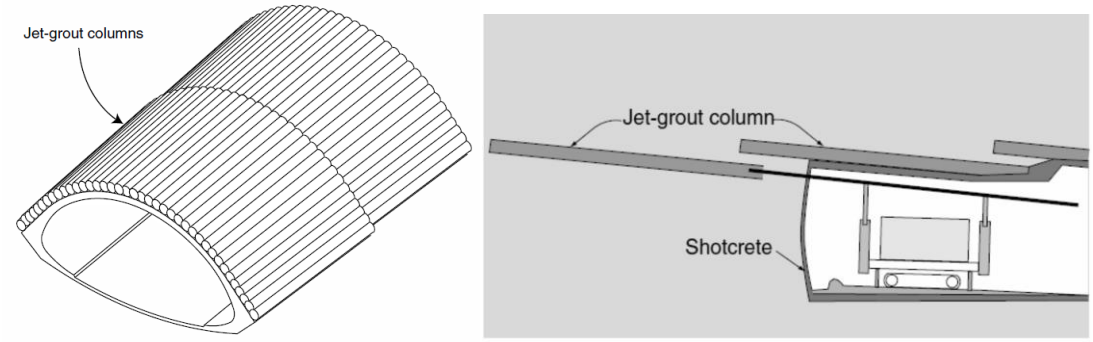

Figure 79: Jet-grouting umbrella

Sub-horizontal jet-grouted umbrellas typically experience loading at their early ages, when their rigidity has just started to develop; as a result of grout hardening, the mechanical behavior of each jet-grouted umbrella varies over time (Coulter and Martin, 2006). Because the jet-grouted ground is a cement-based material, it takes weeks for the jet-grout to achieve an appreciable amount of its final rigidity. On the other hand, for tunnels excavated in ground with time-independent behavior, tunnel convergence typically takes place within a few tunnel diameters (Graziani et al., 2005). Given the practical limitations on the length of sub-horizontal jet-grouted columns (16-20 m) and the excavation rates used in practice (0.6-1.5 m/day), loading of a jet-grouted umbrella begins

right after jet-grouting, during the period of marked mechanical property improvement. When analyzing tunnels with a jet-grouting umbrella, it is not possible to assume that the jet-grout has developed its full stiffness (this would be valid only for unrealistically low advance rates). Even for linings installed in the cavity *behind* the tunnel face (confinement), it is well known that the lining progressive hardening affects the lining stress and deformation especially in ground of low stiffness (e.g., Cosciotti et al., 2001; Oreste, 2003, Boldini et al., 2005; Graziani et al., 2005), where jet-grouting is typically used.

Convergence curves are typically obtained by unloading the tunnel under plane strain conditions. Because of the rate-independent behavior of the materials, the results are independent of the time history of the unloading process. However, in jet-grouted tunnels the ground convergence typically takes place in the same time interval as the jet-grout hardening process. This renders the analysis of these tunnels strongly time-dependent, similar to ground-shotcrete interaction analyzed by Pottler (1990), Oreste and Peila (1997), Boldini et al. (2005), Graziani et al. (2005), and Oreste (2003, 2009), among others.

Quite distinct convergence curves would therefore be obtained assuming different jet-grout rigidities acquired at different ages. For a tunnel with a hardening jet-grouting umbrella, using a mean value for the jet-grout properties would not be realistic and may fail to accurately estimate the true ultimate and transient conditions in the tunnel supports and in the ground. Ignoring jet-grout hardening could even lead to a paradox in the analysis of the tunnel. Recently, Cantieni and Anagnostou (2011) showed that, in an overstressed ground, assuming full stiffness for the shotcrete support may give rise to a counter-intuitive outcome: the tunnel in a ground with higher mechanical properties would require stronger support. The significance of the jet-grout hardening on the behavior of the tunnel thus requires taking jet-grout hardening into account in predicting tunnel deformations and stresses.

Consideration of jet-grout hardening essentially calls for a complex three-dimensional numerical model that incorporates the installation of the jet-grout umbrellas ahead of the face, updates the jet-grout mechanical behavior, and simulates the tunnel incremental excavation advance and possibly the installation of further supports in the cavity (e.g., Pichler et al., 2003). However, at the preliminary design stage, where a number of alternative schemes are to be considered, these sophisticated models would be impractical because they entail substantial time, effort, and skill in setting-up the models and interpreting the output data. Alternatively, the convergence confinement method, hereafter called CCM, provides the designer with a rapid and versatile means for evaluating various preliminary choices. CCM can be effectively used to estimate the supports load, the extent of the ground plastic zone, and the magnitude of the deformations. It can also be used to update the measured geo-mechanical properties of the ground by back analyzing the *in situ* measurements during tunnel excavation (Oreste, 2009).

However, this method does not take into account any time-dependent behavior of the material. In an effort to derive the convergence curve for a shotcreted tunnel incorporating shotcrete hardening, Oreste and Peila (1997) proposed a finite difference procedure, in which the stiffness of the shotcrete lining is updated. The derived convergence curve of the shotcreted tunnel is derived assuming elastic behavior for the shotcrete and a relation between the distance to the face and a fictitious pressure representing the core arch effect.

In this section, CCM is extended for tunnels with hardening jet-grouting umbrellas by employing the tunnel *convergence* as the controlling parameter in the analysis of the tunnel cross-section. The convergence at a given distance to the tunnel face is calculated by exploiting the same relations as used to estimate the initial convergence in the conventional CCM. The progressive hardening of the jet-grouted material is numerically

represented by adding material elements with rigidities equal to the developed increment in the material's rigidity and strength. The applicability of the method is illustrated by an example, where the convergence curves for a jet-grouted tunnel with different rates of excavation are derived. The derived convergence curve allows for the estimation of the stresses developed in the support(s) as well as in the jet-grouting umbrella.

8.2.1. Proposed procedure

The starting point in the proposed procedure is the same basic model used to derive the convergence curves in the conventional CCM, i.e. a two-dimensional plane strain model of the studied circular section of the tunnel.

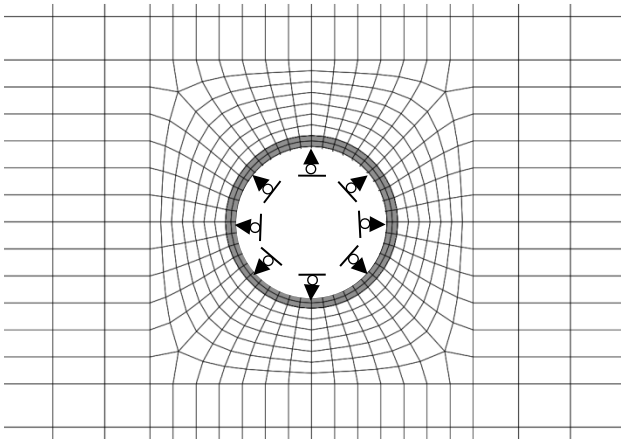

Figure 80: Plane strain finite element model of tunnel

However, the process of de-confining the tunnel is controlled here by using the tunnel convergence as the controlling parameter (Fig. 80): the tunnel convergence is increased by a prescribed amount, and then the pressure needed to reach equilibrium is calculated in the finite element plane strain model. This is in contrast to the conventional

convergence-confinement method, where the internal pressure is used as the controlling parameter, and is progressively decreased to zero (e.g., Panet, 1995).

In order to relate the properties of the jet-grouting to the convergence at a given cross-section, one needs to express the hardening of the jet-grouting in terms of the cross-section distance to the face. This may be accomplished by considering the schedule used for the construction of the tunnel and of the jet-grouting umbrella. Given the excavation advance rate, the age of the jet-grout may readily be calculated at any distance of the studied cross-section to the excavation face. Such a distance increases monotonically from the distance of the cross-section to the face at the instant of the installation of the jet-grouting umbrella (x_{in} in Fig. 77).

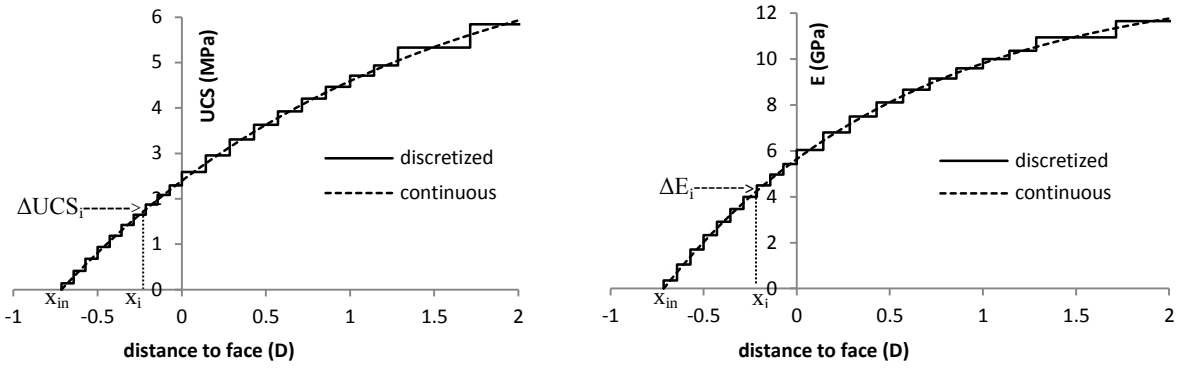

Figure 81: Discretization of jet-grout hardening: (a) strength; (b) stiffness

The pressures and the associated convergences obtained constitute the convergence curve of the tunnel. The algorithm is as follows:

1) Choose a value for the ultimate convergence, u_{ul}.

2) Use Eqn. 1 to find convergence vs. distance to the tunnel face.

3) Let D be the tunnel diameter. Discretize the considered interval of the distance to the tunnel face, e.g., $[-10D,+10D]$, into sub-intervals $[-10D, ..., x_i, ..., +10D]$.

4) For each abscissa x_i:

- Calculate convergence u_i by using Eq. (1) (Fig. 77).
- If $x_i<x_{in}$: The jet-grouting has not yet been installed. Hence, the finite elements at the location of the jet-grouting columns are still composed of the *in situ* ground.
- If $x_i=x_{in}$ (Fig. 77): Replace the ground elements at the location of the jet-grouting columns by stress-free jet-grout elements with $E=\Delta E_1$ and $UCS=\Delta UCS_1$.
- If $x_i>x_{in}$: Calculate the increments in jet-grout Young's modulus, ΔE_i, and strength, ΔUCS_i (Fig. 81), and then embed finite elements with Young's modulus ΔE_i and ΔUCS_i into the existing finite elements for the jet-grout.
- Radially displace the constraints at the tunnel profile (Fig. 80) by the convergence increment u_i-u_{i-1}.
- Run the plane strain finite element model to update stresses and strains in the jet-grout and the ground, as well as the reaction pressures on the supports at the tunnel profile, p_i (Fig. 82).

5) The reaction pressure p_{ul} on the supports at the tunnel profile computed for the last $x_i=10D$ would be the pressure in equilibrium with the convergence u_{ul} (Fig. 82). The point (u_{ul}, p_{ul}) is plotted on the (u,p)-plane of the convergence curve (Fig. 82).

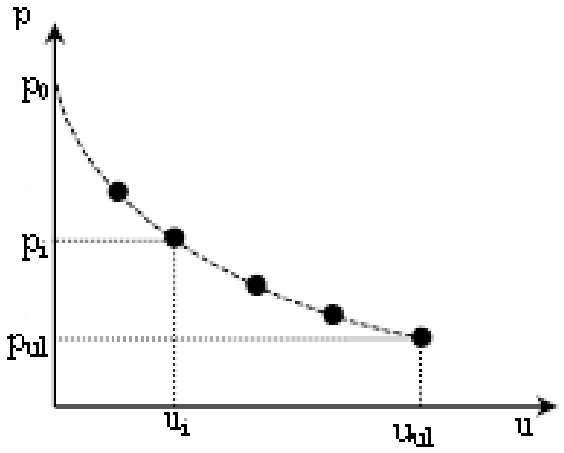

Figure 82: Reaction pressure on supports at tunnel profile vs. tunnel convergence

In addition to the estimation of the stresses and deformations induced in the tunnel supports and the ground, this algorithm also allows for the estimation of the stresses induced in the jet-grout itself. Referring to step (4) above, every single jet-grout element is indeed composed of a number of embedded elements. Therefore, the stresses at a point in the jet-grout are calculated by adding up the stresses in all of the embedded elements at that point.

However, the average ultimate pressure in the jet-grout can be readily estimated by using the convergence curves for the ground with and without jet-grouting. The pressure p_{ul}, associated with the ultimate convergence u_{ul} in the computed convergence curve of the jet-grouted tunnel, represents the pressure between the added support and the jet-grouting umbrella (internal pressure to the jet-grout). On the other hand, the pressure p_{ext}, associated with the same ultimate convergence u_{ul} in the convergence curve of the ground without jet-grouting, reflects the pressure between the ground and the jet-grouting (external pressure to the jet-grout). Having calculated the internal and external pressures across the jet-grouting umbrella, the mean stress p_c, developed in the jet-grout, can be calculated by

taking into account the axisymmetry and equilibrium of the ring according to Mariotte's formula as

$$p_c = (p_{ext} - p_{ul}) \cdot \frac{D}{2t} \quad (2)$$

where t designates the thickness of the jet-grouting ring.

8.2.2. Example and results

This section illustrates the suggested approach by means of a realistic example. The remarkable performance of Eqn. (1) is also verified by comparing the predicted LCP with the result obtained with an axisymmetric analysis incorporating the progressive excavation, and jet-grouting installation and hardening. The convergence curve refers to the ground encountered in the Cassia 2 tunnel constructed in Rome (Italy) using the ADECO (Tonon, 2011). The tunnel analyzed here is 14 m in diameter and jet-grouting is carried out as in the actual tunnel: sub-horizontal columns are 0.5-m thick and 16-m long, with an 8-m overlap. The tunnel is assumed to be excavated at a constant average rate of 1 m/day in the clay of the actual tunnel, which is modeled an elastic-perfect plastic medium of the Mohr-Coulomb type. At difference with the Cassia 2 tunnel, which was a shallow tunnel, the tunnel in this example is assumed to be subjected to a hydrostatic state of stress of 1 MPa. The numerical analyses were carried out using the finite element code ABAQUS. The parameters for the mechanical behavior of the ground and jet-grout used in the analyses are given in Table 7.

Because jet-grouting umbrellas overlap, a typical tunnel cross-section involves layers of jet-grouting with different ages. In this simulation, the jet-grouting umbrella is composed of two layers, the extrados being older. A preliminary axisymmetric analysis was carried out assuming a hardening linear elastic behavior. The results indicated jet-grout stresses greater than the developed strength estimated and the parameters in Table 7. Unlike

permanent tunnel supports, which are designed to behave within their elastic range at the serviceability level, inelastic deformation may be acceptable for the jet-grouting umbrella used as pre-confinement. Nevertheless, the confinement supplied by other supports added in the cavity would preclude structural failure of the jet grouting due to pervasive deformations and cracking. Accordingly, a hardening elastic-plastic behavior of Mohr-Coulomb type with constant friction angle and varying cohesion was assumed for the jet-grout in the computations herein. The varied cohesion is calculated by requiring the model to supply UCS described in section 3.2.

Ground properties	**Value**
Young's modulus (MPa)	200
Poisson's ratio	0.49
Internal friction angle (degrees)	0
Dilation angle (degrees)	0
Cohesion (MPa)	0.2
Jet-grout properties	**Value**
Ultimate Young's modulus (E_{ul}) (GPa)	13.5
Stiffness growth constant (k_s) (day^{-1})	0.054
Poisson's ratio	0.2
Internal friction angle (degrees)	20
Ultimate uniaxial compressive strength (UCS_{ul}) (MPa)	8
Strength growth constant (k_{ucs}) (day^{-1})	0.036

Table 7: Ground and jet-grout mechanical parameters

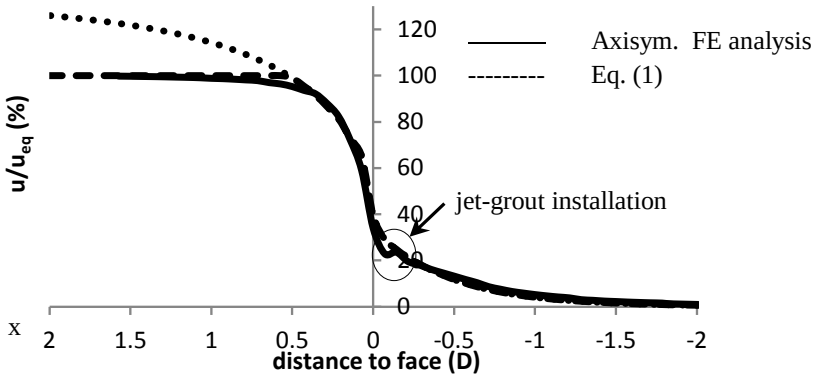

Figure 83: Performance of Eq. (1) vs. axisymmetric analysis result

Shown in Fig. 83 is the LCP predicted by Eq. (1): it is in striking agreement with the profile obtained from the axisymmetric analysis of the jet-grouted tunnel. When young jet-grouted soil material is substituted for the original ground material in a finite element, the pre-stressed soil elements are substituted for by stress-free jet-grouted soil elements. A single jet-grouting umbrella is created by overlapping columns along the tunnel profile; the columns are installed in a particular sequence so that sufficient time is allowed for hardening of adjacent columns before installing the intermediate column. However, in this simulation, for the sake of simplicity, an entire jet-grouting umbrella is implemented at once. Consequently, the contribution of jet-grouting installation in our analysis may be overestimated. Nevertheless, the deviation from the predicted curve in Eq. (1) is negligible.

Fig. 84 (b) shows that the derived convergence curve for the jet-grouted tunnel lies significantly lower than the curve for a tunnel without jet-grouting umbrella. The initial linear part, associated with small tunnel convergence, can be explained by the elastic behavior of the ground and of the jet-grout ring at small deformations. However, it should be noted that such small convergences could not be obtained even if an infinitely rigid cavity support were installed right at the face. As Fig. 84 (a) illustrates, small ultimate convergences (e.g., u_{ul}=1 cm) are associated with LCP's that reach the ultimate

convergence, u_{ul}, ahead of the face. For an infinitely rigid support, the installation abscissa corresponds to the abscissa where the LCP reaches the ultimate convergence. Fig. 84 (a) indicates that such a support must be installed ahead of the face in order to limit the convergence to the elastic range of the ground-jet-grouting composite. The minimum convergence attained by using a cavity support would thus be associated with an LCP that reaches the ultimate convergence at the face, being about 2.5 cm in this example (Fig. 84 (a)); this would be achieved by installing an infinitely stiff lining at the face. The convergence curve for the jet-grouted tunnel ends up with a negative curvature, whereas a positive curvature is displayed by a tunnel with no jet-grouting. The latter implies a softening ground response as a result of progressive expansion of the plastic zone around the tunnel. In the jet-grouted tunnel, the progressive hardening of the jet-grouting umbrella retards this process and ends up dominating (thus controlling) the ground softening. Far from the tunnel face, the convergence for the tunnel with jet-grouting canopy but with no additional support is about 6 cm, whereas it is about 57 cm for the tunnel with no jet-grouting canopy and no additional support. This 90% reduction clearly indicates the high performance of jet-grouting in protecting the tunnel from excessive deformations particularly in ground of low strength (S_u=200 kPa) and Young's modulus (E=200 MPa).

As explained in Section 8.2.1, the ultimate stresses in the jet-grouting umbrella may be readily estimated using the computed convergence curves. The pressures given by the curves in Fig. 84 (b) for an ultimate convergence represent the internal pressure (support-jet-grout) and external pressure (jet-grout-ground) on the jet-grouting umbrella. Hence, the vertical difference between the curves at the ultimate convergence determines the net ultimate pressure, and thus the ultimate circumferential stress developed in the jet-grouting umbrella. If no support is installed, the jet-grouting umbrella in the tunnel considered would undergo a net pressure of about 475 kPa. According to Eqn. (2), the circumferential

stress in the jet-grouting umbrella may be estimated as 3.8 MPa. This jet-grout stress, however, only refers to the ultimate condition far from the tunnel face.

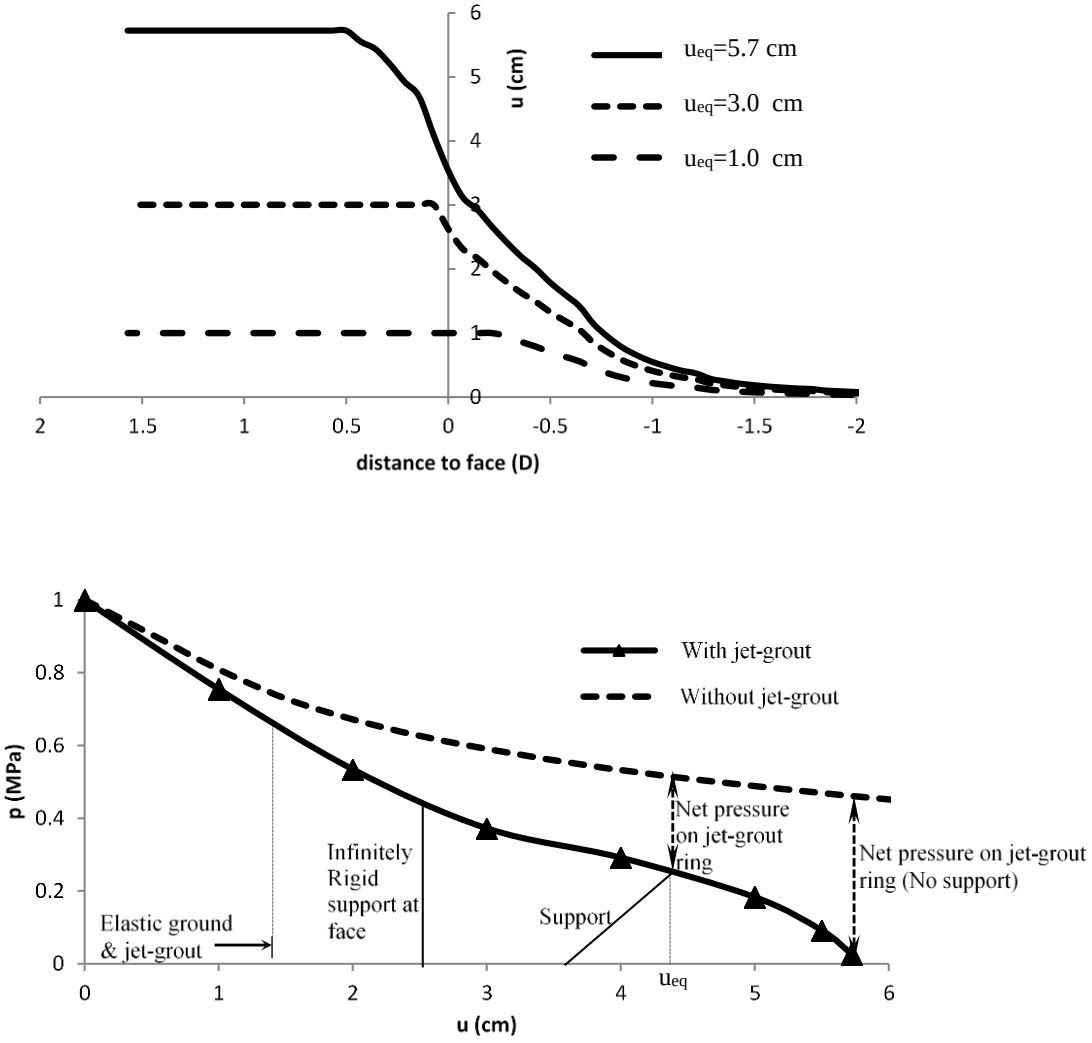

Figure 84: (a) Estimated LCP's; (b) jet-grouted tunnel convergence curve

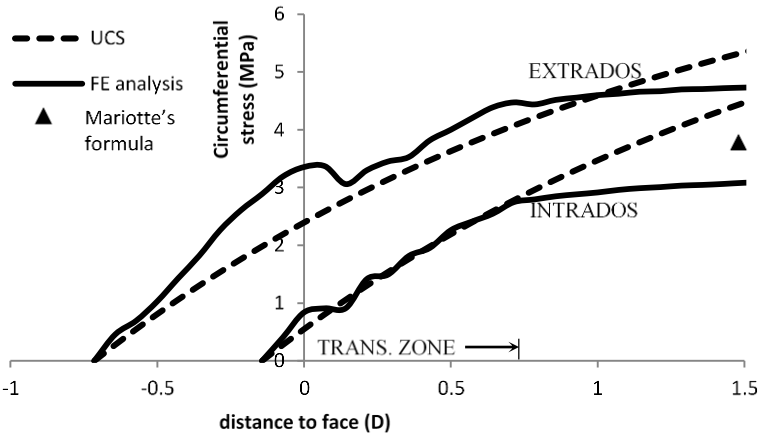

Figure 85: Circumferential stress vs. UCS developed in jet-grouting umbrella (no support)

The developed circumferential stresses as the tunnel face advances are shown in Fig. (85), and are calculated by adding up the circumferential stresses in all of the embedded elements. At a given cross-section, the external element of the jet-grouting umbrella belongs to a jet-grouting umbrella made prior to the internal umbrella. As a result, the mechanical properties and thus the stresses developed in the external and internal elements differ considerably. Nonetheless, the average circumferential stress as estimated before (3.8 MPa) agrees well with the average of the stresses in the two elements at the ultimate state far from the tunnel face (4.6 and 3.1 MPa, respectively). Due to the evolution of the jet-grout strength with time, the ultimate stresses nonetheless would not provide for adequate information on the performance of the jet-grouting. As inferred from Fig. (85), the jet-grouting umbrella undergoes loading as soon as it is installed, and it constantly yields within the entire period of loading (transitional zone). When the excavation face has not reached the studied cross-section (negative distance to the face), the developed circumferential stress in the jet grouting layers could indeed exceed the developed UCS because of the lateral confinement provided by the ground in the tunnel core; when the

excavation face progresses past the cross-section, the intrados is no longer confined (tunnel is assumed to be unsupported), but there is still some confinement applied by the inner umbrella to the outer umbrella. The jet-grout behavior shown here clearly indicates that, in order to obtain an accurate account of jet-grouting performance, the transient behavior of the jet-grouting should be carefully modeled.

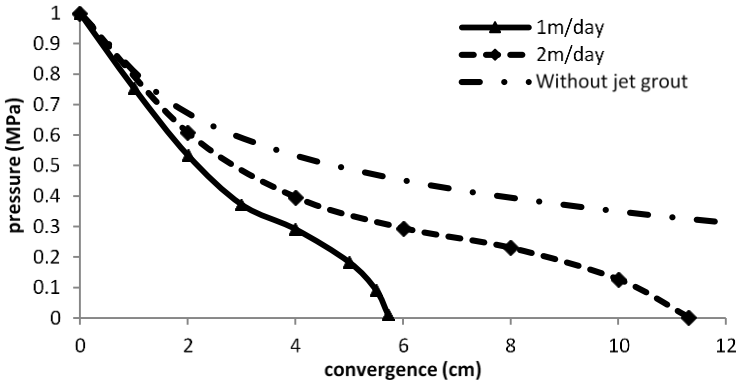

Figure 86: Convergence curves for different advance rates

The significance of jet-grout progressive hardening in the tunnel response may be illustrated by the convergence curves for two different excavation rates of 1 and 2 m/day (Fig. 86). With a higher excavation rate, lower stiffness develops in the jet-grout at the same distance to the face. This reduces the protective effect of the jet-grout and thus gives rise to a convergence curve that lies on top of the 1 m/day curve. The impact of the excavation rate may be evaluated by comparing the convergences computed for the tunnel with no support; the convergence for the unsupported jet-grouted tunnel doubles (11.3 cm vs. 5.7 cm) when the excavation rate increases from 1 m/day to 2 m/day. The excavation rate also affects the stresses developed in the jet-grouting umbrella: slower advance rates would lead to higher ultimate pressures on the ring because of its higher stiffness,

developed over a longer period. All of these results apply if the ground does not exhibit time-dependent deformations (e.g. consolidation, creep) as assumed in this paper.

If the ground does not exhibit time-dependent deformations (e.g. consolidation, creep) as assumed in this paper, an elevated excavation rate may load the jet-grouted soil when it is too young to carry load, and this may yield greater tunnel deformations than in the case of a tunnel without a jet-grouting umbrella (Pichler et al., 2003). The proposed method could thus be very useful in order to optimize the advance rate for a specific tunnel. However, it must be noted that not only does a high advance rate decrease construction time and thus cost but it also reduces ground time-dependent deformations for example in clayey ground (Purwodihardjo and Cambou, 2005). Simulation of the jet-grouted tunnel in viscous ground is the subject of the next section.

8.3. JET-GROUTED VISCOUS GROUND CONVERGENCE CURVE

The following steps give the procedure for the calculation of GCC for tunnels in viscous ground.

1) *Set up a plane strain model of the tunnel with constraints at the tunnel locus:* As depicted in Fig. 8.
2) *Define the LCP for the tunnel in plain ground (no support) excavated at the given construction rate*: This LCP is obtained from an axisymmetric model of the tunnel. Alternatively, it may be obtained based on an LCP for the tunnel with no time effect. The time effect is then superimposed on this LCP by making use of the method suggested by Sulem et al. (1987), for instance.
3) *Suppose a magnitude for the ultimate convergence of the tunnel.*

4) *Modify the LCP in step (2) to accommodate the supposed ultimate convergence (support effect)*: By the value supposed in step (3), the LCP for the unsupported tunnel in step (2) can be adapted to account for the support effect. In this regard, the implicit methods may be employed.

5) *Calculate the installation distance of the jet-grouting rings with respect to the studied cross-section:* given the tunnel construction schedule, the distance at which the jet-grouting rings are installed at the studied cross-section can be determined.

6) *Express the variation of the convergence and the installation distance of the jet-grouting in time:* The LCP in step (4) defines the convergence variation with respect to the face distance. The LCP defined in step (4) and the jet-grouting distance calculated in step (5) can be used to define the time variation of the convergence and the installation instant of the jet-grouting.

7) *Apply the estimated convergence history to the radial constraints at the tunnel locus, and install the jet-grouting extrados and intrados accordingly through the analysis.*

8) *Calculate the pressure on the constraints at the end of the analysis defined in step (7):* This pressure together with the convergence supposed in step (3) define a point of GCC.

9) *Repeat steps (3)-(8):* these steps are repeated until a sufficient number of points on GCC are obtained.

This procedure is used below to construct the GCC for a jet-grouted tunnel in a viscous ground. The calculated GCC takes into account the time-dependency due to the hardening of the jet-grouting as well as the ground viscosity.

1) *Set up a plane strain model of the tunnel with constraints at the tunnel locus:* Fig. 87 shows the plane strain finite element model of the jet-grouted tunnel used in the

following calculations. The model includes a 200 m extension of the ground in each direction surrounding a tunnel with 14 m diameter.

The far field boundary conditions are imposed by constraining the displacement of the ground on one side, and applying the in situ ground stress on the other side in each direction. These boundary conditions prevent any volume-locking issue, particularly in undrained conditions. For a recent account of this issue, the reader is referred to Graziani and Boldini (2012). The highlighted ring around the tunnel represents the jet-grouted zone. Representing the stress conditions at Tartaiguille tunnel (100 m deep), the applied (total) in situ stress is equal to 2000 kPa. Accordingly, the in situ pore water pressure throughout the model is 1000 kPa.

The in situ conditions at the tunnel locus are satisfied by applying radial displacement constraints, which are not shown here. The initial pressure on these constraints will be equal to the in situ ground stress.

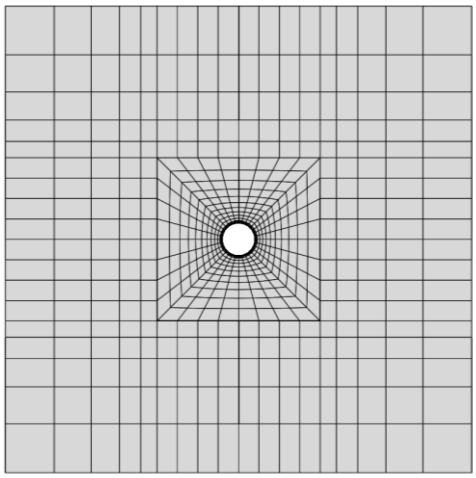

Figure 87: Plane strain finite element model

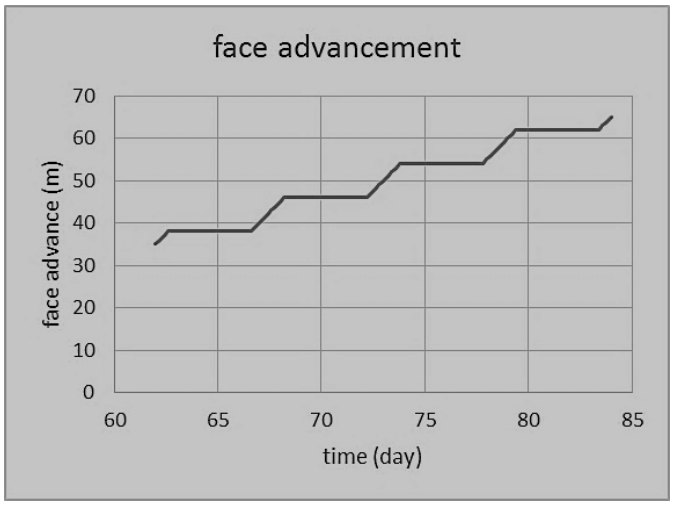

Figure 88: Face advancement in jet-grouted tunnel excavated at 5 m/day and jet-grouted in 4 days

2) *Define the LCP for the tunnel in plain ground (no support) excavated at the given construction rate:* Here, the LCP for the tunnel in plain ground is obtained from an axisymmetric model of the tunnel. The axisymmetric analysis accounts for the ground viscous behavior and the tunnel construction schedule.

In order to represent the viscous behavior of the ground, the advanced viscoplastic model CJS is used. Section 2.4 gives the model details and parameters, which are calibrated for Tartaiguille tunnel. In order to exclude the time-dependency due to ground consolidation, the analysis is carried out in the undrained conditions. Hence, a general uncoupled analysis is used where the ground response is composed of the soil skeleton response described by CJS model and the pore water response described by the water bulk modulus.

Fig. 89 gives the LCP of the tunnel obtained from the axisymmetric analysis of the tunnel in plain ground. This LCP is obtained for a tunnel where the face advances at 5 m/day and, stops for 4 days for jet-grouting operation (Fig. 88). The time-dependent behavior of the ground is implied in the jagged curve. The sharp

convergence increments in the curve represent the time-dependent deformation of the ground during stoppage of the face for the implementation of the jet-grouting. These convergence increments clearly show another adverse effect of jet-grouting. Delayed ground convergence occurs during the time required to implement jet-grouting. This adverse effect is seen to maximize when the jet-grouting takes place in the vicinity of the face. The adversity of the jet-grouting on tunnel deformation can also be seen in the extrusion of the face along the jet-grouting obtained from the axisymmetric analysis (Fig. 90). The face extrusion is seen to increase nearly 25% within the period of jet-grouting operation at the face.

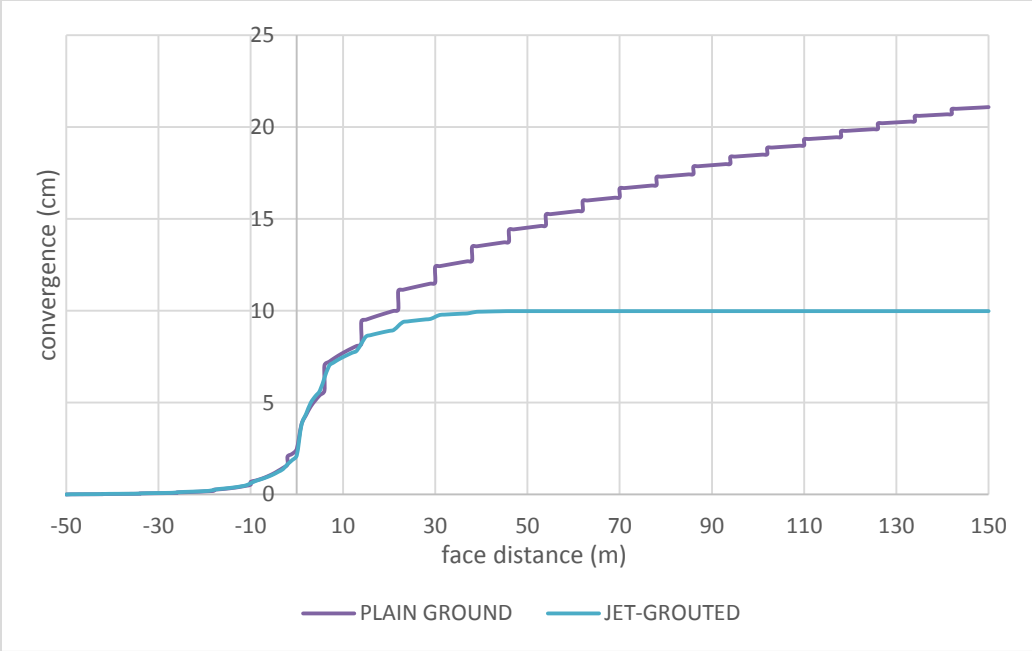

Figure 89: LCP of plain and jet-grouted ground for advance rate 5 m/day

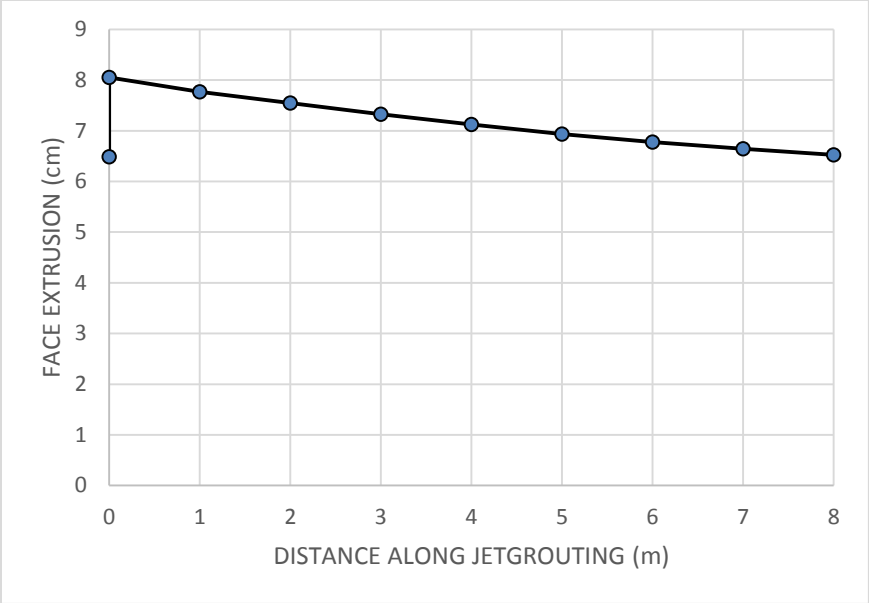

Figure 90: Face extrusion along jet-grouting umbrella for advance rate 5 m/day

3) *Suppose a magnitude for the ultimate convergence of the tunnel, and modify the LCP of the plain ground to accommodate the supposed ultimate convergence (support effect):* Here, for the sake of simplicity, the LCP for the (supported) tunnel with the supposed ultimate convergence is chosen to be identical to the LCP calculated in step (2) but limited to the supposed ultimate convergence.

In order to assess the accuracy of the estimated LCP, the LCP of the jet-grouted tunnel is also obtained from an axisymmetric analysis which takes into account the successive implementation of the jet-grouting. Shown in Fig. 89, the LCP of the jet-grouted tunnel almost coincides with the LCP of the plain ground for convergence values less than the ultimate convergence of the jet-grouted tunnel. This agreement justifies choosing the LCP of the supported tunnel as the LCP of the plain ground bounded by the supposed convergence magnitude.

4) *Calculate the installation distance of the jet-grouting rings with respect to the studied cross-section:* Here, the jet-grouting is modeled in two layers to represent the sub-horizontal (conic) implementation of the jet-grouting. The jet-grouting rings are 16 m long. The first 8 m of the jet-grouting is installed adjacent to the tunnel profile, and the second 8 m is installed farther from the tunnel profile. Hence, at a cross-section, the jet-grouting extrados is installed prior to the jet-grouting intrados. The installation distance of each layer depends on the location of the studied cross-section along the jet-grouting ring. Here, the jet-grouting extrados and intrados are installed 10 m and 2 m behind the studied cross-section, respectively.

5) *Express the variation of the convergence and the installation distance of the jet-grouting in time:* The LCP in step (3) defines the convergence variation with respect to the face distance. The tunnel face advance schedule allows to relate the face distance to time (Fig. 88). Fig. 91 shows the convergence history of the tunnel cross-section for the supposed ultimate convergence of 10 cm, where the installation instants of the jet-grouting extrados and intrados are also demonstrated.

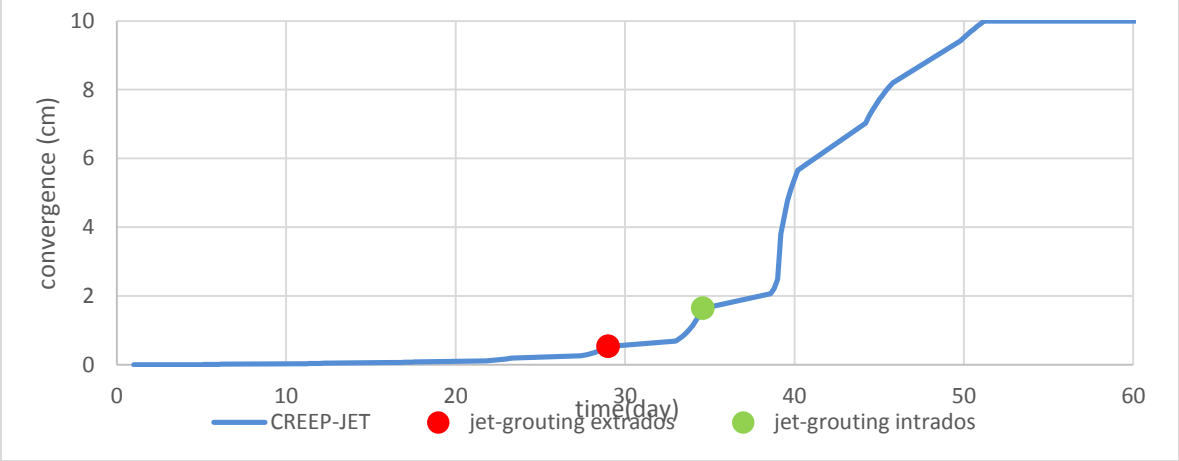

Figure 91: Convergence history for ultimate convergence=10 cm

6) *Apply the estimated convergence history to the radial constraints at the tunnel locus in the finite element analysis, and implement jet-grouting accordingly:* In the plane strain model in step (1), the radial inward displacement of the constraints at the tunnel locus is prescribed by the estimated convergence history. The jet-grouting layers are also installed at the calculated time by replacing the ground elements at the jet-grouting location with the stress-free jet-grouting elements. In order to account for the hardening of the jet-grouting rings, the chemoplastic model explained in section 3.3 is used.

7) *Calculate the pressure on the constraints at the end of the analysis defined in step (6):* The analysis outputs the ultimate reaction forces on the constraints at the tunnel locus. By dividing the sum of these forces by the tunnel perimeter, the ultimate pressure conjugate to the supposed ultimate convergence is obtained.

Ultimate convergence (cm)	Ultimate pressure (kPa)
10	4
8	235
6	502
4	827
2	1516
0	1987

Table 8: Supposed ultimate convergences and calculated conjugate pressures

Table 8 lists a number of supposed ultimate convergence magnitudes along with the calculated pressure for each magnitude. The data in Table 8 indicate that the convergence of the jet-grouted tunnel with no further supports would be nearly 10 cm. This

value agrees with the value obtained from the axisymmetric analysis (Fig. 89). This agreement implies that the LCP for the supported tunnel, as estimated above, could well represent the actual LCP (obtained from the axisymmetric analysis).

Each pair of convergence and pressure in Table 8 constitutes a point on the convergence-confinement plot shown in Fig. 92. These points in turn constitute the GCC of the tunnel.

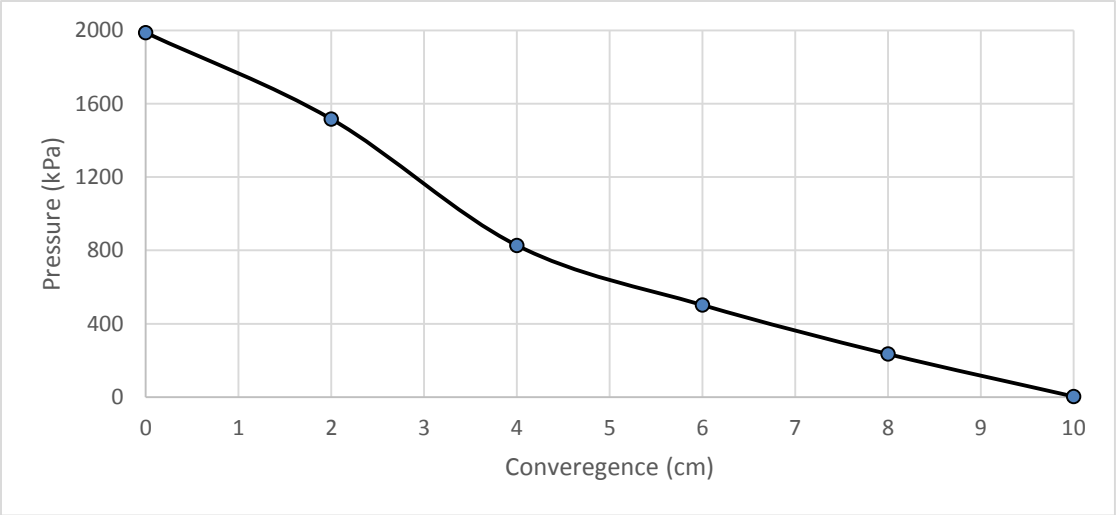

Figure 92: GCC for jet-grouted tunnel excavated at 5 m/day

Now, the effect of the advance rate on the tunnel response is investigated. The response of a tunnel in time-dependent conditions depends on the rate of the tunnel construction. In order to illustrate this dependency, the LCP of the tunnel in plain ground is shown in Fig. 93 for different advance rates. The time for the jet-grouting operation in each case is also extended proportionally. The increase in the advance rate results in reduced tunnel convergence because less delayed plastic deformation develops in the ground. Note that in the calculation of these curves, only the response of the plain ground is involved.

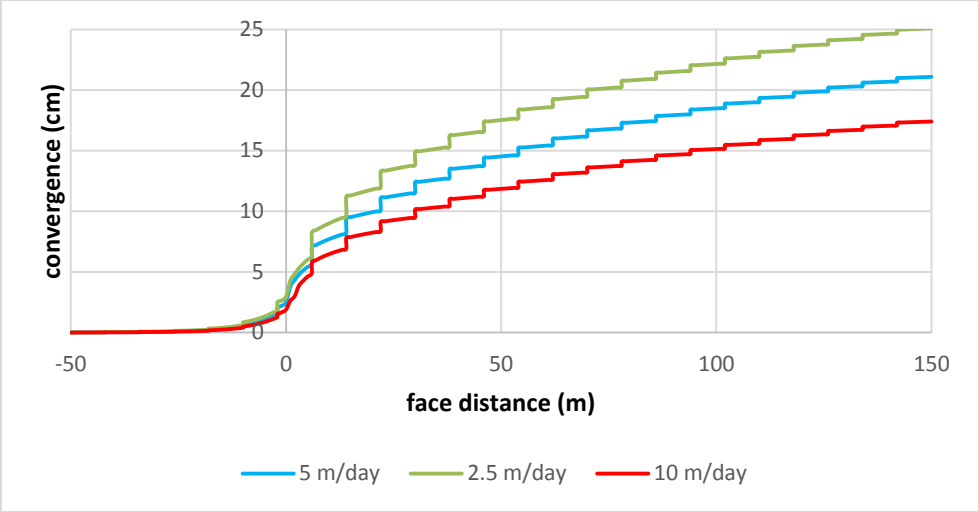

Figure 93: LCP of the plain ground for different advance rates

In order to investigate the effect of the advance rate on the response of the jet-grouted tunnels, the LCP of the jet-grouted ground (jet-grouted tunnel with no further support) is shown in Fig. 94 for different advance rates. By increasing the advance rate, the tunnel convergence increases. This result completely opposes the result obtained for the plain ground. This reversal in the dependency of the tunnel response to the advance rate indicates the dominancy of the jet-grouting time-dependent behavior.

The increase in the advance rate has an adverse effect on the performance of the jet-grouting. This adversity was well characterized in section 8.2.2, where the effect of the ground viscosity was excluded by considering only the immediate ground response. An accelerated tunnel advancement does not allow the freshly cast jet-grouting to harden. Therefore, by increasing the advance rate, the jet-grouting can in effect provide less support for the ground.

The existence of an optimum advance rate may be inferred by the reverse effects of the advance rate on the two time-dependent mechanisms. For the advance rates studied in Fig. 94, this adverse effect on the jet-grouting response overshadows the beneficial effect

in view of the ground viscous response. However, for quite low advance rates, the effect of the ground viscosity may dominate the effect of the jet-grouting hardening. To study this issue, the ultimate convergence of the jet-grouted ground with no support is plotted with respect to the advance rate in Fig. 95.

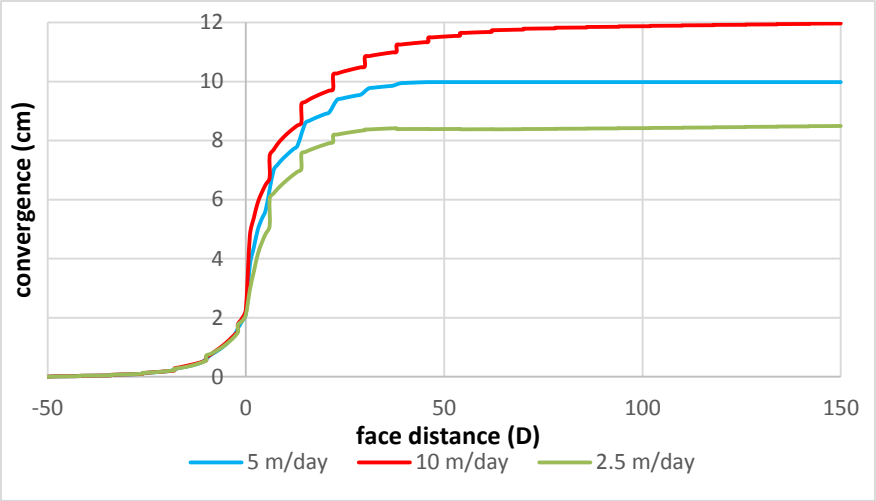

Figure 94: LCP of jet-grouted ground in viscous ground for different advance rates

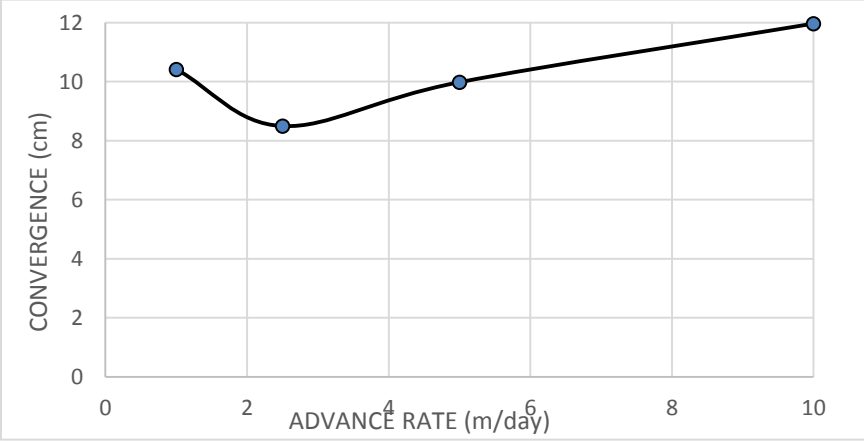

Figure 95: Ultimate convergence of jet-grouted tunnel for different advance rates

The results shown in Fig. 95 confirm the existence of an optimum advance rate at which the convergence of the jet-grouted tunnel minimizes. Fig. 95 indicates that high advance rates may have as adverse effect as low advance rates on the response of the jet-grouted ground. In low rates, the ground delayed deformation develops considerably although the jet-grouting is given adequate time to harden and thus to perform stronger. In high advance rates, the jet-grouting is not allowed to develop its strength and thus underperforms although the ground also does not have time to develop delayed deformation. In high advance rates, the jet-grouting may even escalate the tunnel convergence in the vicinity of the face. Fig. 96 contrasts the LCP of the plain ground and the jet-grouted ground for an elevated advance rate 10 m/day.

The Fig. 96 clearly shows that the tunnel convergence increases as a result of jet-grouting in the vicinity of the tunnel face. In this zone, the jet-grouting is very young with immature mechanical properties. Therefore, the jet-grouting responds even weaker than the in situ ground (Pichler et al., 2003). Furthermore, reaching an equilibrium between the annealed state of the jet-grouting and the surrounding ground entails tunnel convergence.

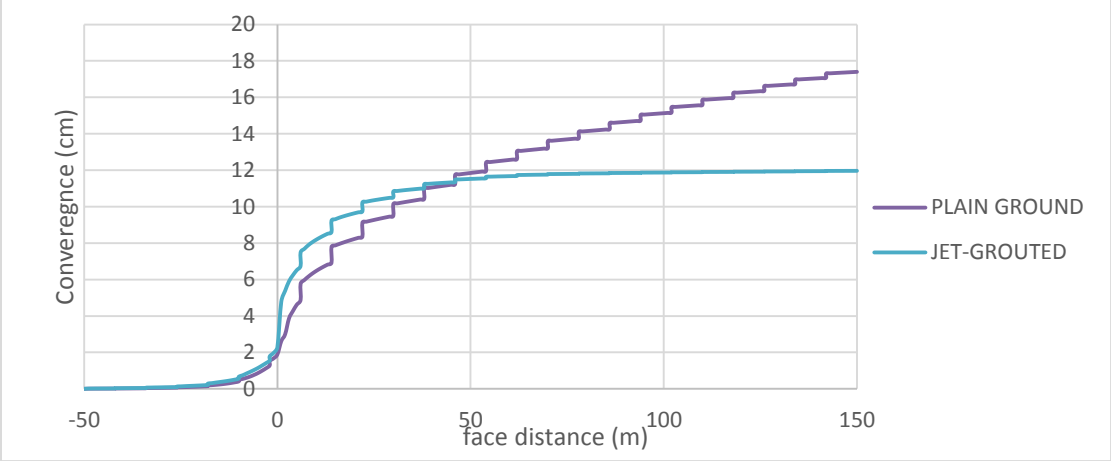

Figure 96: LCP of plain vs. jet-grouted ground for advance rate 10 m/day

Fig. 97 displays the GCC of the tunnel with and without jet-grouting calculated for the optimum advance rate 2.5 m/day. For an identical support system, the convergence of the tunnel in the two cases would be markedly different. This difference could be evaluated with the horizontal distinction between the two GCC's. The distinction is more pronounced for low ultimate pressures. According to the analysis and field measurements given in Mair (2008), the ultimate pressure at tunnels in difficult conditions (low ground strength relative to ground stress) would not exceed 30% of the in situ ground pressure. As indicated by the calculated GCC's, the tunnel convergence would differ by half at this pressure level. This difference dramatically increases for lower pressures, which are more likely in practical cases. This issue is caused by the flattening of the GCC for the tunnel with no jet-grouting at low pressures, indicating the fact that the tunnel with no jet-grouting and support would have unlimited convergence. This flattening also indicates that the use of a supple support system, as recommended in NATM tunneling method, may result in excessive tunnel convergence (collapse) in difficult ground conditions.

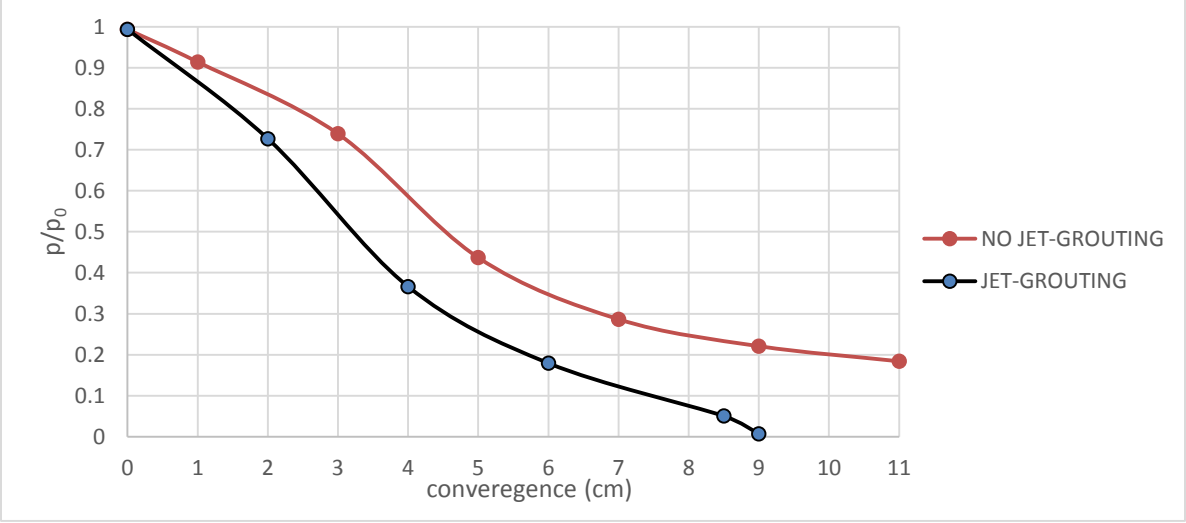

Figure 97: GCC for tunnel with and without jet-grouting

CONCLUSIONS

Chapter 9: Conclusions

This dissertation numerically analyzes the effect of jet-grouting on the response of tunnels in difficult ground conditions. The analysis accounts for the hardening of the jet-grouting and the viscous behavior of the ground. The numerical analysis is conducted using three- and two-dimensional finite element models.

The dissertation begins with three-dimensional undrained analysis of ground excavation using time-independent models such as Mohr-Coulomb and Cam-Clay. The results are shown to agree well with the available analytical solutions. It is shown that representation of the far field boundary conditions by displacement constraints would lead to spurious results in undrained conditions. A margin is also derived for squeezing conditions in terms of the ground strength relative to the in situ stress. The developed model is used to analyze the jet-grouted tunnel.

The sub-horizontal jet-grouting is used to reinforce the ground ahead of the face in difficult conditions. Neglected in the past, the beneficial effect of the ground ahead of the tunnel face (core) on the tunnel stability is markedly exploited in modern tunneling methods. By providing a jet-grouted arch at the tunnel profile ahead of the face, sub-horizontal jet-grouting reinforces the core in difficult ground conditions. The resumption of the tunnel excavation immediately after jet-grouting, however, results in loading of the jet-grouting before it reaches its ultimate maturity. Therefore, the analyses carried out account for the hardening of the jet-grouting by changing the jet-grouting properties through the analysis.

The changing of the jet-grouting properties is accomplished in the finite element model by successive element embedment. The continuous growth of the jet-grouting

properties is discretized into a number of increments. Each increment is assigned to a duplicate of the jet-grouting zone. These duplicates are embedded in the jet-grouted zone through the analysis at the due time. The jet-grouting is shown to significantly reduce the magnitude of the stress and deformation at the tunnel wall and face, particularly in poor ground conditions.

The model of the jet-grouted tunnel is then used to analyze the effect of the core reinforcement by dowels. Dowels are plastic rods inserted into the face to reinforce the tunnel core. This type of core reinforcement is represented in the model by embedding the dowels into the core elements. As such, the displacement of the dowel and the core elements are constrained. The results show that the dowels reduce the tunnel deformation in the vicinity of the tunnel face. This temporary support would be of key importance, particularly in jet-grouted tunnels. This support at the face helps delay the loading of the fresh jet-grouting arch at the face. The model developed for the jet-grouted tunnel is used to analyze time-dependent mechanisms such as ground consolidation and viscous behavior.

The effect of ground consolidation is studied by allowing water inflow at the tunnel wall and face. An identical permeability is assumed for the jet-grouting and the ground. The effect of the ground consolidation is shown to depend markedly on the ground over-consolidation ratio.

Delayed ground response is one of the essential characteristics of tunneling in difficult ground conditions. In order to represent the viscous behavior of the ground, an advanced viscoplastic model is adopted. Three important mechanisms are considered in this model: a non-linear elastic mechanism, an isotropic plastic mechanism, and a deviatoric plastic mechanism. The evolution of the yield surface is represented by an isotropic hardening, which is suitable for monotonic loading paths such as in tunneling. The model accounts for fundamental concepts such as critical state, strain softening, non-

associativity, and bounding surface theory. By introducing a viscous surface, the model can also account for the strain rate effects and the primary and tertiary creep behaviors. The viscoplastic model is numerically integrated using the backward Euler scheme. This ensures the convergence of the integrated equations.

The finite element model of the jet-grouted tunnel is used in conjunction with the implemented viscoplastic model to compare the performance of two different tunneling methods. In the full-face method, the tunnel face is entirely excavated. The full-face excavation allows for the accelerated completion of the support structure by installation of the tunnel invert adjacent to the tunnel face. In the sequential method, the tunnel face is segmented, and each segment is excavated with some distance along the tunnel. As such, in this method, it takes longer for the support at a cross-section to complete. The effect of this delay is analyzed by comparing the deformation and stress fields in the tunnel excavated in full-face and also sequentially. The full-face method is shown to result in less tunnel deformation and stresses than the sequential method. In fact, less delayed deformation is developed in the full-face method because of the accelerated installation of the tunnel invert.

In order to make the three-dimensional time-dependent analyses achievable in practice, similar analyses are performed within the two-dimensional convergence-confinement method (CCM). CCM is based on the analysis of the tunnel cross-section in plane strain conditions and the longitudinal profile of the tunnel deformation (LCP) in the vicinity of the face. The plane strain model is used to calculate the ground (GCC) and the support convergence curves, representing the response of the ground and the support to excavation, respectively.

In order to incorporate time-dependent mechanisms such as jet-grouting hardening and ground viscous behavior in CCM, a new approach is proposed to calculate GCC. In

this approach, the plane strain model is analyzed by controlling the convergence of the jet-grouted ground. The prescribed convergence history is derived from the tunnel LCP. The tunnel LCP is shown to depend on the tunnel advance rate.

The effect of the tunnel advance rate is investigated by comparing the GCC of the tunnel with different advance rates. The increase in the advance rate is shown to result in higher tunnel convergence considering only the jet-grouting hardening. At increased rates, the jet-grouting is not allowed to harden and thus underperforms. On the contrary, increased advance rates are shown to result in lower tunnel convergence considering only the ground viscosity. The reverse dependency of the jet-grouting performance and the ground viscous response on the advance rate leads to an optimum advance rate, at which minimum tunnel convergence is obtained. The GCC calculated for the optimum advance rate shows that the jet-grouting can considerably reduce the tunnel deformation.

The analyses performed in this dissertation may be improved by incorporating the followings:

- Jet-grouting shrinkage and creep behavior during hardening
- Thermal behavior of the jet-grouting during hardening
- Improved representation of the jet-grouting permeability
- Improved estimation of the support effect on LCP in viscous ground conditions
- Ground consolidation in the calculation of GCC
- The effect of face doweling on LCP
- Improved representation of ground-dowel interaction
- Analysis of the model mesh-dependency

References

Adachi, T, Kikuchi, T, Kimura, H., 1988. Behaviour and simulation of soil tunnel with thin cover. In: Proceedings of the 6th Int. Conf. Num. Meth. Geomech., Innsbruch; 3–12.

Adachi, T., Oka, F., 1982. Constitutive equations for normally consolidated clays based on elasto-viscoplasticity. Soils and foundations, Vol. 22, No. 4, 57-70.

Adachi, T., Oka, F., Mimura, M., 1990. Elasto-Viscoplastic constitutive equations for clay and its application to consolidation analysis. J. Engng. Mat. Tech., Vol. 112, 202-209.

Adachi, T., Oka, F., Mimura, M., 1996. Elasto-viscoplastic constitutive equations and its application to consolidation analysis. J. Engng. Mat. Tech. 112, 202‑209.

A.F.T.E.S., 2001. Recommandations relatives a` la methode convergence-confinement. Association Franc¸aise des Travaux en Souterrain, Groupe de travail n_7 (anime´ par M. Panet avec la collaboration de A. Bouvard, Dardard B, Dubois P, Givet O, Guilloux A, Launay J, Nguyen Minh Duc, Piraud J, Tournery H, Wong H). Tunnels et Ouvrages Souterrains 170, 79–89.

Akai, K., Adachi, T., Nishi, K., 1977. Mechanical Properties of Soft Rocks. 9th International Conference on Soil Mechanics and Foundation Engineering, July, Tokyo, 7-10.

Alejano, L.R., Alonso, E., Rodriguez-Dono, A., Fernández-Manín, G., 2010. Application of the convergence-confinement method to tunnels in rock masses exhibiting Hoek–Brown strain-softening behaviour. Int. J. Rock Mech. Min. Sci., 47, 150–160.

Aristorenas, G.V., 1992. Time-dependent behaviour of tunnels excavated in shale. PhD dissertation, MIT.

Aubry, D., Kodaissi, E., Meimon, E., 1985. A viscoplastic constitutive Equations for clays including damage law. Proc, 5th ICONMG, Vol. 1, 421-428.

Barton, N., Lien, R., Lunde, J., 1974. Engineering Classification of Rock Masses for the design of Tunnel Support. Rock Mechanics, Vol. 6 n° 4, 189-236.

Berest, P., Nguyen-Minh, D., 1983. Mode`le viscoplastique pour le comportement d'un tunnel reveˆtu. Rev Fr Ge´otech, 24, 19–25.

Bernaud, D., De Buhan, P., Maghous, S., 1995. Calcul numérique des tunnels boulonnés par une méthode d'homogénéisation. Revue Française de Géotechnique, N° 73, 4ème trisemestre, 53 - 65.

Bernaud, D., Rousset, G., 1996. The new implicit method for tunnel analysis. Int. J. Numer. Anal. Meth. Geomech. 20, 673–690.

Bieniawski, Z.T., 1979. Engineering Rock Mass Classifications. Wiley-interscience publications, U.S.A.

Bishop, A.W., 1966. The strength of soil as engineering materials. Geotech, 16, 91-128.

Bjerrum, L., 1973. Problems of soil mechanics and construction of soft clays and structurally unstable soils. Proceedings 8th Int. Conf. Soil Mech. Found. Engng., Moscow, 3, 111-159.

Bobet, A., 2003. Effect of pore water pressure on tunnel support during static and seismic loading. Tun. Undergr. Space Tech., 18, 377–393.

Boidy, E., Bouvard, A., Pellet, F., 2002. Back analysis of time-dependent behavior of a test gallery in clay stone. Tunn. Undergr. Spa. Tech., 17, 415-424.

Boldini, D., Lackner, R., Mang, H.A., 2005. Ground-shotcrete interaction of NATM tunnels with high overburden. J. Geo. Geoen. Engng. 131 (7), 886-897.

Borja, R., Kavazajian, E., 1985. A constitutive model for the stress-strain-time behavior of wet clays. Géotechnique 35, No. 3, 283-298.

Broms, B. B., Bennermark, H., 1967. Stability of Clay at Vertical Openings. J. Soil Mech. Found. Div., 71 – 94.

Brown, E.T., Bray, J.W., Ladanyi, B., Hoek, E., 1983. Ground response curves for rock tunnels. J. Geotech. Engng. 109, 15-39.

Callari, C., 2004. Coupled numerical analysis of strain localization induced by shallow tunnels in saturated soils. Computers and Geotechnics, 31, 193–207.

Cambou, B., Jafari, K., A constitutive model for granular materials based on two plasticity mechanisms. In Constitutive Equations for Granular Non-Cohesive Soils, Saada A.S, Bianchini G (eds). Balkema: Rotterdam, 149‑167.

Cantieni, L., Anagnostou, G., 2009. The effect of the stress path on squeezing behavior in tunneling. Rock Mech. Rock Engng. 42, 289–318.

Cantieni, L., Anagnostou, G., 2011. On a paradox of elasto-plastic tunnel analysis. Rock Mech. Rock Engng. 44, 129–147.

Caquot, A., Kerisel, J., 1966. Traité de mécanique des sols, 4ème éd., Gauthier-Villars, Paris.

Carranza-Torres, C., Fairhurst, C., 1999. The elasto-plastic response of underground excavations in rock masses that satisfy the Hoek-Brown failure criterion. Int. J. Rock Mech. Mining Sci., 36, 777-809.

Carranza-Torres, C., Zhao, J., 2009. Analytical and numerical study of the effect of water pressure on the mechanical response of cylindrical lined tunnels in elastic and elasto-plastic porous media. Int. J. Rock Mech. Min. Sci., 46, 531–547.

Carter, J.P., Booker, J.R., 1983. Creep and consolidation around circular openings in infinite media. Int. J. solids Str., 19, 663-675.

Chang, Y., Stille, H., 1993. Influence of Early Age Properties of Shotcrete on Tunnel Construction Sequences. Shotcrete for Underground Support VI, Proceedings of The Engineering Foundation Conference, Canada, 110 - 117.

Chen, R., Tonon, F., 2011. Closed-form solutions for a circular tunnel in elastic-brittle-plastic ground with the original and generalized Hoek–Brown failure criteria. Rock Mech. Rock Engng. 44, 169–178.

Chern, J. C., Yu, C. W., Shiao, F. Y., 1998. Tunneling in squeezing ground and support estimation. Proc. Reg. Symp. Sedimentary Rock Engineering, Taipei, 192–202.

Corbetta, F., 1990. Nouvelles me´thodes d' e´tude des tunnels profonds—calculs analytiques et nume´riques. PhD thesis, Ecole des Mines de Paris.

Corbetta, F., Nguyen-Minh, D., 1992. New methods for rock-support analysis of tunnels in elastoplastic media. In: Kaiser, P., McCreath Rock Support in Mining and Underground Construction, 83–90.

Cosciotti, L., Lembo Fazio, A., Boldini, D., Graziani, A., 2001. Simplified behavior models of tunnel faces supported by shotcrete and bolts. *Mod. Tunn. Scie. Tech., Adachi et al. (eds), Swets* & *Zeitlinger*.

Coulter, S., Martin, C.D., 2006. Single fluid jet-grout strength and deformation properties. Tun. Undergr. Spa. Tech. 21, 690–695.

Cristescu, N., 1985. Viscoplastic creep of rocks around horizontal tunnels. Int J Rock Mech Min Sci Geomech Abstr, 22 (6), 453–459.

Cristescu, N., 1988. Viscoplastic creep of rocks around a lined tunnel. Int. J. Plas. 4, 393–412.

Dafalias, Y. F., Herrmann, L. R., 1982. A Generalized Bounding Surface Constitutive Model for Clays. Application of plasticity and Generalized stress-strain relations in Geotechnical Engineering, ASCE, special publication volume.

Debernardi, D., Barla, G., 2009. New Viscoplastic Model for Design Analysis of Tunnels in Squeezing Conditions. Rock Mech Rock Engng, 42, 259–288.

Eisenstein, Z., Kuwajima, F. M., Heinz, H. K., 1991. Behaviour shotcrete tunnel linings. 10th Proceedings of the Rapid Excavation and Tunnling Conference, Seattle, June, 47– 57.

Einstein, H.H., Schwartz, C.W., 1979. Simplified analysis for tunnel supports. J. Geotech. Engng. Div., ASCE, vol 105, No GT4; 499-518.

Fahimifar, A., Zareifard, M., 2009. A theoretical solution for analysis of tunnels below groundwater considering the hydraulic–mechanical coupling. Tun. Undergr. Space Tech., 24, 634–646.

Fang, Q., Zhang, D., Zhou, P., Wong, L., 2013. Ground reaction curves for deep circular tunnels considering the effect of ground reinforcement. Int. J. Rock Mech. Mining Sci., 60, 401–412.

Fodil, A., Aloulou, W., Hicher, P. –Y., 1998. Comportement viscoplastique d'une argile naturelle. Ouv. Géomat. Interac. Model. Multi., Editions Hermes, Paris, 377–396.

Fritz, P., 1984. An Analytical Solution for Axisymmetric Tunnel Problems in Elasto-Viscoplastic Media. Int. J. Num. Anal. Meth. Geomech., Vol. 8, 325 – 342.

Garlanger, J. E., 1972. The consolidation of soils exhibiting creep under constant effective stress. Géotechnique, Vol. 22, No. 1, 71 – 78.

Gioda, G., Swoboda, G., 1999. Developments and applications of the numerical analysis of tunnels in continuous media. Int. J. Numer. Anal. Meth. Geomech., 23, 1393-1405.

Giraud, A., Rousset, G., 1996. Time-dependent behaviour of deep clays. Engineering Geology, 41, 181-195.

Graziani, A., Boldini, D., 2012. Remarks on axisymmetric modeling of deep tunnels in argillaceous formations. I: Plastic clays. Tun. Undergr. Space Tech., 28, 70–79.

Graziani, A., Boldini, D., Ribacchi, R., 2005. Practical estimate of deformations and stress relief factors for deep tunnels supported by shotcrete. Rock Mech. Rock Engng. 38 (5), 345–372.

Gschwandtner, G.G., Galler, R., 2012. Input to the application of the convergence confinement method with time-dependent material behaviour of the support. Tun. Undergr. Space Tech., 27, 13–22.

Heidari, M., Tonon, F., 2013. Convergence curve for tunnels with hardening jet-grouting umbrella. Submitted to Tun. Undergr. Space Tech.

Hellmich, C., Ulm, F.-J., Mang, H.A., 1999. Multisurface chemoplasticity, I: material model for shotcrete. J. Eng. Mech., 125, 692-701.

Hicher, P. -Y., 1985. Comportement mécanique des argiles saturées sur divers chemins de solicitations. Thèse de Doctorat d'Etat, Université Paris.

Hicher, P.-Y., Shao, J.-F., 2008. Constitutive Modeling of Soils and Rocks. ISTE, John Wiley, Great Britain.

Hoek, E., 2001. Big tunnels in bad rock. J. Geotech. Geoenvir. Eng., 127, 726-740.

Hoek, E., Kaiser, P.K., Bawden, W.F., 2000. Support of Underground Excavations in Hard Rock. Balkema, Rotterdam, Netherlands.

Holtz, R.D., Kovacs, W.D., Sheahan, T.C., 2010. An Introduction to Geotechnical Engineering. 2nd ed., Prentice Hall.

Kaliakin, V.N., Dafalias, Y., 1989. Simplification to the Bounding Surface Model for Cohesive Soils. Int. Num. Anal. Meth. Geomech., Vol. 13, No. 1, 90-100.

Kaliakin, N., Dafalias, F., 1990. Theoretical aspects of the elastoplastic‐viscoplastic bounding surface model for cohesive soils. Soils and Foundations 30, 11‐24.

Karakus, M., 2007. Appraising the methods accounting for 3D tunneling effects in 2D plane strain FE analysis. Tun. Undergr. Spa. Tech. 22, 47–56.

Katona, M. G., 1984. Evaluation of viscoplastic cap model. J. Geotech. Engng., Vol. 110, No. 8, 1107-1125.

Kavanzanjian Jr., E., Mitchell, J. K., 1980. Time-Dependent Deformation Behaviour of Clays. J. Geotech. Enging. Division, 106, No. 6, 611–630.

Kharchafi, M., Descoeudres, F., 1995. Comportement différé des roches marneuses encaissant les tunnels. Colloque Craies et Schistes, GBMR, Bruxelles, 1.2.58 – 1.2.67.

Kolymbas, D., Wagner, P., 2007. Groundwater ingress to tunnels- the exact analytical solution, Tun. Undergr. Space Tech., 22, 23-27.

Komamura, F., Huang, R. J., 1974. New Rheological Model for Soil Behavior. J. Geotech. Engng. Div., Vol. 100, No. 7, 807 – 824.

Lackner, R., Hellmich, C., Mang, H.A., 2002. Constitutive modeling of cementitious materials in the framework of chemoplasticity. Int. J. Num. Meth. Engng., 53, 2357-2388.

Ladanyi, B., 1980. Direct determination of ground pressure on tunnel lining in a non-linear viscoelastic rock. In: Proceedings of 13th Canadian Rock Mech. Symp. CIM, Montreal, 126–132.

Lade, P.V., Liu, C-T., 1998. Experimental study of drained creep behavior of sand. J. Engng Mech. 124, 912‐920.

Laigle, F., Kolmayer, P., 1998. Modélisation numérique du comportement à long terme des ouvrages souterrains. Revue Française de géotechnique, No. 85, 65 – 77.

Li, X., Flores-Berrones, R., 2002. Time-dependent behavior of partially sealed circular tunnels. Computers and Geotechnics, 29, 433–449.

Lin, H. D., Wang, C. C., 1998. Stress-Strain-Time Function of Clay. J. Geotech. Geoenviron. Engng., Vol. 124, No. 4, 289 – 296.

Lunardi, P., 1998. Convergence - confinement au extrusion – préconfinement. Mécanique & Géotechnique, Luong (eds), 41 – 57.

Lunardi, P., 2000. The design and construction of tunnels using the approach based on the analysis of controlled deformation in rocks and soils. T&T International ADECO-RS Approach.

Lunardi, P., 2008. Design and Construction of Tunnels: Analysis of controlled deformation in rocks and soils (ADECO-RS). Springer-Verlag, Berlin.

Madejski, J., 1960. Theory of non-stationary plasticity explained on the example of thick-walled spherical reservoir loaded with internal pressure. Archiwum Mechaniki Stosowanej, 5/6, n°12, 775 – 787.

Maekawa, H., Miyakita, K., Sekiguchi, H., 1991. Elasto-Viscoplastic consolidation of Diatomaceous Mudstone. Soil and Foundation, 31, No. 2, 93-107.

Mair, R. J., 2008. Tunnelling and geotechnics: new horizons. Geotechnique, 58, 695–736.

Maleki, M., 1998. Modelisation hierarchisee du comportement des sols. Ph.D. Thesis, Ecole Centrale de Lyon, Montreux.

Mimura, M., Sekiguchi, H., 1985. A review of existing viscoplastic models with particular emphasis on stress-rate effect. Proc. 20th Japan Nat. Conf. SMFE, 403-406.

Murakami, S., Yasuhara, K., Bessho, K., 1996. Prediction of time-dependent behavior of remolded soft marine clay in axisymmetric undrained conditions. Measuring and Modeling Time Dependent Soil Behavior, Ed.: T. C. Sheahan, V.N. Kaliakin, Geotechnical Special Publication, 181-194.

Nguyen-Minh, D., 1986. Modèles rhéologiques pour l'analyse du comportement différé des galeries profondes. Proceedings Int. COng. On Large Underground Openings, Vol. 2, Italy, 659 – 666.

Nguyen-Minh, D., Guo, C., 1998. A new approach to convergence confinement method. Advances in Rock Mechanics, ed. by Lin, Y., 267-279.

Nomikos, P., Rahmannejad, R., Sofianos, A., 2011. Supported Axisymmetric Tunnels Within Linear Viscoelastic Burgers Rocks. Rock Mech Rock Eng, 44, 553–564.

Ohtsu, H., Ohnishi, Y., Taki, H., Kamemura, K., 1999. A study on problems associated with finite element excavation analysis by the stress flow coupled method. Int. J. Num. Anal. Meth. Geomech., 23, 1473–92.

Olszak, W., Perzyna P., 1966. The Constitutive Equations Of The Flow Theory for A Non-Stationary Yield Condition. Proc. 11th Int. Cong. Applied Mechanics, Springer Verlag, 545 – 552.

Oreste, P.P., 2003. A procedure for determining the reaction curve of shotcrete lining considering transient conditions. Rock Mech. Rock Engng. 36, 209–236.

Oreste, P.P., 2009. The convergence-confinement method: roles and limits in modern geomechanical tunnel design. Am. J. App. Sci. 6 (4), 757-771.

Oreste, P. P., Peila, D., 1997. Modeling progressive hardening of shotcrete in convergence-confinement approach to tunnel design. Tun. Undergr. Spa. Tech. 12 (3), 425-431.

Pan, Y.-W., Huang, Z.-L., 1994. A Model of the Time-dependent Interaction Between Rock and Shotcrete Support in a Tunnel. Int. J. Rock Mech. Min. Sci. & Geomech. Abstr., 31, 213-219.

Panet, M., 1979. Time-dependent deformations in underground works. In: Proceedings of 4th Int Conf. Rock Mech., Montreux, Balkema, Rotterdam, 279–290.

Panet M., 1995. Le calcul des tunnels par la me´thode convergence–confinement. Presses de L'e´cole Nationale des Ponts et Chausse´es, Paris.

Panet, M., Guenot, A., 1982. Analysis of convergence behind the face of a tunnel. In: Tunneling 82, Proceedings of the 3rd International Symposium, Brighton, 197–204.

Peck, R.B., 1969. Deep excavations and tunneling in soft ground. In: Proceedings of the 7th ICSMFE, Mexico. State of the Art, vol. 3, 225–90.

Peila, D., 1994. A theoretical study of reinforcement influence on the stability of a tunnel face. Geotech. Geolog. Engng., 12, 145 – 168.

Pelizza, S., Peila, D., 1993. Soil and Rock Reinforcements in Tunnelling. Tun. Undergro. Spa. Tech. 8, 3, 357-372.

Pelizza, S., Peila, D., Oreste, P.P., 1994. A new approach for ground reinforcing design in tunneling. Tunnelling and Ground Conditions, Abdel Salam (ed.), Balkema, Rotterdam, 517 – 522.

Perzyna, P., 1966. Fundamental problems in viscoplasticity. Advances in Applied Mechanics 9, 243‑277.

Pestana, J. M., Whittle, A. J., 1998. Time effects in the compression of sands. Geotechnique, Vol. 48, 695 – 701.

Pichler, C., Lackner, R., Spira, Y., Mang, H.A., 2003. Thermochemomechanical assessment of ground improvement by jet-grouting in tunneling. J. Engng. Mech. 129 (8), 951-962.

Pilgerstorfer, T., Radonc˘ic´, N., 2009. Prediction of spatial displacement development. Geomech. Tunnel. 2, 250–259.

Pottler, R., 1990. Time-dependent rock-shotcrete interaction, a numerical shortcut. Computers and Geotechincs, 9, 149-169.

Poulos, H.G., Davis, E.H., 1974. Elastic solutions for Soil and Rock Mechanics. John Wiley and sons, Inc. – Series in Soil Engineering.

Purwodihardjo, A., 2004. Modelisation des deformation differees lors du creusement des tunnels. Ph.D. Thesis, Ecole Centrale de Lyon.

Purwodihardjo, A., Cambou, B., 2005. Time-dependent modeling for soils and its application in tunneling. Int. J. Numer. Anal. Meth. Geomech. 29, 49–71.

Rabcewicz, L. v., 1969. Stability of Tunnels under Rock Load. Water Power, 225-229.

Ramoni, M., Anagnostou, G., 2011. The interaction between shield, ground and tunnel support in TBM tunnelling through squeezing ground. Rock Mech. Rock Engng., 44, 37–61.

Rousset, G., 1988. Comportement Mécanique des Argiles Profondes. Thèse de doctorat l'Ecole Nationale des Ponts et Chaussées.

Rousset, G., 1990. Les Sollicitations à Long Terme des Revêtements des Tunnels. Revue Française Géotechnique, n° 53, 5 – 20.

Sagaseta, C., 1988. Discussion: Analysis of undrained soil deformation due to ground loss, Géotechnique, vol. 38, No. 4, 647 – 649.

Sandrone, F., Labiouse, V., 2010. Analysis of the evolution of road tunnels equilibrium conditions with a convergence–confinement approach. Rock Mech Rock Eng., 43, 201–218.

Sekiguchi, H., 1984. Theory of undrained creep rupture of normally consolidated clays based on elasto-viscoplasticity. Soils and foundations, 24, No. 1, 129-147.

Sezaki, M., Kawata, T., Swoboda, G., Aydan, Ö, Moussa, A., 1992. Numerical Modelling for The Representation of Shotcrete Hardening and Face Advance of Tunnels Excavated by Bench Excavation Method. Num. Models in Geomech., Pande & Pietruszczak (eds), Balkema, Rotterdam, 707 - 717.

Shin, J. H., Potts, D. M., Zdravkovic, L., 2002. Three-dimensional modeling of NATM tunneling in decomposed granite soil. Géotechnique, Vol. 52, No. 3, 187 – 200.

Singh, A., Mitchell, J. K., 1968. General Stress-Strain-Time Function for Soils. J. Soil Mech. Found. Div., Proceedings of ASCE, 21 – 46.

Sterpi, D., Gioda, G., 2009. Visco-Plastic Behaviour around Advancing Tunnels in Squeezing Rock. Rock Mech Rock Engng, 42, 319–339.

Stille, H., Holmberg, M., Nord, G., 1989. Support of weak rock with grouted bolts and shotcrete. Int. J. Rock Mech. Min. Sci. Geomech. Abstr., 26, 99–113.

Sulem, J., Panet, M., Guenot, A., 1987. An Analytical Solution for Time-dependent Displacements in a Circular Tunnel. Int. J. Rock Mech. Min. Sci.& Georaech. Abstr. Vol. 24, No. 3, 155-164.

Tavenas, F., Leroueil, S., La Rochelle, P. et Roy, M., 1978. Creep Behaviour of An Undisturbed Lightly Overconsolidated Clay. Canadian Geotechnical Journal, vol. 15, 402 – 423.

Tonon, F., 2010. Sequential Excavation, NATM and ADECO: What They Have in Common and How They Differ. Tun. Undergr. Spa. Tech. 25, 245–265.

Tonon, F., 2011. ADECO full-face tunnel excavation of two 260 m^2 tubes in clays with sub-horizontal jet-grouting under minimal urban cover. Tun. Undergr. Spa. Tech. 26, 253–266.

Ulm, F.-J., Coussy, O., 1995. Modeling of thermochemomechanical couplings of concrete at early ages. J. Engng. Mech., 121, 785-794.

Ulm, F.-J., Coussy, O., 1996. Strength growth as chemo-plastic hardening in early age concrete. J. Engng. Mech., 122, 1123-1132.

Unlu, T., Gercek, H., 2003. Effect of Poisson´s ratio on the normalized radial displacements occurring around the face of a circular tunnel. Tunnel. Undergr. Space Technol. 18, 547–553.

Vlachopoulos, N., Diederichs, M.S., 2009. Improved longitudinal displacement profiles for convergence confinement analysis of deep tunnels. Rock Mech. Rock Engng. 42, 131–146.

Zhu, J., Yin, J., 2000. Strain-Rate-Dependent Stress-Strain Behavior of Overconsolidated Hong Kong Marine Clay. Canadian Geotechnical Journal, Vol. 37, 1272 – 1282.

Zhu, J.-G., Yin, J.-H., Luk, S.-T., 1999. Time-Dependent Stress-Strain Behavior of Soft Hong Kong Marine Deposits. Geotech. Testing J., Vol. 22, No. 2, 112 – 120.